Constraints on the thermal state of the continental lithosphere

A dissertation presented by

Matthew Gard

In fulfilment of the requirements
for the degree of
Doctor of Philosophy

THE UNIVERSITY
of ADELAIDE

Submitted to the
Department of Earth Sciences,
School of Physical Sciences, Faculty of Sciences

Adelaide, November 2021

It's the job that's never started as takes longest to finish.
– Samwise Gamgee

CONTENTS

LIST OF TABLES

LIST OF FIGURES

ABSTRACT

The thermal state of the lithosphere is an important driver of many physical and chemical processes within the Earth. Understanding the distributions of heat flow and radiogenic heat production provides an important constraint on lithospheric thermal models. By some estimates nearly 40% of continental heat flow is produced by radioactive decay in the crust, however the distribution of heat producing elements is poorly constrained.

Creating robust models of radiogenic heat production requires an understanding of its natural variability. The creation of a global whole-rock geochemical database provides a framework for discussing global distributions of thermal parameters. I have collated over one million digital rock entries with a range of sample data including major and trace element concentrations, isotopic ratios, and other metadata. Associated naming schema and physical parameter estimates are also computed in a standardised manner, including radiogenic heat production.

I then present a new model for continental igneous heat production from ~4 Ga to the present using a novel silica-normalised igneous data set and compare to previous discussions of granitic and sedimentary trends in the literature. Crude normalization for composition indicates lithological control is the dominant factor on heat production after the influence of decay is removed. I find that heat production at formation for different rock types has been relatively constant through time except for the early Archean to ~2.7 Ga. I suggest the heat production–age pattern does not significantly reflect the influences of erosion, secular cooling, depletion, or the supercontinent cycle as suggested by some previous studies, but instead either reflects a shift in the bulk composition of the crust or evidence for bias in the rock record due to thermal stability.

Geophysical proxies provide additional constraints on the crustal thermal state. I have developed a global Curie Depth model from the latest satellite-derived lithospheric magnetic model using the equivalent source magnetic dipole method. Forward modelling was conducted to simulate the observed lithospheric magnetic field. Our updated methodology involves additional vector components utilised in the forward modelling calculations, a differing long-wavelength model, and inclusion of a spatially variable magnetic susceptibility estimate. Resultant continental Curie depth estimates show good agreement with observed heat flow observations and provide further evidence that Curie depth estimates can assist in estimates of the thermal state of the lithosphere.

Finally, I assess various heat flow models for Antarctica derived from geophysical proxies. Extrapolation from isotherm estimates at depth require models of heat production and thermal conductivity to model surface heat flow. Differences in models can have non-trivial influences on the results produced. Quantifying the uncertainty associated with these thermal parameters is also critical for understanding and interpreting the heat flow solutions. I propose a set of models derived from whole-rock geochemical data, and guided by compositional studies of the crust. Uncertainties associated with this model are estimated via the Monte Carlo method. I show that applying models guided by global insights provides a reasonable fit to the Antarctica continent, and a method of estimating uncertainty in thermal parameters for regions lacking basement geology constraints.

Thesis Supervisors: Derrick Hasterok, Graham Heinson, and Martin Hand

STATEMENT OF ORIGINALITY

I certify that this work contains no material which has been accepted for the award of any other degree or diploma in my name, in any university or other tertiary institution and, to the best of my knowledge and belief, contains no material previously published or written by another person, except where due reference has been made in the text.

In addition, I certify that no part of this work will, in the future, be used in a submission in my name, for any other degree or diploma in any university or other tertiary institution without the prior approval of the University of Adelaide and where applicable, any partner institution responsible for the joint-award of this degree.

I acknowledge that copyright of published works contained within this thesis resides with the copyright holder(s) of those works.

I also give permission for the digital version of my thesis to be made available on the web, via the University's digital research repository, the Library Search and also through web search engines, unless permission has been granted by the University to restrict access for a period of time.

I acknowledge the support I have received for my research through the provision of an Australian Government Research Training Program Scholarship.

Signed

03/06/2021

Date

ACKNOWLEDGEMENTS

Thank you to my primary supervisor Derrick Hasterok for the tremendous amount of time given for assistance over the course of this thesis. You made yourself available in times of need, and instilled in me the same drive you have to code everything yourself (for better or for worse!). Secondly, thank you to my co-supervisors Martin Hand and Graham Heinson for their insights and advice over the years.

To my family, thank you for everything. Mum and Dad - knowing you were there for me gave me the confidence to tackle everything that came my way. Maybe with this PhD you'll finally trust me to drink the right amount of water. Emma - although you may have (..arguably..) beaten me to being the first doctor in the family, thank you for all the support. I'm constantly inspired by the things you have achieved, and I'm also sure you'll find another way to one-up me by 0.05.

To my Nanna and Pa, I'm sorry you didn't get to see me finish this PhD. Your unwavering encouragement over the years, and the looks of pride every time I described what I was working on is something I'll keep with me forever.

I am also grateful for the support of Geoscience Australia over the last couple of years. The study assistance program gave me the flexibility to juggle work and study.

Finally, thank you Tasha for helping me in this final year. Our burrito dates got me through a lot of difficult study periods.

CHAPTER

ONE

INTRODUCTION

1.1 Contextual statement

Heat transfer influences a wide range of geological processes; from the microscopic scale and its role in metamorphic reactions, to macroscopic systems such as differentiation of the crust, and planetary forces such as plate tectonics. Understanding the thermal state of the continental lithosphere is paramount for not only improving our knowledge of evolving Earth systems, but it is also important economically for geothermal energy resources and predicting maturation of hydrocarbons. Despite influencing a range of geological systems, continental lithospheric temperatures are often poorly constrained, owing largely to the scarcity and heterogeneous spatial distribution of direct heat flow measurements around the globe, and the highly variable nature of critical parameters such as radiogenic element enrichment and its distribution in space and time. Often regions lacking data are either ignored or interpolated through.

Radioactive decay constitutes one of the primary sources of heat generation in the continental crust. This radiogenic heat production can vary by several orders of magnitude, and it's distribution is both laterally and vertically heterogeneous. Thus, it comes as no surprise that one of the challenges facing the heat flow community is the characterisation of reasonable estimates for the continental crust when developing thermal mod-

els. Estimates of the average enrichment of heat producing elements in the continental crust as well as its simplified vertical stratification are variable, particularly for the lower crust (e.g. Condie, 1993; Taylor and McLennan, 1995; Hans Wedepohl, 1995; Gao et al., 1998; Rudnick and Gao, 2003; Hans Wedepohl, 1995). Understanding the nature of the variability of radioactive heat production and heat flow, and how they might correlate to other factors such as lithology and age, is critical in determining reasonable uncertainty estimates that might help guide improved predictions of intracrustal temperatures, particularly in regions with little to no data.

1.2 Objectives and thesis outline

In this thesis I examine a range of methods to expand our understanding of heat flow and heat production in the continental crust. I use a range of geological, geophysical and geochemical proxies to constrain numerically derived estimates and associated uncertainty of heat flow and heat production. The work in this thesis helps improve constraints and uncertainty estimates in generalised heat production models, for example, geothermal resources exploration, petroleum maturation models, thermal buoyancy, and studies of the cryosphere.

This thesis is presented in seven chapters to address these questions;

- Chapter 2 provides a summary of the state of the field in relation to our understanding of surface heat flow and crustal radiogenic heat production.
- The initial content chapter of this dissertation, Chapter 3, provides a framework for quantifying and discussing global distributions of geochemistry and heat production through the collation of a global geochemical database, which contains just over one-million samples with associated sample data including major and trace element concentrations, isotopic ratios, and location information. Also included are physical parameter estimates, including heat production, that are computed in a standardised manner. The global geochemical database has been published as Gard, M., Hasterok, D., and Halpin,

J. A. (2019). Global whole-rock geochemical database compilation. Earth System Science Data, 11(4):1553–1566, doi:10.5194/essd-11-1553-2019.

- Chapter 4 outlines a new model for continental igneous heat production from ~4 Ga to the present, using a subset of the global geochemical database in Chapter 3 which consists of 75,800 whole-rock analyses and associated continental heat production estimates. The content of this chapter has been published as Gard, M., Hasterok, D., Hand, M., and Cox, G. (2019). Variations in continental heat production from 4 Ga to the present: Evidence from geochemical data. Lithos, 342-343:391–406, doi:10.1016/j.lithos.2019.05.034.

- Chapter 5 describes an updated methodology for a global Curie depth estimate using the equivalent source magnetic dipole method to fit the lithospheric magnetic field model LCS-1 from spherical harmonic degree 16 to 100. This model makes use of the three vector components of the magnetic field model and includes a laterally variable magnetic susceptibility model. This work has been published as Gard, M. and Hasterok, D. (2021). A global Curie depth model utilising the equivalent source magnetic dipole method. Physics of the Earth and Planetary Interiors, page 106672, doi:10.1016/j.pepi.2021.106672.

- Chapter 6 presents an analysis of Antarctic heat flow estimates derived from geophysical proxy methods, with particular focus on uncertainty estimates associated with the selection of thermal parameters. Variance in thermal parameter models contribute significantly in some regions to the variance observed in the surface heat flow estimates for Antarctica, and I suggest recommendations for future models and avenues of research.

- Finally, Chapter 7 discusses the contributions of this thesis in relation to heat flow modelling and the thermal state of the continental crust, as well as suggests future research directions.

CHAPTER

TWO

BACKGROUND

2.1 Heat flow

Surface heat flow is a measure of the transfer of heat energy from the interior of the Earth to the surface, with standard units of milliwatts per meter squared (mWm^{-2}). In steady-state this is Fourier's Law;

$$q(z) = -K(z)\frac{\partial T(z)}{\partial z}, \tag{2.1}$$

where $q(z)$ is heat flow, $K(z)$ is thermal conductivity, z is depth, and $\frac{\partial T(z)}{\partial z}$ is the thermal gradient.

Surface heat flow, and the insights it can give us into temperatures of the crust and mantle, are critical for understanding a host of processes; from studies of lithospheric strength (Sonder and England, 1986; Sandiford and McLaren, 2002; Jiménez-Díaz et al., 2012), the evolution and thermal state of the lithosphere and mantle (Furlong et al., 1995; Korenaga, 2008), economic drivers such as the associations with the maturation of source rocks in the petroleum industry (Palumbo et al., 1999) or geothermal resource assessment (Middleton, 2016), and studies impacting climate change models such as assessments of subglacial conditions (Pattyn, 2010) or carbon

and methane degassing models from the lithosphere (Mörner and Etiope, 2002).

Although lithospheric temperatures impart notable influence on a range of geological processes at all scales in space and time, it is often poorly constrained owing to the highly heterogeneous and predominantly sparse distribution of direct measurements. A number of studies have worked to collate the scattered measurements of surface heat flow (e.g. Pollack et al., 1993; Hasterok et al., 2011; Lucazeau, 2019), with some applying additional constraints from alternative models of lithospheric temperatures derived from geophysical and geological proxies in attempts to infill regions with sparse or no data (e.g. Lucazeau et al., 2011; Davies, 2013; Lucazeau, 2019)

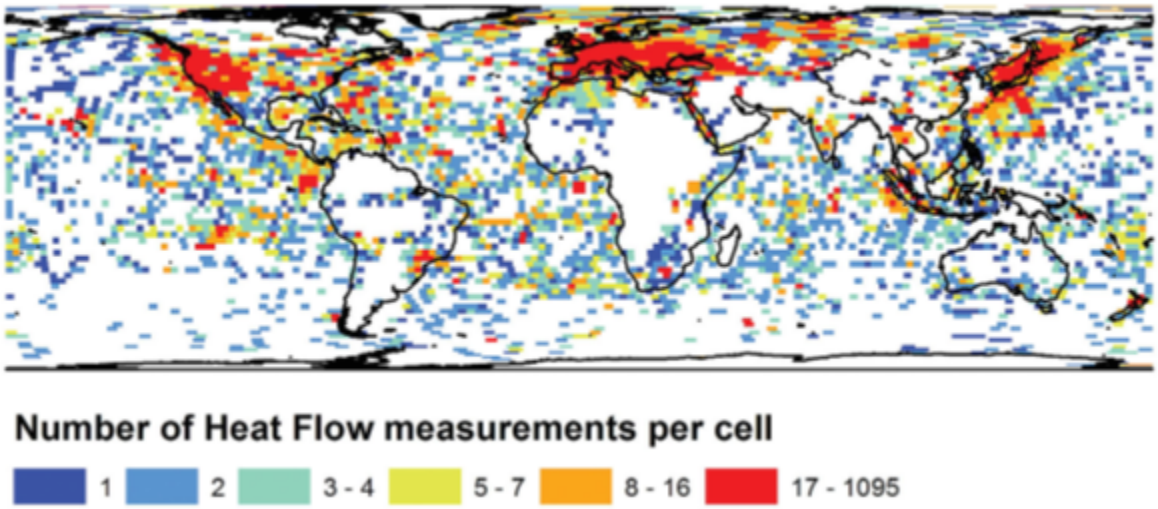

Figure 2.1: Heat flow data collated in Davies (2013). The Earth surface is broken up into a regular grid, with the colour of the cells representing the number of heat flow measurements in the cell. Note the large gaps in the data set, as well as large amounts of underrepresented regions with only 1-4 heat flow measurements

However, the inhomogeneous distribution and poor spatial density of surface heat flow data points for large areas of the continental crust makes analysis difficult. As seen in Figure 2.1, there are large regions of the Earth lacking any direct surface heat flow measurements, and much of the world has less than 4 measurements per 2° cell. One problem with such sparse data is that surface heat flow data can be heavily controlled by extreme local anomalies, such as magmatic or fluid circulation processes, and this

can bias estimates of the deeper thermal structure of the crust in a larger region towards anomalous values in poorly sampled regions (Chapman, 1986; Goes et al., 2000)

These heat flow and temperature gradient measurements are generally attained in the oceans via penetrator probes, or via downhole probe readings and poorer quality petroleum well bottom-hole temperatures for the continents (Drury, 1984). These bottom hole temperatures must be corrected to estimate the equilibrium temperature (Goutorbe et al., 2007), but are not always done in a consistent fashion. Thus, not only is the distribution of these data points highly variable, but also the quality of the readings attained.

2.1.1 Global heat loss, heat generation and redistribution

A range of processes work to generate and redistribute heat and energy within the Earth. Most studies of total heat loss estimate the sum of the Earth's heat loss is on the order of 44-49 TW (e.g. Pollack et al., 1993; Jaupart et al., 2007; Davies and Davies, 2010). Within the Earth there are two primary sources of heat that contribute to the heat observed at the surface;

- Heat generated internally from the decay of radioactive isotopes (also known as heat producing elements (HPEs)); and
- Primordial heat associated with accretion of the Earth and formation of the core.

At present day it has been estimated from a suite of observables including heat production, surface heat flow, xenoliths and seismic tomography that heat generated via radioactive decay in the lithosphere contributes 25 to 45% of the total heat loss (Pollack and Chapman, 1977a; Artemieva and Mooney, 2001; Hasterok and Chapman, 2011; Jaupart and Mareschal, 2014). Additionally, magmatic activity and viscous dissipation (Pollack and Chapman, 1977b), frictional heating due to kinetic effects such as plate movement (Zhu, 2016), some exothermic metamorphic processes such as serpentinization (Fyfe, 1974), and redistribution of heat via hydrothermal

circulation of fluids can also impact crustal temperatures and measured surface heat flow.

For large amounts of the continental lithosphere the thermal system is presumed to be in 'steady-state', which is where the surface heat flow is equal to the heat flow into the base of the lithosphere and the heat generated internally within the lithosphere due to radioactive decay.

For a system in steady-state i.e. no transient heating or cooling effects, the 1-D steady-state heat conduction equation is given by the following:

$$\frac{\partial}{\partial z}\left(K\left(z\right)\frac{\partial T\left(z\right)}{\partial z}\right) = -A\left(z\right), \tag{2.2}$$

where $K\left(z\right)$ is the thermal conductivity, $T\left(z\right)$ is the temperature, z is depth and $A\left(z\right)$ is the heat production.

While this assumption is not always valid, for example following a major tectonic event, it has been empirically shown to be suitable for large swathes of the lithosphere (Lucazeau et al., 2011). Generally, if a region has been tectonically inactive for a period on the order of 50-300 My, it is assumed to be in steady-state, or close enough to be reasonably approximated by it, but the amount of time depends a lot on the vertical distribution of the heat producing elements through the lithospheric column (Jaupart and Mareschal, 2007).

2.2 Radiogenic heat production

The primary source of internal heat generation within the continental lithosphere is via the decay of radionuclides (e.g. Birch, 1954; Taylor and McLennan, 1995; Wasserburg et al., 1964), whereby a radioactive isotope transitions to a more stable energy state with an associated release of energy (McDonough, 2021).

While this parameter is critical for determining intracrustal temperatures, most studies utilise overly simplified vertical (and even more rarely, lateral)

variations models (e.g. McKenzie et al., 2005; Artemieva, 2006; Martos et al., 2017).

Surface heat flux often varies on scales smaller than those permitted by variations due to deep sub-lithospheric heat flow sources, most commonly influenced by upper crustal variations in radiogenic heat production (Mareschal and Jaupart, 2004). Despite this, radiogenic heat production information is not routinely collected alongside heat flow measurements. As detailed in Jaupart et al. (2016), a global compilation of heat flow data consisting of some 17,000 data points was only associated with around 1,800 with measured heat production values.

Of the radioactive isotopes present in the Earth, four of these contribute around 99% of the total heat produced at present day; ^{238}U, ^{235}U, ^{232}Th, and ^{40}K (Rybach, 1988; McDonough, 2021) (Figure 2.2). Isotopes of ^{87}Rb and ^{144}Sm which are the next largest contributors only produce <1% to the total heat production (Korenaga, 2008).

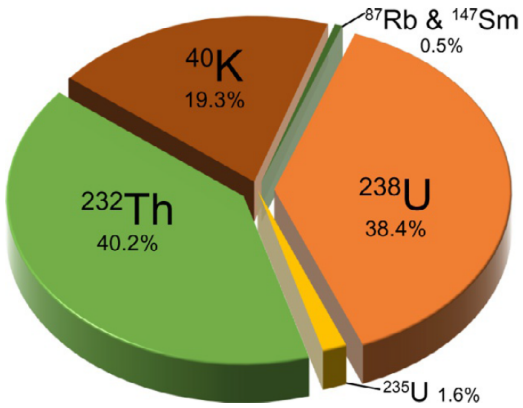

Figure 2.2: Most common isotopes contributing to Earth's total radioactive heat generation. Figure sourced from McDonough (2021).

Internal heat generation owing to radioactive decay has been in constant decline since the formation of the Earth. As radioactive isotopes decay into stable isotopes, their relative proportion in the bulk Earth decreases. The total heat loss due to radioactive decay around 3 billion years ago was almost double that of today, purely as a result of radioactive decay. This difference has important implications for the thermal evolution of the

Earth and systems such as mantle convection (Schubert, 1997; Jaupart and Mareschal, 2010). Additionally, due to the large differences in half-lives of the various heat producing isotopes, the relative proportions and contributions to the total heat output due to different radionuclides has also changed through time. For example, ^{26}Al is a relatively short-half lived isotope and its influence on the bulk radiogenic heat at present day is negligible, although for the first 10 Ma of Earth's formation this was not the case (Urey, 1955; McDonough, 2021). Similarly, although ^{238}U and ^{232}Th contribute the most to the present day heat generation, in the Hadean the shorter half-life ^{235}U and ^{40}K would have contributed around 22% and 46% to the total radiogenic heat output, respectively (Turcotte and Schubert, 2002; McDonough, 2021). At present day the relative proportions of ^{238}U, ^{235}U, ^{232}Th, and ^{40}K are listed in Table 2.1, along with their relative half-lives and heat production per unit mass. While ^{235}U only exists as around 0.7% of the total naturally occurring uranium at present day, it remains a major isotope to the total heat generated as it produces an order of magnitude more energy during it's decay series (Table 2.1).

Table 2.1: Decay series contributing to the bulk heat generation within the Earth. Values from McDonough (2021).

Decay system	Natural abundance (%)	Half-life (Ga)	Decay energy (MeV)
^{40}K	0.01167	1.412 (^{40}Ar)	1.5044 (^{40}Ar)
		1.192 (^{40}Ca)	1.3109 (^{40}Ca)
^{238}U	99.274	4.4683	51.6942
^{235}U	0.72033	0.70348	46.3965
^{232}Th	100	14.1	42.6459

Radioactive elements decay towards more stable daughter nuclei. This process is associated with emission of energy in the form or alpha, beta, and/or gamma radiation depending on the decay pathway. Of these, gamma radiation is the most penetrating, and is thus the target of in-situ measurements of radiogenic heat production. Portable gamma ray spectrometers can detect an integrated heat production estimate over roughly 1 m^2. Aerial surveys are also possible and can rapidly capture large swathes of radiometric data, as gamma rays do not attenuate as rapidly though air as they do rock and regolith. However, penetration is relatively shallow due to the rapid attenuation of gamma rays through solid material, with most of the

emissions detected coming from only the top 15 cm of material (McCay et al., 2014).

Alternatively, heat production may be estimated via geochemical data. Geochemical data by contrast uses smaller volumes of samples that have been powdered and mixed. As many as 90 elements may be analyzed at a time, but for radiogenic heat production estimates only three are needed (K, Th and U). Geochemical data have some advantages over traditional gamma ray spectral measurements despite their smaller volume of sampling. For instance, geochemical samples are far more commonly made by geochemists and petrologists than gamma-ray spectra measured by geothermicists. The precise chemistry of samples and known rock type provide a wealth of information that can be used to study in great detail the effects of composition, tectonic setting, and physical processes have on heat production. Methods for gathering geochemical concentrations of the heat producing elements can include ICP-MS and ICP-AES (Inductively coupled plasma mass spectrometry/atomic emission spectrometry), and XRF (X-ray fluorescence spectrometry) with differing levels of utility and precision (Rybach, 1988; Vilà et al., 2010).

Given the chemical composition of a rock sample, the heat production per unit volume (at present day, given modern isotopic ratios) can be calculated by summing the contributions of each element given the natural abundance and decay energy of the radioactive isotopes;

$$A(\mu\mathrm{Wm}^{-3}) = \rho\left(9.67\mathrm{C_U} + 2.56\mathrm{C_{Th}} + 2.89\mathrm{C_{K_2O}}\right) \times 10^{-5}, \qquad (2.3)$$

where A is the heat production, $\mathrm{C_U}$ and $\mathrm{C_{Th}}$ are the concentrations of uranium and thorium in parts per million (ppm), $\mathrm{C_{K_2O}}$ is the concentration of potassium in wt%, and ρ is the density of the rock sample (Rybach, 1988).

Each of the three primary heat producing elements (potassium, uranium and thorium) are classified as large-ion lithophile elements (LILE). These LILE elements are strongly incompatible (particularly uranium and thorium) and partition strongly to the melt phases during melting. This has several implications, the most notable of which is that for igneous

and metaigneous rocks heat production generally increases with increasing silica content (Artemieva, 2006; Vilà et al., 2010). Through time, these elements have concentrated primarily in the upper crust due to the processes of crustal differentiation. A present day example of this process can be observed at mid-ocean ridges, where oceanic crust (i.e. the basaltic melts derived from partial melting of the mantle) is enriched by a factor of 4 with respect to the heat producing elements compared to the mantle it was derived from (Turcotte and Schubert, 2002). While there is a crude correlation to lithology due to incompatibility, the concentration of the heat producing elements uranium and thorium is a much more complex interaction heavily influenced by an individual sample's petrological history. Potassium occurs in a number of minerals that form significant fractions of igneous rocks such as feldspars and micas, however uranium and thorium are generally concentrated in accessory minerals such as zircon and monazite, which means their correlation to major element geochemistry, and physical properties such as density and seismic velocity are generally considered weak (Jaupart and Mareschal, 2014; Artemieva et al., 2017).

Heat flow in geological provinces also shows a crude correlation with age. This influence is due in part to two conditions; time since last tectonothermal event, and also radiogenic heat generation. However, within any time period significantly variability in heat flow is observed, and this association is mainly present in the global heat flow data sets, and not necessarily true for local scale models (Morgan, 1985; Jaupart and Mareschal, 2014). Although time since last tectonothermal event imparts some of this observed effect in recently active regions, for most regions older than about 50–300 Mya this is primarily due to a decrease in heat producing element enrichment with age, as a result of the decay process (Jaupart and Mareschal, 2014).

A study of sedimentary rock heat producing element enrichment and its relationship to age has also been conducted by McLennan and Taylor (1980). They noted a stark shift in Th and U concentrations at the Archean–Proterozoic boundary which they attributed to a shift in the bulk composition of the upper crust brought on by emplacement of significant volumes of felsic material at the end of the Archean in agreement of other studies (e.g. Veizer, 1983).

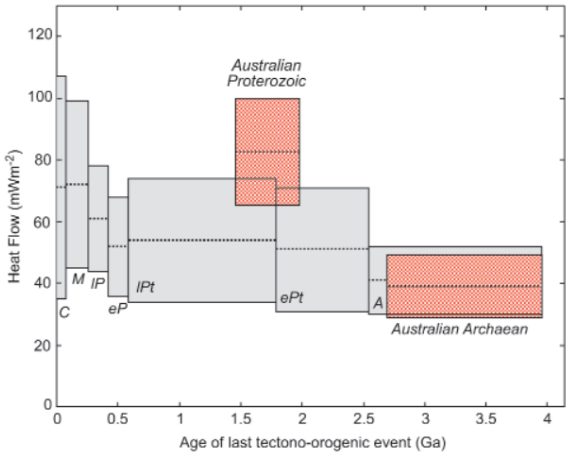

Figure 2.3: Histogram of heat flow data by age from Morgan (1985) (Figure derived from McLaren et al. (2003))

2.2.1 Variability of heat production

Radiogenic heat production is highly variable both laterally and vertically; varying at all spatial scales and up to two orders of magnitude (Kukkonen and Lahtinen, 2001; Slagstad, 2008; Jaupart and Mareschal, 2014), even within regions such as plutons (e.g. Sawka and Chappell, 1988; Brady et al., 2006). Selection of heat production estimates are thus often poorly constrained within a large uncertainty window, and this has important implications for the vertical temperature distributions derived from these estimates.

It is often suggested that, on average, heat production must decrease with depth, otherwise observed surface heat flow would be exceeded (Sandiford and McLaren, 2002). Lower crustal structure shows variability on similar scales as that of the surface heat production measurements as evidenced from exhumed crustal cross-sections, xenoliths, and deep boreholes (e.g. Ketcham, 2006; Fountain and Salisbury, 1981; Rudnick, 1992; Brady et al., 2006; He et al., 2008). While these crustal profiles may help improve estimates of vertical profiles for a particular province, they are rare and may not necessarily reflect the average crust (Hasterok and Chapman, 2011). Additionally, the heat producing elements enrichment of xenoliths may become altered by the magmatic fluids that are providing the medium to reach the upper crust (Dawson, 1984).

Thus, quantifying the vertical heat production profile is plagued with considerable uncertainty, and variations in heat production with depth are a function of the unique local geologic history of a region (Mareschal and Jaupart, 2013). A direct consequence of this large variability is that models for average concentrations of heat producing elements in the continental crust show non-trivial disparities (e.g. Rudnick and Fountain, 1995; Taylor and McLennan, 1995; Hans Wedepohl, 1995; Rudnick and Gao, 2003) depending on the data sets used to constrain these estimates.

2.3 Proxies for estimating the lithospheric thermal state

While the thermal state of oceanic lithosphere is quite well understood (e.g. Hasterok et al., 2011), the thermal state of the continental lithosphere is appreciably more heterogeneous. As discussed previously, this is due to lateral and vertical variations in radiogenic heat production, complex and highly variable geological histories and large differences in lithology and vertical stratification. As a result, a number of proxy methods exist to estimate the thermal state of the continental lithosphere.

Temperature profiles through the Earth can be estimated through extrapolation of the surface measurements, under the assumption that the heat transport is entirely conductive (Čermák and Bodri, 1995; Pollack and Chapman, 1977b). However, the spatial density of heat flow measurements is highly heterogeneous as discussed in Section 2.1, with a number of countries and regions considerably under sampled. Another problem with this information is that surface heat flow data can be heavily controlled by extremely local anomalies, and in underrepresented regions in particular, bias estimates of the deeper thermal structure of the crust in a larger region towards anomalous values (Chapman, 1986; Goes et al., 2000). Addition of thermotectonic age constraints and lithological estimates has also been used in conjunction with surface heat flow data to produce models that can be applied to regions with little to no heat flow data themselves (e.g. Davies and Davies, 2010).

Geothermobarometry of xenoliths and xenocrysts, which are pieces of host rock from deep crust or upper mantle rapidly brought to the surface via magmatism, can also be utilised to estimate a temperature profile through the lithosphere (Y. O'Reilly and Griffin, 1985; Xu et al., 1996). However, these samples represent a geotherm at the time of their eruptive host and may not be indicative of the current thermal state. Even in the case that they do represent the current geotherm, they may not adequately sample the lower crust and upper mantle in a representative manner. Additionally, xenoliths are only found in magmatic environments and some have suggested they may instead signify the localised and transient thermotectonic environment due to the source that is inducing the magmatism (e.g. Eaton et al., 2009), or may have their geochemistry altered by the fluids they used to ascend (Dawson, 1984). The sparseness of heat flow and xenolith data suffer from localisation effects and uncertainties due to temporal lag respectively.

Incorporating other independent models can assist in constraining estimates of the thermal structure rather than relying on interpolation. Geophysical derived proxies for temperature can aid in this pursuit, most notably of which include studies of thermal isostasy, magnetotelluric studies and models of electrical conductivity, modelling of the relationship between seismic velocities and temperature, and magnetic Curie depth estimations.

Thermal isostasy is where the deep thermal state of the crust and lithosphere can impart influences on a regions elevation through thermal expansion and buoyancy forces. While this methodology has been primarily used in the oceans whereby bathymetry away from the oceanic ridge follows a reasonable well-defined relaxation curve (e.g. McKenzie, 1967; Sclater et al., 1980), it has also found application in the continents in regions such as continental rifts, and more holistically via adjustments to elevation to correct for compositional variations and its influence on buoyancy such as those applied by Hasterok and Chapman (2007) and Hasterok and Gard (2016).

Seismic velocities have also been used to invert for temperature, but are dependent on many physical properties other than temperature as well such as composition, presence of partial melts, anisotropy, anelasticity, and grain size (Liu et al., 1976; Faul and Jackson, 2005; Dalton et al.,

2009; Takei, 2017). Previous studies have highlighted the density of rock at depths shallower than around 250 km are most commonly the result of temperature variations (e.g. Sobolev et al., 1996; Goes et al., 2000). As such, estimations and models for the thermal state can be produced from seismic velocities through inversion, in combination with laboratory measured elastic moduli of common lithospheric materials (Sobolev et al., 1996; Goes et al., 2000; Cammarano et al., 2003; An et al., 2015), or including additional constraints from measurements such as gravity and electrical conductivity (e.g. Afonso et al., 2013; Jones et al., 2017)

Many studies have also documented that there is a crude relationship between surface heat flow and the depth to the bottom of the magnetized layer in the crust (e.g. Mayhew, 1982; Okubo and Matsunaga, 1994). The primary contribution to the observable magnetic field of the Earth is that from the core; however at shorter wavelengths, shallower anomalies due to magnetisation within the crust can be identified. Two components comprise the crustal field: magnetisation due to the remanent field, and magnetisation due to the induced field. The latter is dependent on multiple properties, including the magnetic susceptibility of the rocks and the thickness of the magnetised layer within the Earth, known as the magnetic crust (Maus et al., 2002). Magnetic material becomes functionally non-magnetic above a temperature known as the Curie temperature (Wasilewski and Mayhew, 1992), and through forward modelling either in spatial domain (e.g. Purucker et al., 2002; Fox-Maule et al., 2009; Hojat et al., 2016) or in the frequency domain (e.g. Bouligand et al., 2009; Li et al., 2017; Martos et al., 2017) can solve for the depth of this isotherm. Both methodologies suffer from differing assumptions and limitations: the spatial domain method must make assumptions on magnetic susceptibility distributions across continental and oceanic regions, and the fractal process is constrained by other limitations such as selection of window size which has a direct result of maximum resolvable Curie depth and often fixed fractal scaling factors. Additionally, the depth to the bottom of magnetisation is not always associated with the Curie isotherm, and instead be associated with lithological boundaries such as the Moho as mantle rocks are commonly assumed to have low susceptibility (Wasilewski and Mayhew, 1992), and also the magnetic signature may be significantly influenced by

lateral variations in magnetic susceptibility (Hemant, 2003; Hemant and Maus, 2005).

CHAPTER

THREE

GLOBAL WHOLE-ROCK GEOCHEMICAL DATABASE COMPILATION

Gard M.[1] and Hasterok D.[12]

[1]School of Physical Sciences,
University of Adelaide, Adelaide, Australia
[2]Mawson Centre for Geoscience (MCG),
University of Adelaide, Adelaide, SA, 5005, Australia

Published in *Earth System Science Data* https://doi.org/10.5194/essd-11-1553-2019

Statement of Authorship

Title of Paper	Global whole-rock geochemical database compilation
Publication Status	☑ Published ☐ Accepted for Publication ☐ Submitted for Publication ☐ Unpublished and Unsubmitted w ork w ritten in manuscript style
Publication Details	Gard, M., Hasterok, D., Halpin, J. A., 2019. Global whole-rock geochemical database compilation. Earth System Science Data, v. 11 pp. 1553-1566. doi: 10.5194/essd-11-1553-2019.

Principal Author

Name of Principal Author (Candidate)	Matthew Gard		
Contribution to the Paper	Conception of ideas Collated data Programming, visualisation, and database structure Manuscript writing		
Overall percentage (%)	60		
Certification:	This paper reports on original research I conducted during the period of my Higher Degree by Research candidature and is not subject to any obligations or contractual agreements with a third party that would constrain its inclusion in this thesis. I am the primary author of this paper.		
Signature		Date	02/06/2021

Co-Author Contributions

By signing the Statement of Authorship, each author certifies that:

i. the candidate's stated contribution to the publication is accurate (as detailed above);

ii. permission is granted for the candidate in include the publication in the thesis; and

iii. the sum of all co-author contributions is equal to 100% less the candidate's stated contribution.

Name of Co-Author	Derrick Hasterok		
Contribution to the Paper	Conception of ideas Collated data Assistance with programming and visualisation Manuscript editing and feedback		
Signature		Date	5/5/21

Name of Co-Author	Jacqueline A. Halpin		
Contribution to the Paper	Collated data (Antarctic data set) Manuscript editing and feedback		
Signature		Date	6/12/20

Please cut and paste additional co-author panels here as required.

Abstract

Collation and dissemination of geochemical data are critical to promote rapid, creative and accurate research and place new results in an appropriate global context. To this end, we have compiled a global whole-rock geochemical database, sourced from various existing databases and supplemented with an extensive list of individual publications. Currently the database stands at 1,022,092 samples with varying amounts of associated sample data including major and trace element concentrations, isotopic ratios, and location information. Spatial and temporal distribution is heterogeneous, however temporal distributions are enhanced over some previous database compilations, particularly in ages older than ~1000 Ma. Also included are a range of geochemical indices, various naming schema and physical property estimates computed on a major element normalized version of the geochemical data for quick reference. This compilation will be useful for geochemical studies requiring extensive data sets, in particular those wishing to investigate secular temporal trends. The addition of physical properties, estimated from sample chemistry, represent a unique contribution to otherwise similar geochemical databases. The data are published in .csv format for the purposes of simple distribution, but exists in a structure format acceptable for database management systems (e.g. SQL). One can either manipulate this data using conventional analysis tools such as MATLAB®, Microsoft® Excel, or R, or upload to a relational database management system for easy querying and management of the data as unique keys already exist. The data set will continue to grow and be improved, and we encourage readers to contact us or other database compilations within about any data that is yet to be included. The data files described in this paper are available at https://doi.org/10.5281/zenodo.2592822 (Gard et al., 2019a).

3.1 Introduction

Geochemical analyses in conjunction with other temporal, spatial, and physical property information have been vital sources of information for understanding the Earth and investigating both local, and global geodynamic histories (e.g. Keller and Schoene, 2018). Effective collection, collation and dissemination of this type of data is critical to promote rapid, creative and accurate research. Every year, the amount of data recorded globally increases, dispersed among many hundreds of individual publications. Since the 1960's and 70's, broad element suites have been promptly accumulated due to the commercial availability of methods such as x-ray fluorescence (XRF) and inductively coupled plasma mass spectrometry (ICP-MS), and thus modern publications are swiftly expanding our cumulative global data records. However, due to the rate of new publications, in conjunction with significant partitioning between different journals, this data is not always easy to find and can be incredibly time consuming to collate. It is pertinent that this information be readily available for future studies as all benefit from taking advantage of the full suite of data available to produce more robust models and constrained analyses.

Geochemical compilations have been used in a range of studies such as examining crustal magma reservoirs (e.g. Carbotte et al., 2013), proposing changes in mantle dynamics (e.g. Iwamori and Nakamura, 2015), to look at regional and global tectonic histories (e.g. Keller and Schoene, 2018), and examine the connections between life and the solid Earth (e.g. Cox et al., 2018). Not only does this information have implications for the scientific community, but also for issues such as environmental management, land use, and mineral resources development.

In this paper we present a global whole-rock geochemical database compilation consisting of modified whole-rock subsets from existing database compilations, in conjunction with significant supplementation from individual publications not yet included in these other collections. Additionally, we have generated naming schema, various geochemical indices, and other physical property estimates including density, seismic velocity and heat production for a range of the data contained within.

3.2 Existing Initiatives

Many existing initiatives have worked to construct and maintain database compilations with great success, but often restrict themselves to certain tectonic environments or regimes, regions, or rock types. EarthChem (https://www.earthchem.org) is currently the most notable general use geochemical data repository. It consists of many federated databases such as NAVDAT, PetDB, GEOROC, SedDB, MetPetDB and the USGS National Geochemical Database, as well as other individually submitted publications. The constituent databases are mostly more specialized compilations, for example the following:

- The North American Volcanic and Intrusive Rock Database (NAVDAT) has existed since 2002 and is primarily aimed at geochemical and isotopic data from Mesozoic and younger igneous samples of western North America (Walker et al., 2006). (http://www.navdat.org/)
- The Petrological Database of the Ocean Floor (PetDB) is the premier geochemical compilation suite for the igneous and metamorphic hosted data from mid-ocean ridges, back-arc basins, sea-mounts, oceanic crust and ophiolites (https://www.earthchem.org/petdb).
- Geochemistry of Rocks of the Oceans and Continents (GEOROC) is a more holistic compilation effort of chemical, isotope, and other data for igneous samples, including whole-rock, glass, minerals and inclusion analyses and metadata (http://georoc.mpch-mainz.gwdg.de).
- SedDB focuses on sedimentary samples, primarily from marine sediment cores. It has been static since 2014, and includes information such as major and trace element concentrations, isotopic ratios, and organic and inorganic components. (http://www.earthchem.org/seddb).
- MetPetDB is a database for metamorphic petrology, in a similar vein to PetDB and SedDB. This database also hosts large swathes of images collected through various methods such as x-ray maps and pho-

tomicrographs, although this information is not utilized in this paper (http://metpetdb.com/).

- The USGS National Geochemical Database archives geochemical information and its associated metadata from USGS studies and made available online (https://www.usgs.gov/energy-and-minerals/mineral-resources-program/science/national-geochemical-database).

Many other government initiatives and national databases exist, with notable examples including PETROCH from the Ontario Geological Survey (Haus and Pauk, 2010), New Zealand's national rock database (Petlab) (Strong et al., 2016), Australia's national whole-rock geochemical database (OZCHEM) (Champion et al., 2007), the Finnish lithogeochemical rock geochemistry database (RGDB) (Rasilainen et al., 2007), the Newfoundland and Labrador Geoscience Atlas (Newfoundland and Labrador Geological Survey, 2010), and the basement rock geochemical database of Japanese islands (DODAI) (Haraguchi et al., 2018).

While all of these are generally exceptional enterprises, we personally found that the variety of structures were cumbersome to reconcile or otherwise deficient in some respect for our own research. Some examples included databases being deficient in aged data (>1000 Ma), or lacking many recent publications. Some issues in certain existing databases were also evident; we found many samples missing information available in the original individual publications. It was quite common for age resolutions to be significantly larger than the values quoted within the paper itself, of the order of hundreds of millions of years in some cases, or not included at all because they were not found in a table but within the text itself.

Thus, we sought to produce a database incorporating refined samples from previous databases, and supplementing significantly from other, often recent, publications. Computed properties, naming schemes, and various geochemical indices have also been calculated where the data permits. Smaller subsets of previous iterations of this database have already been utilized for studies of heat production and phosphorus content (Hasterok and Webb, 2017; Hasterok et al., 2018; Cox et al., 2018; Gard et al., 2019c; Hasterok et al., 2019b), and this publication represents the totality of geo-

chemical information gathered. As an ongoing process we have corrected some errors or omissions from previous databases as we have come across them, but have not undergone a systematic effort to quality check the prior compilations. We intend to continue updating the database both in additional entries and in further clean up when necessary.

3.3 Database aggregation and structure

While other database structures are incredibly efficient, some of the intricacies of the systems make it difficult to utilize the information contained within. For example, we had issues when seeking estimated or measured ages of rock samples. In order to examine temporal variations of chemistry and physical properties, an accurate and precise age is required. Under some of the present data management schemes it may be difficult to recover the desired data. Crystallization ages for older samples are often determined by U-Pb or Pb-Pb measurements from a suite of zircons. For a given sample, the individual zircon dates may be contained within the database, and stored under mineral analyses. However, a search for rock chemistry may only return an estimated age (often a geologic timescale division). To get the crystallization age one would have to also download the individual mineral analyses, conduct an analysis on a concordia diagram (or similar), determine whether each individual analysis was valid, and then associate the result with the bulk chemistry. This process can be tedious and may be intractable. Had the estimated crystallization age been attributed to the sample directly as often reported in the original study, much of this process could be shortened. Instead, our database attributes these estimated crystallization ages directly to the whole rock sample entry, which allows us to include estimated ages for the same unit or formation more readily. As a result the database presented here allows for a higher density of temporal sampling than other compilations.

The database is provided in two formats; the first as a compressed single spreadsheet for people unfamiliar with database management systems, and the second as a mixed flat file and relational database structure. Codd (1970) was the first to propose a relational model for database management. A relational structure organizes data into multiple tables, with

a unique key identifying each row of the sub-tables. These unique keys are used to link to other sub-tables. The main advantages of a relational database over a flat file format are that data is uniquely stored just once, eliminating data duplication, as well as performance increases due to greater memory efficiency and easy filtering and rapid queries.

Rather than utilize an entirely relational database format, we have adopted some flat file formats for the sub tables as to reduce the number of total tables to an amount more manageable for someone unfamiliar with SQL database structure. This format raises storage memory due to data duplication in certain fields (e.g. repetition of certain string contents across multiple samples, such as rock name). However, we believe this is a reasonable trade off for an easier to utilize structure for distribution, and makes using this data for someone unfamiliar with SQL simpler. Ideally we would host a purely relational database structure online and be accessed via queries similar to the EarthChem Portal, but this is yet to be done.

PostgreSQL was utilized as the relational database management system (RDBMS) to update and administer the database. PostgreSQL contains many built in features and useful addons including the geospatial database extender PostGIS which we utilize, has a large open source community and runs on all major operating systems.

Python in conjunction with a PostgreSQL database adapter Psycopg are used to import new data efficiently. Data is copied into a .csv template directly from publications to reduce any chance of transcribing errors, and dynamically uploaded to a temporary table in PostgreSQL. From here, the desired columns are automatically partitioned up and added to the database in their respective sub-tables. We iterate through a folder of new publications in this way, and are able to add data rapidly as a result.

The database consists of 10 tables: trace elements, major elements, isotope ratios, sample information, rock group/origin/facies triplets, age information, reference information, methods, country, and computed properties. The inter-connectivity of these tables is depicted in Figure 3.1, with tables linked via their respective id keys. A description of each of these tables is included in Table 3.1, and column names that require further details

as well as computed property methods are detailed in Table 3.3. Individual sub-tables have been output as csv files for use. We suggest inserting these into a RDBMS for efficient queries and extraction of desired data. However, we have exported these in csv format in case people not familiar with database systems wish to work with them in other programs such as Microsoft®Excel, MATLAB® or R. While technically inefficient, the largest sub-table currently stands at only 280 MB uncompressed, which we believe to be an acceptable size for data manipulation. The compressed merged spreadsheet is only 130 MB.

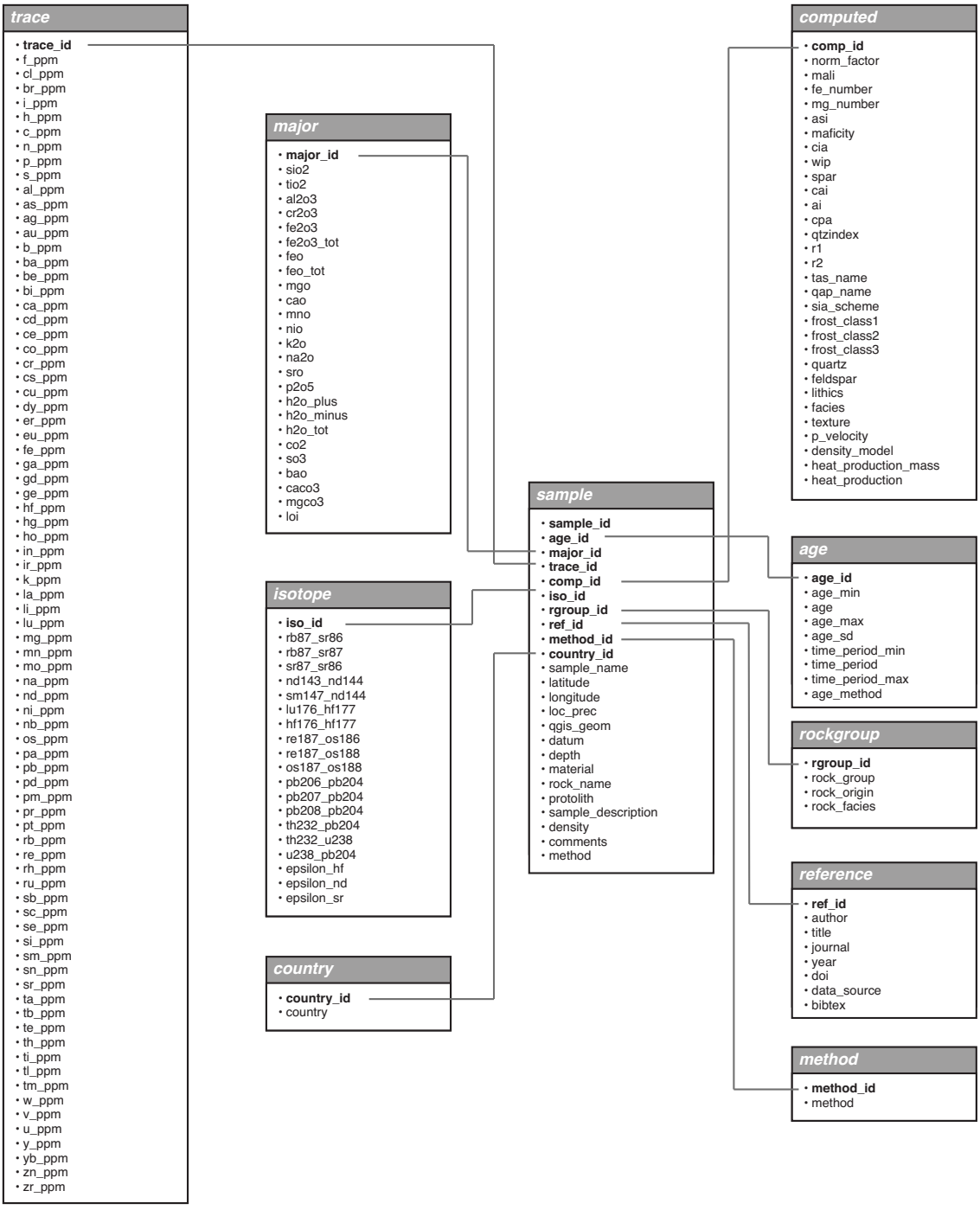

Figure 3.1: Database relational structure. Sub-tables are linked through foreign id keys. Ambiguous field names are described in detail in the supplemental material.

Many samples include multiple geochemical analyses. These can vary from separate trace and major measurements with no overlap, to duplicate element analyses using different methods. In the case of some subsets of this data we have chosen to merge these multiple analyses into a singular entry in the database. This methodology has both benefits and drawbacks. While it reduces the difficulty in selecting individual samples analyses, it means that lower resolution geochemical methods are sometimes averaged with higher precision ones. In the future we hope to prioritise these higher precision methods where applicable (e.g. ICP-MS for many trace elements over XRF). Using a singular entry is simpler for many interdisciplinary scientists who don't wish to be slowed down by the complexity of managing duplicate samples and split analyses. We have generally kept track of this with the method field; where merging has occurred and both methods are known, we have concatenated the method in most cases.

3.4 Data statistics

3.4.1 Raw data

The largest existing database contributions to this database are listed in Table 3.2. Individual publication supplementation includes both new additions we have found in the literature, as well as cleaned up and modified entries from existing databases. The subsets of existing databases do not represent the entire collections for many of these programs as we have done pre-filtering to remove non-whole rock data or encountered issues with accessing the entire data set using online web forms.

Figure 3.2 denotes histograms of the various major, trace and isotope analyses within the database. The majority of isotope data was recently sourced from the GEOROC database. Unsurprisingly, major element analyses in general dwarf the number of trace element measurements recorded.

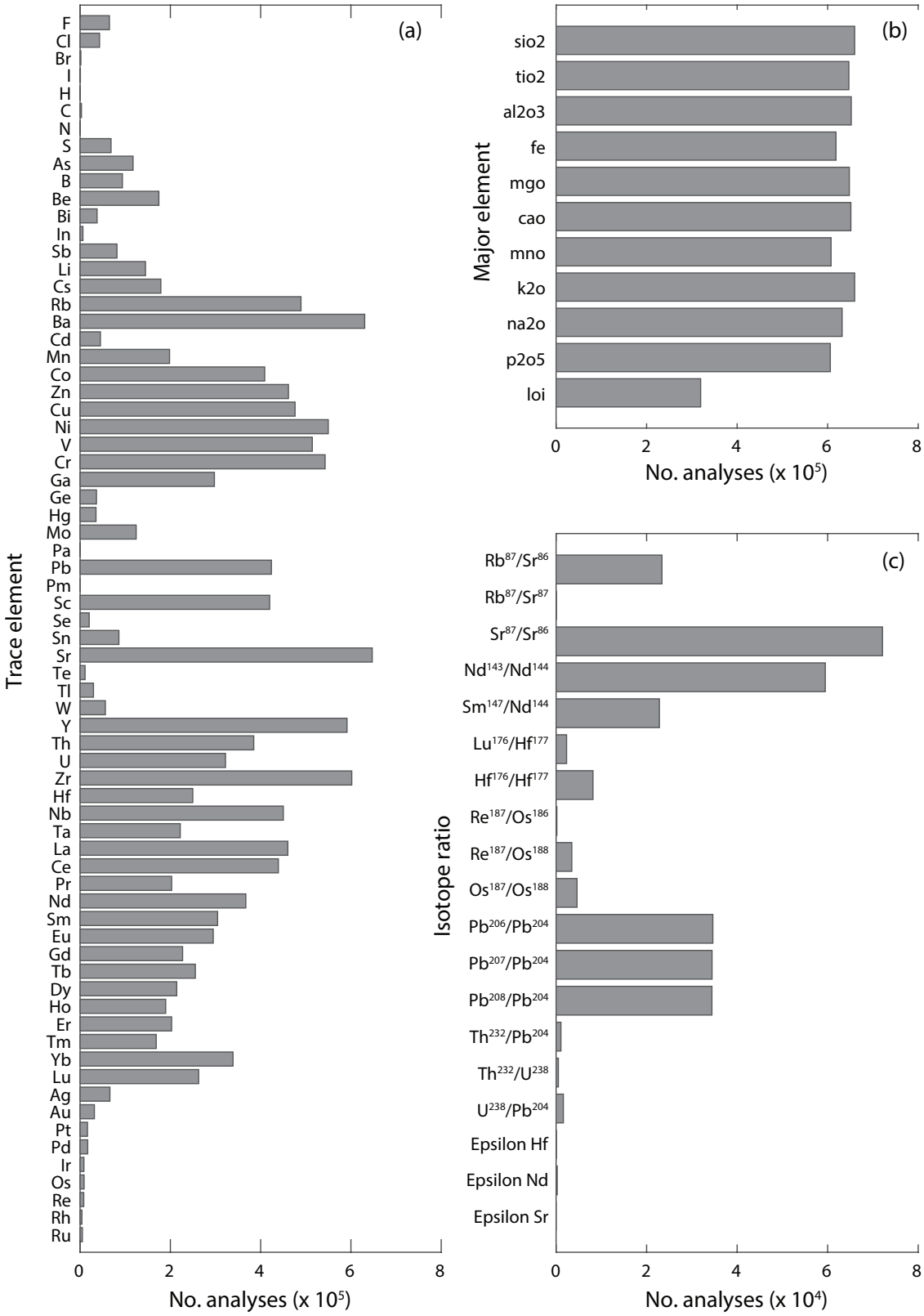

Figure 3.2: Histogram of analyses. a) Trace elements b) Major oxides. Fe denotes any one or more entries for feo, feo total, fe2o3, or fe2o3 total. c) Isotope ratios and episilon values

Despite the heterogeneous nature of geochemical sampling, there is still reasonable spatial coverage around the world. However, there are a noticeable dominance of samples sourced from North America, and additionally Canada, Australia, and New Zealand (Figure 3.3). The United States tops of the list with 352,761 samples, including those from their non-contiguous states. The African continent suffers the most from lack of data with regards to the rest of the globe (Figure 3.3).

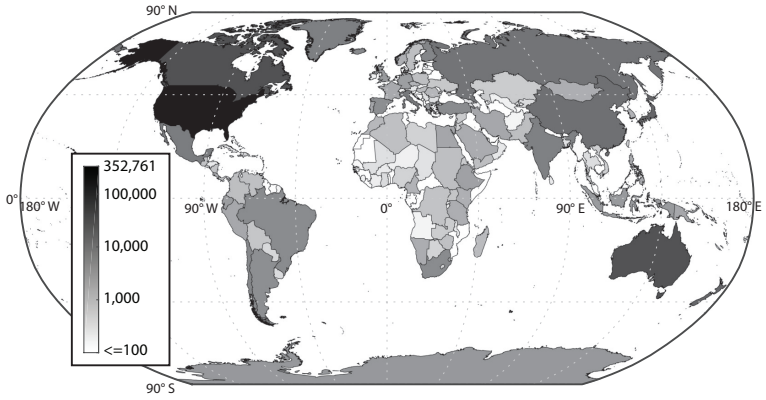

Figure 3.3: Spatial distribution of geochemical samples. Countries are shaded based on the amount of data points within the polygons.

Age distributions unsurprisingly show a significant dominance towards very recent samples (<50 Ma), due largely to the oceanic subset (Figure 3.4b). Age here is indicated as being an assumed crystallization age. Excluding major time-period associated ages (e.g. Paleoproterozoic age range of 2,500–1,600 Ma as the max and min age of a sample), there are 355,467 samples with estimated crystallisation age values. Of these, 282,147 have age uncertainty estimates and observing the cumulative distribution function of these values indicates that ~ 99% of the age uncertainties fall below ~150 Ma (Figure 3.4a).

Rock group and rock origin are described in Table 3.3. There is a clear dominance towards igneous samples, making up 72.37% of the data with known rock group information (Figure 3.5). About 99% of these igneous samples have a distinction noted as volcanic or plutonic in the rock origin field, with just over two thirds of these being volcanic. Sedimentary samples are the next most common rock group, however the vast majority of these have no classification in rock origin, and we aim to improve this

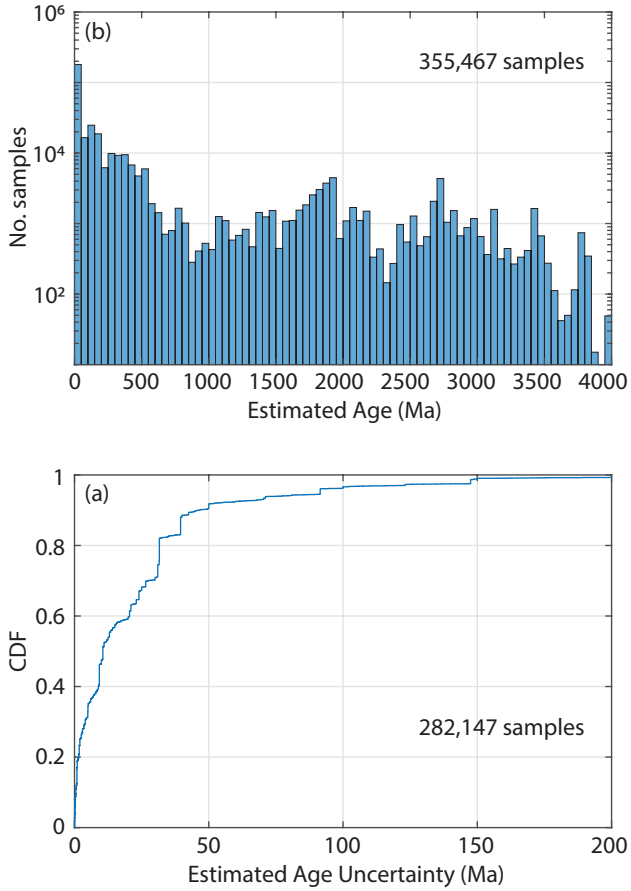

Figure 3.4: Temporal distribution of geochemical samples. a) Histogram of mean ages in 50 Ma intervals b) Empirical cumulative distribution function of age uncertainty (major time-period associated ages removed)

in future updates. Finally metamorphic rocks have ~ 44% of the samples with rock origin classifications. Meta-sedimentary origin is slightly more common than meta-igneous, however meta-igneous includes two further subdivisions of meta-volcanic and meta-plutonic where known.

3.4.2 Naming schema - rock_type

Nomenclature varies significantly within geology and unsurprisingly rock names within the database differ wildly as a result. Different properties such as texture, mineralogical assemblages, grain sizes, thermodynamic histories, and chemistry make up the majority of the basis for the various naming conventions utilized throughout, interspersed with author assumptions and/or inaccuracies. Thus, we sought a robust and consistent

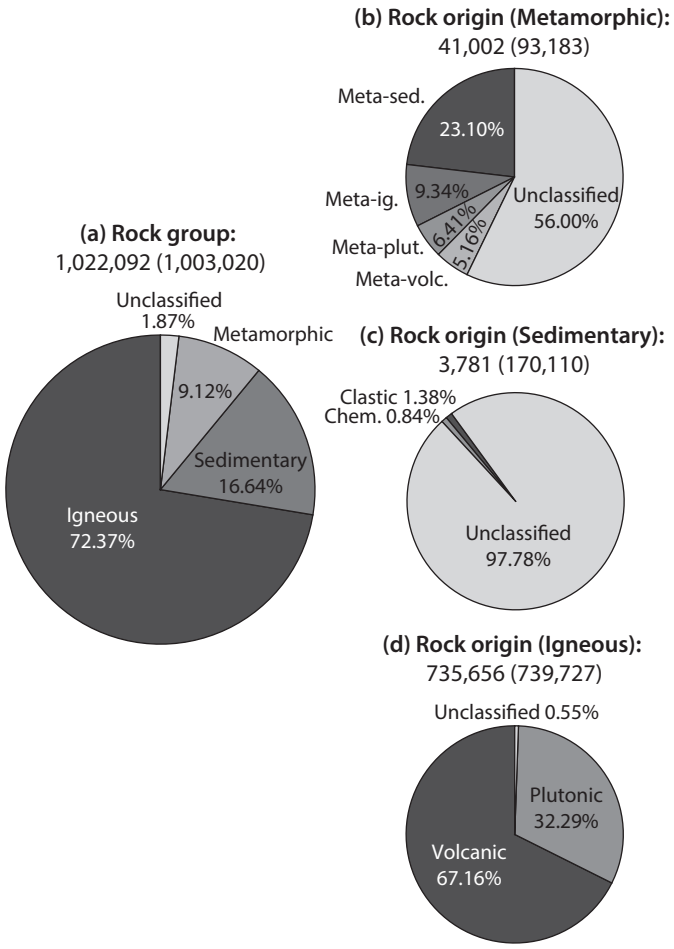

Figure 3.5: Rock group partitioning. a) Pie chart depicting distribution of samples containing a rock group, b) c) and d) denote the rock origin distributions of the rock group fields where rock origin is listed.

chemical classification scheme to assign rock names to the various samples of the database. This chemical basis classification scheme is stored in the computed table, within the rock_type field.

Differing naming work flows are applied to (meta-)igneous, and (meta-)sedimentary samples. For igneous, meta-igneous, and unknown protolith origin metamorphic samples, we use a total alkali-silica (TAS) schema (Middlemost, 1994) modified to include additional fields for further classification of high-Mg volcanics (Le Bas and Streckeisen, 1991). See Figure 3.6c and d for a partial visual description of the process. Furthermore we classify igneous rocks as carbonatites when the CO2 concentration exceeds 20 wt. %. These entries are assigned either the plutonic or volcanic

equivalent rock names depending if the sample is known to be of plutonic or volcanic origin.

For sedimentary and meta-sedimentary rocks, we first separate out carbonates and soils using ternary plot divisions of SiO_2, $Al_2O_3 + Fe_2O_3$, and $CaO + MgO$ (Mason, 1952; Turekian, 1969). Additionally, we further partition clastic sediments using the SedClass™classification method from Herron (1988). Quartzites are identified separately where SiO_2 exceeds 0.9 in the ternary system. See Hasterok et al. (2018) for further discussion.

A break down of the classification distributions are included in Figure 3.6a and b. Sub-alkalic basalt/gabbro is a significantly large contribution to the volcanic samples, due to the extent of samples of oceanic nature.

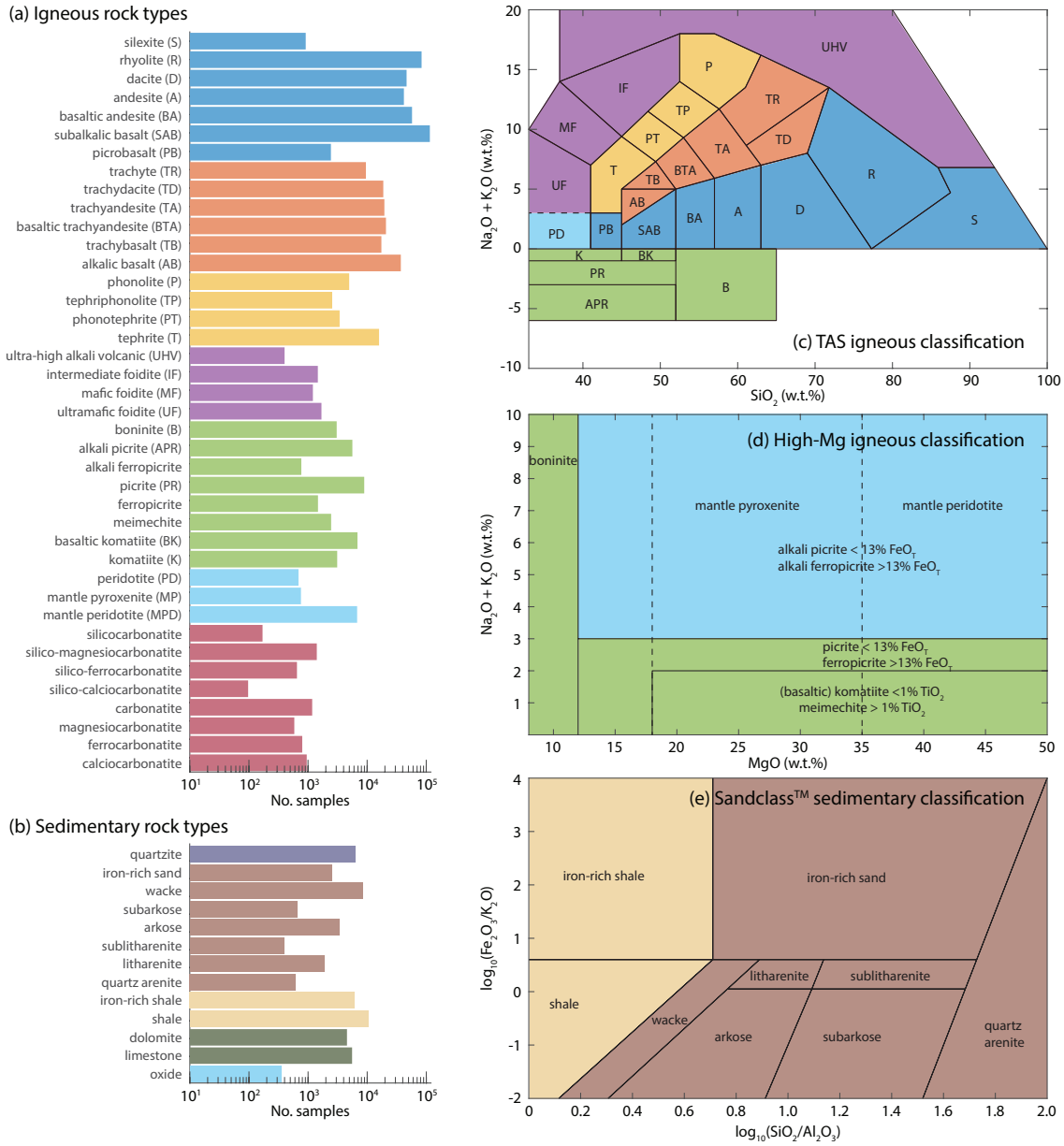

Figure 3.6: Rock type classification information. a) Igneous and metaigneous sample histograms of assigned rock names b) Sedimentary and metasedimentary sample histograms of assigned rock names c) TAS igneous classification (Middlemost, 1994) d) High-Mg igneous classification. See Le Bas and Streckeisen (1991) for further information on classification methods. e) Sedimentary classification, after Herron (1988) (Sandclass™)

3.4.3 Computed properties

In numerical models, rock types are often assigned physical property estimates that have been derived from limited data sets. We compute a number of properties and naming schema for a significant subset of the database, a new addition over many previous database compilations. This includes heat production, density and p-wave velocity estimates, as well as various geochemical indices and descriptors such as modified TAS, QAPF and SIA classifications. A full list of referenced methods and computed columns are given in Table 3.3.

Where computed values require major element concentrations, these properties and values have been calculated based on an LOI free major element normalised version of the database i.e. major element totals are normalised to 100, while preserving the relative proportions of each individual elements contribution to the total. This normalisation occurs only on samples with major element totals between 85 and 120 wt. %. Totals lying outside this range are ignored, and properties requiring these values are not computed. The exact value of normalisation for each sample is recorded in the computed table, within the norm_factor field. Figure 3.7a, b and c denote some property estimates calculated from the normalised analyses.

Density estimates

Density is an important input for a wide range of models but only a small fraction of samples have measured density values associated with them. Contained within the database are a number of publications hosting density observations (e.g. Haus and Pauk, 2010; Barette et al., 2017; Slagstad, 2008). Following the method of Hasterok et al. (2018), we produce a set of simple oxide-based linear regression density models.

$$\rho_{\text{Low-Mg}} = 2506.22 + 204.82 \times \text{Fe} + 791.72 \times \text{Maficity} - 4.56 \times \text{MALI}$$
$$\rho_{\text{High-Mg}} = 3159.18 - 10.40 \times \text{MgO} + 1.36 \times \text{CaO},$$
$$\rho_{\text{Carb.}} = 3268.04 - 6.23 \times \text{SiO}_2 - 6.37 \times \text{CaO} - 2.88 \times \text{MgO}$$

where Fe* is iron number, MALI is modified alkali-lime index, oxides are in weight percent and ρ is density in kg m^{-3}. Misfits for the above are 97, 149, and 147 kg m^{-3} respectively. Low-Mg, High-Mg and Carb. (carbonated rocks) refer to the specific models for different rock groups. See Hasterok et al. (2018) for further discussion of the model fits. Density estimates peak at ~2680 and ~2946 kg m^{-3} due to mafic and felsic sample medians respectively

Seismic velocity

We utilize the empirical model of Behn and Kelemen (2003) for estimating anhydrous p-wave seismic velocity. Their model was calibrated on ~ 18,000 igneous rocks and validated against 139 high quality laboratory measurements. However this model does have limitations, as it was calibrated to anhydrous compositions only. utilizing their 3 oxide model, estimated uncertainty (1σ) is ~ ±0.13 km s^{-1}. P-wave velocity estimates depict maximums at ~6.2 and ~7.1 m s^{-1} (Figure 3.7c). For further details or discussion, refer to Behn and Kelemen (2003) and Hasterok and Webb (2017).

$$Vp = 6.9 - 0.011 \times \mathrm{SiO_2} + 0.037 \times \mathrm{MgO} + 0.045 \times \mathrm{CaO},$$

where oxides are in weight percent and Vp is in m s^{-1}.

Heat production

Heat production is computed by employing the relationship from Rybach (1988). Heat production estimates are resolved by a smoother distribution in log-space than the dichotomous nature of the density and Vp estimates.

$$A(\mu W m^{-3}) = \rho \times \left(9.67 \times \mathrm{U} + 2.56 \times \mathrm{Th} + 2.89 \times \mathrm{K_2O}\right) \times 10^{-5},$$

with concentrations of U, Th in ppm, K_2O in weight-percent and ρ in kg m^{-3}. Heat production has a median value of ~ 1.0 μW m^{-3}, with first and third quartiles (25th and 75th percentiles) of 0.39 and 2.2 μW m^{-3} respectively.

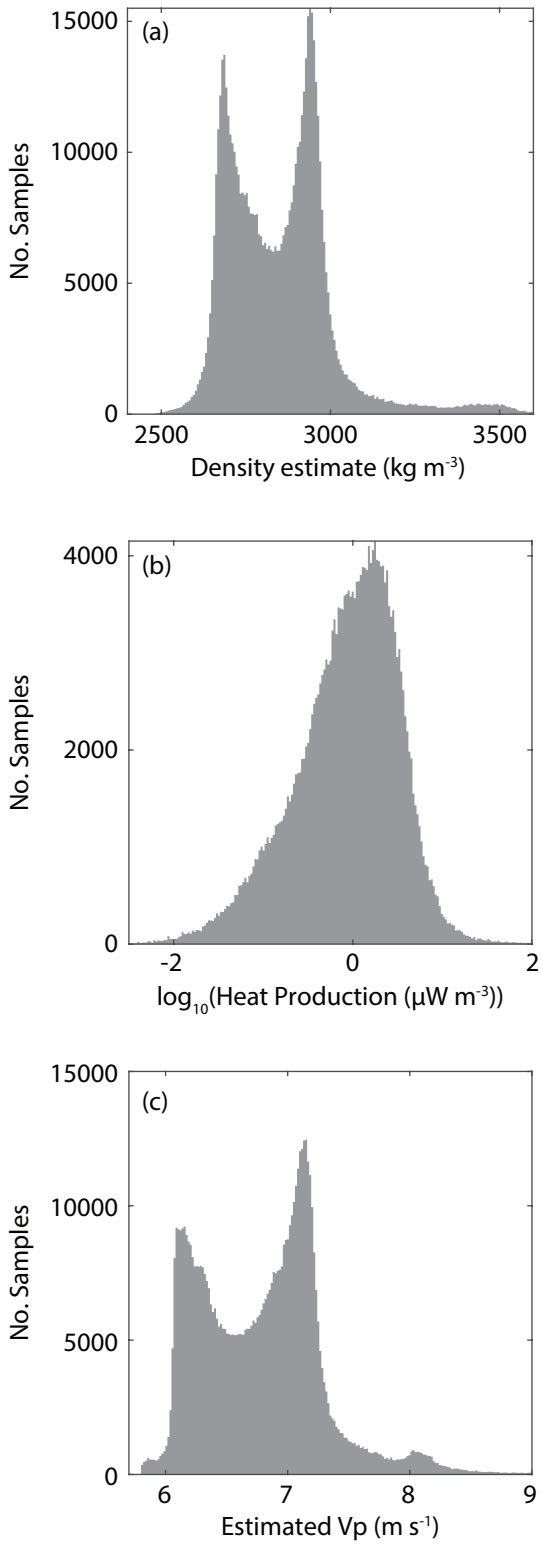

Figure 3.7: Example computed physical property estimate distributions. a) Density b) Heat Production c) P-wave velocity

3.5 Improvements and future developments

Bibliographic information

Due to a high variety of sources and database formats, merging bibliographic information proved difficult. For individual publications and adjustments made manually, we have collated bibliographic information in higher detail. We hope to expand this .bib file as we continue to clean up the reference lists and make adjustments to other compilations. For other inherited bibliographic information from external databases, the exact format can vary. These details are contained within the reference .csv and linked to each sample through the ref_id as seen in Figure 3.1.

Ownership and accuracy

Although every effort is made to ensure accuracy, there are undoubtedly some errors, either inherited or introduced. We make no claims to the accuracy of database entries or reference information. It is up to the user to validate subsets for their own analyses, and ideally contact the original authors, previous database compilation sources, or ourselves to correct errors where they exist. We make no claim on ownership of this data; when utilizing this database additionally cite the original authors and data sources.

Future Work

We have published portions of the database in the course of prior studies and will continue to expand this data set for our own research purposes. Small individual corrections have occurred incrementally with every version, and unfortunately we did not keep records of these improvements. Going forward, we plan to include a record of these corrections and forward them to the other database compilations as needed. We hope to work with existing compilation authors in the future to assist with new additions as well. This version of the database may be of use for these database initiatives to supplement their own records.

Utilizing this database we have worked on methods for predicting protoliths of metamorphic rocks (Hasterok et al., 2019a). As over 57% of the samples lack that information (Figure 3.5) this methodology may be included in future database versions. We are also making progress on a geologic provinces map that captures tectonic terranes.

3.6 Data availability

The .bib file and .csv tables of this data set are available on Zenodo: https://doi.org/10.5281/zenodo.2592822 (Gard et al., 2019a). An associated set of software that can be used in MATLAB® to explore the database, including many of the individual methods cited above for the computed properties is also available on github at https://github.com/dhasterok/global_geochemistry.

Acknowledgements

We thank Bärbel Sarbas for supplying the GEOROC database in its entirety. We would also like to thank the following individuals for providing data sets and/or personal compilations: David Champion (GA) Dick Claeson (SGU), Trond Slagstad (NGU), Lorella Francalanci (UNIFI), Yuri Martynov (FEGI-RAS), Takeshi Hanyu (JAMSTEC), John Clemens (SUN), Harald Furness (UIB), Alex Burton-Johnson (BAS) and Marlina Elburg (UJ). Peter Johnson provided a collection of papers with data for the Arabian-Nubian Shield. M. Gard is supported by Australian Government Research Training Program Scholarship. This research was supported partially by the Australian Government through the Australian Research Council's Discovery Projects funding scheme (project DP180104074), and the Australian Research Council's Special Research Initiative for Antarctic Gateway Partnership SR140300001. The views expressed herein are those of the authors and are not necessarily those of the Australian Government or Australian Research Council.

Table 3.1: Brief table content information

Table name	Table description
sample	Lists all samples, where sample_id uniquely describes each row. Contains all foreign keys linking to the other tables. Other information such as coordinates, measured density and depth of sample, analysis method, as well as author prescribed sample descriptions, comments and rock names are also included.
major	Unique major analyses, linked via the key major_id to sample list. Includes major element oxides as well as volatile, carbonate and LOI content where available.
trace	Unique trace element analyses analyses, linked via the key trace_id to sample list.
isotope	Unique isotopic ratio analyses, including epsilon values for Hf, Nd and Sr. Linked via the key iso_id to sample list.
computed	List of physical properties including heat production and density estimates, and classifications and indices based on schemes such as TAS (Total alkali-Silica) and ASI (aluminum-saturation index). Theses values are computed on a major element normalised (LOI free) version of the associated sample's trace and major compositions and may not match the raw values listed. We preserve the raw data in the database, and methods for normalisation and computed properties are included in the appendices if one wishes to recompute these computed properties and indices with different parameters. comp_id uniquely describes each row and is linked to the sample table.
reference	Includes information on the author of the original paper the data was sourced from, and/or reference to database or other previous compilation the data was sourced from e.g. EarthChem. ref_id links the reference table to the sample table.
rockgroup	Uniquely links triplets of rock group, rock origin and rock facies to sample table. For definitions of rock group, origin and facies see Table 3.3.
age	Uniquely links sets of age and time period information to sample table
country	Unique list of countries (ISO 3166 ALPHA-2 codes) as well as ocean
method	Lists unique method strings detailed in previous publications or databases

Table 3.2: Data sources

Data source	No. data
EarthChem family (excluding GEOROC) (https://www.earthchem.org/)	380,532
GEOROC (http://georoc.mpch-mainz.gwdg.de)	349,037
OZCHEM (Champion et al., 2007)	65,391
Petlab (Strong et al., 2016)	35,499
Petroch (Haus and Pauk, 2010)	27,388
Newfoundland and Labrador Geoscience Atlas (Newfoundland and Labrador Geological Survey, 2010)	10,073
The British Columbia Rock Geochemical Database (Lett and Ronning, 2005)	8,990
Canadian Database of Geochemical Surveys Open File Reports	8,766
DODAI (Haraguchi et al., 2018)	6,588
Finnish Geochemical Database (Rasilainen et al., 2007)	6,543
Ujarassiorit Mineral Hunt (Geological Survey of Greenland, 2011)	6,078
The Central Andes Geochemical GPS Database (Mamani et al., 2010)	1,970
Geochemical database of the Virunga Volcanic Province (Barette et al., 2017)	908
Other sources (~1,900 sources, misc. files, see reference csv and bib file)	123,095
Total	1,022,092

Table 3.3: Potentially ambiguous column information

Column name	Description
sample_name	Author denoted title for the sample. Often non-unique e.g. numbered.
loc_prec	Location precision
qgis_geom	PostGIS ST_Geometry object based on the latitude and longitude of the sample.
material	Material/source of the sample e.g. Auger sample, core, drill chips, xenolith, vein
rock_name	Rock name designated by the original author
sample_description	Sample description mostly inherited from previous databases. Highly variable field.
density	Measured density
comments	Misc. comments, often additional information not included in the sample description field.
method	Method utilized to analyse chemistry and/or age. Variable due to inheritance from previous databases. Multiple methods may be listed, separated by semicolons.
norm_factor	Major element normalisation factor applied to the samples major element chemistry before computing properties
MALI	Modified alkali–lime index (Frost et al., 2001)
fe_number	Iron number (Frost et al., 2001)
mg_number	Magnesium number. Fe2+ estimated using 0.85 × FeO^T.
asi	Alumina Saturation Index (Frost et al., 2001)
maficity	$n_{Fe} + n_{Mg} + n_{Ti}$
cia	Chemical index of alteration (Nesbitt and Young, 1989). Generally CaO* includes an additional correction for CO_2 in silicates, but CO_2 is not reported for a large fraction of the data set so we do not include this term for consistency.
wip	Weathering Index of Parker (Parker, 1970)
spar	Modified from (Debon and Le Fort, 1983) to remove apatite
cai	Calcic-alkalic index (Frost et al., 2001)
ai	Alkalic index (Frost et al., 2001)
cpa	Chemical proxy of alteration (Buggle et al., 2011)

qtzindex	Quartz Index (Debon and Le Fort, 1983)
r1	R1R2 chemical variation diagram (la Roche et al., 1980)
r2	R1R2 chemical variation diagram (la Roche et al., 1980)
rock_type	Compositionally based rock names, discussed in Section 3.4.2, following similar methods of Hasterok et al. (2018)
sia_scheme	S-, I-, and A-type granite classification. For felsic compositions, A- and I-types are not properly discriminated with this method. (Frost et al., 2001)
frost_class1	Magnesian or Ferroan (Frost et al., 2001)
frost_class2	Calcic, calc-alkalic, alkali-calcic, alkalic(Frost et al., 2001)
frost_class3	Metaluminous, peraluminous, peralkaline (Frost et al., 2001)
quartz	Estimate of quartz content from major element analyses. SiO_2/M_{SiO_2} where M_X is the molecular weight of the oxide X (Mason, 1952; Turekian, 1969)
feldspar	Estimate of feldspar/clay/Fe-Al oxide content from major element analyses. $Al_2O_3/M_{Al_2O_3} + Fe_2O_3(t)/M_{Fe_2O_3}$ where M_X is the molecular weight of the oxide X (Mason, 1952; Turekian, 1969)
lithics	Estimate of lithics (carbonate) content from major element analyses. $MgO/M_{MgO} + CaO/M_{CaO}$ where M_X is the molecular weight of the oxide X (Mason, 1952; Turekian, 1969)
facies	Metamorphic facies information pulled from rock_name via partial string search
texture	Metamorphic texture information pulled from rock_name via partial string search
p_velocity	To estimate seismic velocity we use an empirical model developed by Behn and Kelemen (2003), and utilized in Hasterok and Webb (2017). We use the compositional model $V_p(km/s) = 6.9 - 0.011C_{SiO_2} + 0.037C_{MgO} + 0.045C_{CaO}$ where the concentration of each oxide is in wt.%.

density_model	We utilize the multiple density estimate methods as outlined by Hasterok et al. (2018) for each compositional group, using multiple linear regression on the data set
heat_production_mass	Determined from the chemical composition with the relationship $HP_{mass} = 10^{-5}(9.67C_U + 2.56C_{Th} + 2.89K_2O)$ where C are the concentrations of the HPEs in ppm except K_2O in wt.% (Rybach, 1988)
heat_production	Heat production mass multiplied by the density estimate (in kg m^{-3}) (Rybach, 1988)
age_ or time_period_ min	Minimum crystallisation age estimate
age or time_period	Mean crystallisation age estimate
age_ or time_period_ max	Maximum crystallisation age estimate
age_sd	Age uncertainty
age_method	Method of age estimation, variable due to inheritance from previous databases
rock_group	The highest order rock type classifications: Igneous/metamorphic/sedimentary
rock_origin	Second order classifications of the rock groups - e.g. plutonic/volcanic, metaplutonic/metaigneous/metased, clastic/chemical
rock_facies	Third order classifications, mostly restricted to metamorphic rock facies e.g. granulite
data_source	Field reserved for existing database compilation e.g. if a sample is derived from EarthChem
bibtex	Bibtex key corresponding to further reference information if it exists, contained in the attached bib file for easier citation

CHAPTER

FOUR

VARIATIONS IN CONTINENTAL HEAT PRODUCTION FROM 4 GA TO THE PRESENT

Gard M.[1], Hasterok D.[12], Hand M.[12] and Cox G.[1]

[1]School of Physical Sciences,
University of Adelaide, Adelaide, Australia
[2]Centre for Tectonics Research and Exploration (TRaX),
University of Adelaide, Adelaide, Australia

Published in *Lithos* https://doi.org/10.1016/j.lithos.2019.05.034

Statement of Authorship

Title of Paper	Variations in continental heat production from 4 Ga to the present: Evidence from geochemical data
Publication Status	☑ Published ☐ Accepted for Publication ☐ Submitted for Publication ☐ Unpublished and Unsubmitted w ork w ritten in manuscript style
Publication Details	Gard, M., Hasterok, D., Hand, M., Cox, G., 2019. Variations in continental heat production from 4 Ga to the present: Evidence from geochemical data. Lithos, v.342-343, pp. 391-406. doi: 10.1016/j.lithos.2019.05.034

Principal Author

Name of Principal Author (Candidate)	Matthew Gard		
Contribution to the Paper	Conception of ideas Collated data Programming, visualisation, and modelling Data interpretation Manuscript writing		
Overall percentage (%)	75		
Certification:	This paper reports on original research I conducted during the period of my Higher Degree by Research candidature and is not subject to any obligations or contractual agreements with a third party that would constrain its inclusion in this thesis. I am the primary author of this paper.		
Signature		Date	03/06/2021

Co-Author Contributions

By signing the Statement of Authorship, each author certifies that:

i. the candidate's stated contribution to the publication is accurate (as detailed above);

ii. permission is granted for the candidate in include the publication in the thesis; and

iii. the sum of all co-author contributions is equal to 100% less the candidate's stated contribution.

Name of Co-Author	Derrick Hasterok		
Contribution to the Paper	Conception of ideas Collated data Assistance with programming and modelling Supervised and aided data interpretation Manuscript editing and feedback		
Signature		Date	5/5/21

Name of Co-Author	Martin Hand		
Contribution to the Paper	Assistance with conception of ideas and contribution of knowledge Feedback on modelling		
Signature		Date	25/05/2021

Name of Co-Author	Grant Cox		
Contribution to the Paper	Assistance with conception of ideas and contribution of knowledge Feedback on modelling		
Signature		Date	9/12/2020

Abstract

Crustal heat production accounts for 30 to 40% of continental heat loss and enhances thermally controlled processes such as melting and metamorphism, yet is in general poorly constrained. We present a new model for continental igneous heat production from ~4 Ga to the present using a global geochemical database of 75,800 whole-rock analyses providing the highest resolution record to date. Hypotheses advanced to explain past heat production–age variations include erosion of the enriched felsic upper crust, decay of the radioactive elements, geodynamic processes such as the supercontinent cycle, secular cooling, lithological controls, and/or a major shift in the bulk composition in the crust during the late Archean. However, previous heat production–age models are often coarsely resolved, poorly sampled, and/or spatially biased. To test these hypotheses and refine secular trends in crustal heat production, we construct a model by correcting for radioactive decay and normalizing by SiO_2 content to remove the gross influence of lithology. The variations through time are highly correlated among both plutonic and volcanic samples, as well as mafic and felsic distributions. Unsurprisingly, compositional normalization indicates lithological control is the dominant factor on heat production after the influence of decay is removed. Following these adjustments, we find heat production has been relatively constant from ~2.8 Ga to the present, with an increase from ~3.4 Ga to ~2.8 Ga. We suggest the heat production–age pattern does not significantly reflect the influences of erosion, secular cooling, depletion, or the supercontinent cycle as suggested by some previous studies. Heat producing element distributions might be expected to be similar regardless of the age of melt generation, once compositionally normalised and adjusted for the decay of the various isotopes. Compared to this reference model, we observe a heat production and heat producing element enrichment deficit, particularly for the Archean and Paleoproterozoic. This deficit is accounted for by a rapid increase in heat producing element concentrations associated with a shift in the bulk composition of the crust from the early Archean to ~2.7 Ga. Additionally, we suggest that the heat production record may also represent a biased sample set, perhaps as a result of selective preservation due to thermal stability. This

new model will lead to better crustal heat production and global heat loss estimates both at present and within Earth's past.

4.1 Introduction

Processes contributing to continental crust generation are suggested to have changed significantly throughout Earth's history (Belousova et al., 2010; Hawkesworth et al., 2016; Campbell, 2003). Fundamental changes such as the shift from vertical to horizontal tectonics and the supercontinent cycle are largely driven by the thermal evolution of the mantle (Condie et al., 2016). Factors such as the decay of radioactive isotopes through time, and depletion of the upper mantle in heat producing elements (HPEs) due to crustal formation have drastically changed the energy partitioning of heat between the crust and mantle through time. However, the temporal variations in heat production in the crust and mantle are poorly constrained.

Nearly 99% of radiogenic heat production is due to the decay of ^{40}K, ^{235}U, ^{238}U and ^{232}Th (Rybach, 1988; Wasserburg et al., 1964). Within the continental crust, heat production typically accounts for 30 to 40% of the heat loss (Pollack and Chapman, 1977b; Artemieva and Mooney, 2001), but could in some cases account for 75% or more (Hasterok and Gard, 2016). As such, the distribution of HPEs affects the geotherm and influences thermally-controlled processes such as melting and metamorphism, as well as physical properties such as density, seismic velocity and viscosity (Sandiford and McLaren, 2006; Kelsey and Hand, 2015; McKenzie and Priestley, 2016). Heat production variations have the largest influence on heat loss in regions that are near thermal equilibrium (Cooper et al., 2004). Since stable regions account for nearly 85% of the continental crust by area (Gordon, 1998), understanding temporal variations in crustal heat production is important.

Past models for temporal variations in global HP are based on observations of heat production and/or surface heat flow (Vitorello and Pollack, 1980; Jaupart and Mareschal, 2014; Jaupart et al., 2016; Artemieva et al., 2017). These models are typically low in temporal resolution and/or contain ge-

ographic and lithological bias, generally a result of low sample numbers. A few studies address regional variations of heat production with time, though these models are limited to the types and timing of magmatism of the area, making it difficult to draw direct inferences about globally extensive trends (Kukkonen and Lahtinen, 2001; Slagstad, 2008).

Despite variations in interpretations, nearly all models agree that present-day crustal heat production is systematically lower in Archean terranes relative to modern ones. Several hypotheses have been advanced to account for the variations through time, and can be explained broadly in two categories;

1. the rock record preserves a representative distribution of the heat production of the crust, with the variations in response to physical or geodynamic processes operating at the time, and/or
2. the rock record is biased or modified to preserve only selected samples.

We consider the following hypotheses from the literature in this manuscript:

1. decay of the radioactive elements through time leads to a first order monotonic decrease in heat production with increasing age (Jaupart and Mareschal, 2014; Jaupart et al., 2016);
2. lithological variations are the primary control on heat production, and may mask any temporal signals attributed to other secular or cyclical Earth processes (Kukkonen and Lahtinen, 2001; Slagstad, 2008);
3. heat producing element enrichment increased at the Archean-Proterozoic boundary, associated with a significant episodic shift towards more felsic compositions in the crust (McLennan et al., 1980);
4. heat production through time exhibits a non-monotonic trend with an approximate first order correlation with plate velocity, the supercontinent cycle and/or geodynamic setting (Artemieva et al., 2017);
5. erosion of an enriched radioactive upper crust leads to a decrease in heat production in older terranes as deeper, less enriched crust is exhumed (Vitorello and Pollack, 1980); and

6. selective preservation due to thermal stability has shifted older terranes to lower heat production distributions (Morgan, 1985).

In this study, we have estimated the heat production from an expanded compilation of igneous rock geochemistry with associated crystallization ages and heat production estimates. We evaluate the contributions of the aforementioned hypotheses to the temporal heat production record. By improving our understanding of the temporal variations in heat production, it will be possible to develop more accurate estimates of heat production and heat loss with few direct measurements. Furthermore, the understanding of heat production variations through time yields important constraints on the physical and chemical processes operating over the past 4 Ga.

4.2 Review of Previous Models

4.2.1 Radioactive Decay

The radioactive isotope abundance in a rock at present-day does not equate to its abundance at formation. Heat production is the result of the decay of the unstable radioactive isotopes, whereby a fraction of the original mass is converted to energy. Jaupart and Mareschal (2014) showed such a systematic decrease in average heat production with increasing age, albeit in conjunction with large scatter on account of lithology variations. By fitting an average composition decay curve to the heat production trend, Jaupart and Mareschal (2014) proposed that there is little difference in the heat production distribution for any age interval at formation (Figure 4.1b). This model suggests the average heat production of newly formed crust is initially the same throughout geologic time, which implies the thermal conditions for crustal stabilization have remained largely unchanged since the Archean. In contrast, some regional studies do not necessarily observe such a defined trend (e.g. Kukkonen and Lahtinen, 2001; Slagstad, 2008), likely due to unique tectonic histories and varying lithologies.

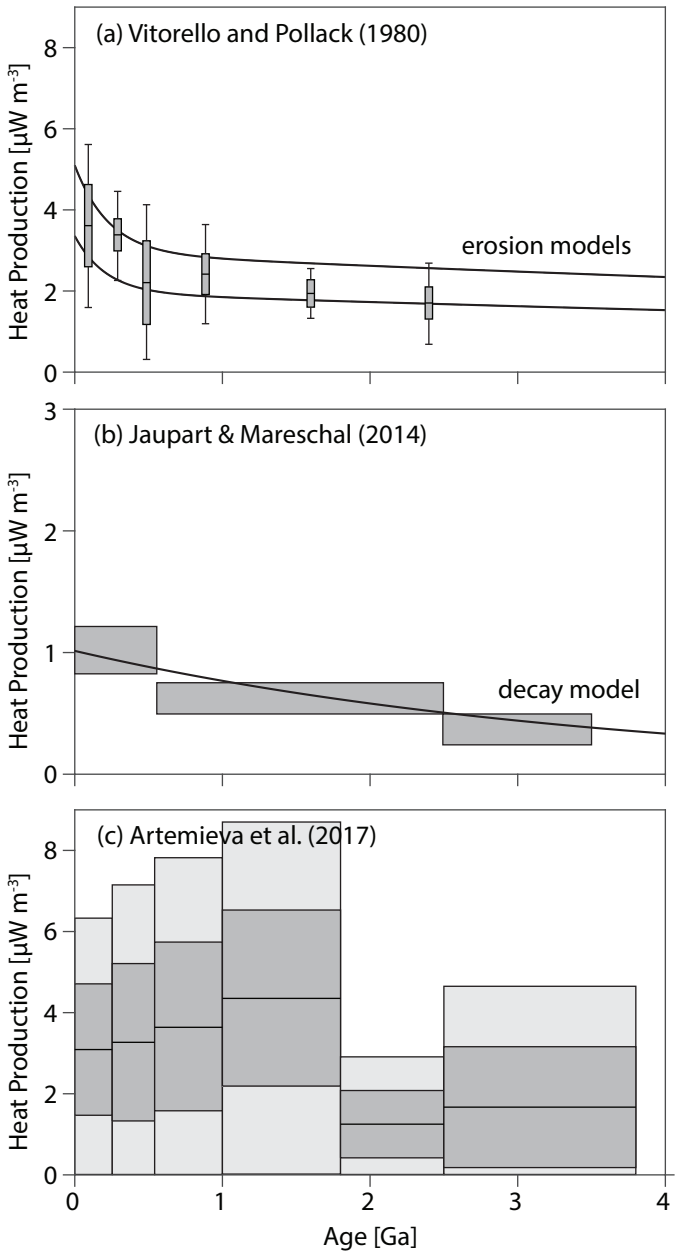

Figure 4.1: Previous models of heat production with age: (a) erosional model by Vitorello and Pollack (1980); (b) radioactive decay model by Jaupart and Mareschal (2014); (c) granite heat production model by Artemieva et al. (2017).

4.2.2 Lithological controls

It is well documented that a rough first-order correlation exists between heat production and relative silica enrichment (Wollenberg and Smith, 1987; Kukkonen and Lahtinen, 2001; Hasterok and Webb, 2017). Felsic rocks are typically more enriched in heat producing elements; with

enrichment generally decreasing with increasing maficity. For instance, median heat production declines from granite (3.54 μW m^{-3}), to diorite (1.20 μW m^{-3}), to gabbro (0.46 μW m^{-3}) (Hasterok and Webb, 2017). However, this trend is weak as natural variability is high (standard deviations of 0.74, 0.74 and 1.23 $\log_{10}$-units for granite, diorite, and gabbro, respectively). This lithological control hinders identification of any other temporal heat production signal. Regional studies in Norway and Finland do not produce clear relationships between heat production and age (Kukkonen and Lahtinen, 2001; Slagstad, 2008). Heat production of the Fennoscandian shield, Paleoproterozoic Transscandinavian Igneous Belt, and the Permian Oslo Rift, for example, overlap significantly in median heat production values regardless of age, tectonic environment and lithology. As HPEs are mostly concentrated in trace minerals, vast differences in concentrations between similar rock types can result from different alteration and enrichment histories (Kukkonen and Lahtinen, 2001). While Kukkonen and Lahtinen (2001) found a weak increase in heat production from Archean to Proterozoic-aged metasedimentary samples, both studies ultimately concluded that the lithologic controls on heat production make it difficult to assess temporal variations in heat production on a regional data set.

4.2.3 Shift in the bulk composition of the crust

While not specifically calculating past heat generation, McLennan et al. (1980) did investigate the temporal record for thorium and uranium enrichment for relatively uniform composition sedimentary and metasedimentary samples. They found that Th (and U) enrichment showed a monotonic increase in enrichment within samples at, and leading up to, the Archean-Proterozoic boundary, and then remained relatively constant moving towards the present. It was proposed that these observations were consistent with previous studies; that there was a significant episodic shift in the composition of the exposed crust, associated with an influx of granitic intrusions at the end of the Archean (e.g. Taylor and McLennan, 1985; Condie, 1993; Dhuime et al., 2015; Tang et al., 2016, and references therein). These intrusions would have contained much higher concentrations of Th and U than existing crustal material, and marked a step change in the average

composition of the crust (from mafic to felsic), evidenced by no significant changes in element enrichments from ~2.5 Ga to present.

4.2.4 Geodynamic Controls and Crustal Reworking

Since the difference in median heat production between felsic and mafic rocks is approximately an order of magnitude, shifts in average rock compositions may dominate the temporal record. These variations in composition may potentially reflect periodic or secular changes in dominant geodynamic and crustal reworking processes, e.g. the change from vertical to horizontal tectonics, or correlations to supercontinent formation and breakup. A recent study of heat production analyzed the temporal record of a restricted rock database (granites only); Artemieva et al. (2017).

Artemieva et al. (2017) utilized 445 globally distributed heat production estimates from gamma-ray spectrometry and found a highly variable, rather than monotonically decreasing heat production–age relationship, in contrast to some previous studies on a larger range of compositions (e.g. Vitorello and Pollack, 1980; Jaupart et al., 2016). They suggest a rapid increase, followed by a slow decline in heat production from the Mesoproterozoic to the present is correlated to similar variations in plate velocities, possibly associated with the assembly of the supercontinent Nuna (Figure 4.1c). However, their interpretations are tenuous given the significant spatial biases within their dataset; a point recognized by the authors themselves.

4.2.5 Erosion of Enriched Upper Crust

Early studies of heat flow suggested that surface heat flow and heat production were linearly related, leading to the concept of reduced heat flow (Roy et al., 1968; Birch et al., 1968). Under a reduced heat flow model, the crust is conceptualized as a high upper crustal heat producing layer (intercept) with a characteristic thickness (slope). This model only survives under erosion if heat production exponentially decreases with depth (Lachenbruch, 1970). Surface heat production observations in some obliquely exposed crustal sections, such as the Idaho and Closepet batholiths, appear to

support the exponential model, either as a result of pluton emplacement or through the redistribution from fluid flow (Gosnold, 1987; Kumar and Reddy, 2004).

However, more recent evidence does not support a clear relationship between depth and heat production. In contrast, variations in heat production with depth in deep drill cores and along exposed crustal cross-sections exhibit more complex patterns of heat production with depth, rarely suggestive of an exponential decrease (Hasterok and Chapman, 2011). Even in some obliquely exposed crustal sections such as the Sierra Nevada Batholith, the apparent heat production depth relationship appears somewhat inconsistent with the generalized exponential distribution function (Sawka and Chappell, 1988; Brady et al., 2006). Lateral variations in heat production can alter the slope of the reduced heat flow–heat production relationship, further complicating the connection to depth dependence on heat production (Jaupart, 1983). Furthermore, indiscriminate studies of reduced heat flow lack a trend between heat flow and heat production (Sandiford and McLaren, 2002). More recently, Alessio et al. (2018) also showed that in metasedimentary crust, increasing depth as recorded by increasing metamorphic grade did not result in reduced heat production.

Vitorello and Pollack (1980) had this concept of reduced heat flow and differential erosion in mind when proposing an erosional control on the average heat production through time. They assumed older terranes have generally undergone greater exhumation, and thus exhibit lower heat production at the surface today (Figure 4.1a). Although this concept of reduced heat flow tailored their models, the erosional hypothesis is not necessarily negated by the complications discussed. The original reduced heat flow studies applied this method only to cogenetic plutons (Roy et al., 1968; Birch et al., 1968). Heat production decreases almost exponentially with SiO_2 content, on average, for igneous rocks (Hasterok and Webb, 2017), which could explain why the Idaho and Closepet batholiths are the exceptions that validate the exponentially decreasing heat production with depth and the differential erosion hypothesis. Inconsistencies arise when the dominant lithology in the vertical structure is not co-genetic, for example the metasediments atop the Sierra section, or as a result of their natural variability when considering individual point departures. In

a perfectly co-genetic system, an exponential decrease with depth may be a reasonable model, but these idealised zones are few and far between and variance is high.

Furthermore, there is good observational evidence from holistic studies of continental crust composition that suggests heat production should decrease with depth from upper to lower crust because of a general increase in mafic compositions at depth (Rudnick and Gao, 2003, and references therein). Although recent studies challenge the assumption that mafic proportions general increase with depth (e.g. Hacker et al., 2011, 2015; Williams et al., 2014), heat production must decrease with depth, otherwise surface heat flow would be higher than observed (Taylor and McLennan, 1985).

4.2.6 Selective Preservation due to Thermal Stability

From observations on Precambrian cratons, there is qualitative evidence to suggest that terranes with relatively low radiogenic heat production may be less susceptible to reworking by orogenesis than regions with high heat production (and thus higher geotherm). Such cratons have generally remained relatively stable while surrounding provinces have often undergone rigorous deformation and magmatism (e.g. Clifford, 1970). High heat-producing terranes can be thermally weak as a result of the increased geotherm and susceptible to deformation, particularly when these HPEs are distributed at depth (Hand and Sandiford, 1999; Sandiford et al., 2002).

Morgan (1985) suggested that the early Earth rock record may not be a representative sample of the original heat production distribution, owing largely to these qualitative observations of Precambrian cratons and reduced standard deviations in Archean heat flow globally. Crust with low heat production, and thus lower geotherms, may have a much higher probability of stabilization and survival. Due to relatively high mantle temperatures, and higher average concentrations of heat producing isotopes globally than present-day (due to radioactive decay), average geotherms in the Archean crust were likely of higher temperature and greater variability than geotherms today. However higher mantle temperatures do not automatically imply higher mantle heat flow and vice versa, for instance,

higher temperatures below a thick lithosphere can have lower heat flow than lower temperatures beneath a thin lithosphere. In the Archean, low heat production crust was far more likely to stabilize, according to Morgan (1985), while higher heat production terranes (even values that would be considered normal today) were more likely to be reworked and effectively removed from the record. Morgan (1985) observed an Archean–Proterozoic transition in the heat production record, where Archean samples seemed systematically lower than Proterozoic samples even when considering decay. He proposed that this may have indicated the last remobilisation of the high heat producing Archean crust, and the onset of a mantle thermal regime in which the range in crustal heat production typical of Proterozoic and younger crust would no longer be a major factor in localizing crustal remobilisation.

4.3 Geochemical data set

To examine the heat production–age record, we utilise a large whole-rock geochemical database, comprised of existing databases, and supplemented with geological survey compilations and individual data sets we have collated from the literature. The existing databases utilised include first and foremost EarthChem (https://www.earthchem.org/), which consists of many federated databases such as The Petrological Database of the Ocean Floor (PetDB) (https://www.earthchem.org/petdb), The North American Volcanic and Intrusive Rock Database (NAVDAT) (Walker et al., 2006), the USGS National Geochemical Database (https://mrdata.usgs.gov/ngdb/rock/) and Geochemistry of Rocks of the Oceans and Continents (GEOROC) (http://georoc.mpch-mainz.gwdg.de), as well as individually submitted publications. Additional databases utilised include the Newfoundland and Labrador Geoscience Atlas (Newfoundland and Labrador Geological Survey, 2010), Australia's national whole-rock geochemical database (OZCHEM) (Champion et al., 2007) and the Finnish lithogeochemical rock geochemistry database (RGDB) (Rasilainen et al., 2007). A complete list of references and link to the database are included in the supplementary material. These samples are sourced from a variety of locations and depths including drill cores, xenoliths etc., however

the vast majority are surface samples from outcrop. The full database is available online at Zenodo (1,023,491 samples) (Gard et al., 2019a) (https://zenodo.org/record/2592823), and the subset utilised in this manuscript is provided as supplementary data (75,800 samples).

For our analyses, we chose to focus on igneous and meta-igneous samples only, as these rocks make up the bulk of the continental crust. Furthermore, sedimentary and meta-sedimentary samples are excluded because these rocks generally represent an integration of material from a variety of sources that may have radically different ages, thus convoluting any potential heat production–age variations. SiO_2 is also restricted to between 40 and 85 wt.% and normalized to anhydrous conditions. This restriction only excludes ~1.7% of samples. Extreme silica concentrations outside this range generally represent insignificant fractions of crustal samples, and statistically very little is lost due to their removal.

Rather than relying on highly variable and inconsistent rock naming schemes supplied by the various authors and sources, we chose to classify rock types using a total alkali–silica (TAS) naming scheme, modified from Middlemost (1994), to additionally classify high-Mg volcanics, as recommended by Le Bas and Streckeisen (1991). An advantage of such a scheme is that it is based on major element chemistry and can be used to directly compare plutonic and volcanic rocks of similar compositions.

We chose to only utilize samples with a reported/estimated age with an uncertainty of ≤200 Ma. Dating of rocks can be complicated as the radiometric dates of samples can be influenced by crystallization, metamorphism and/or inheritance. We use crystallization ages associated with the samples as that most likely represent the time at which heat production is set.

After the above filtering, the number of samples available for analysis is 75,800 (Table 4.1). The database represents measurements spanning a significant fraction of the continental area (Figure 4.2a). While some large gaps persist, the sampling is sufficient to characterize many common rock types for most age intervals. The lowest populated age bins are mostly concentrated in the oldest age intervals, with the lowest containing 127 samples (3.8 to 4 Ga), and the largest hosting >34,000 (0 to 0.2 Ga) (Fig-

ure 4.2b, Table 4.1). The majority of age bins hold >500 samples, with 13 of the 20 bins containing 1000 samples or more. This constitutes a respectable increase in sample numbers over past studies.

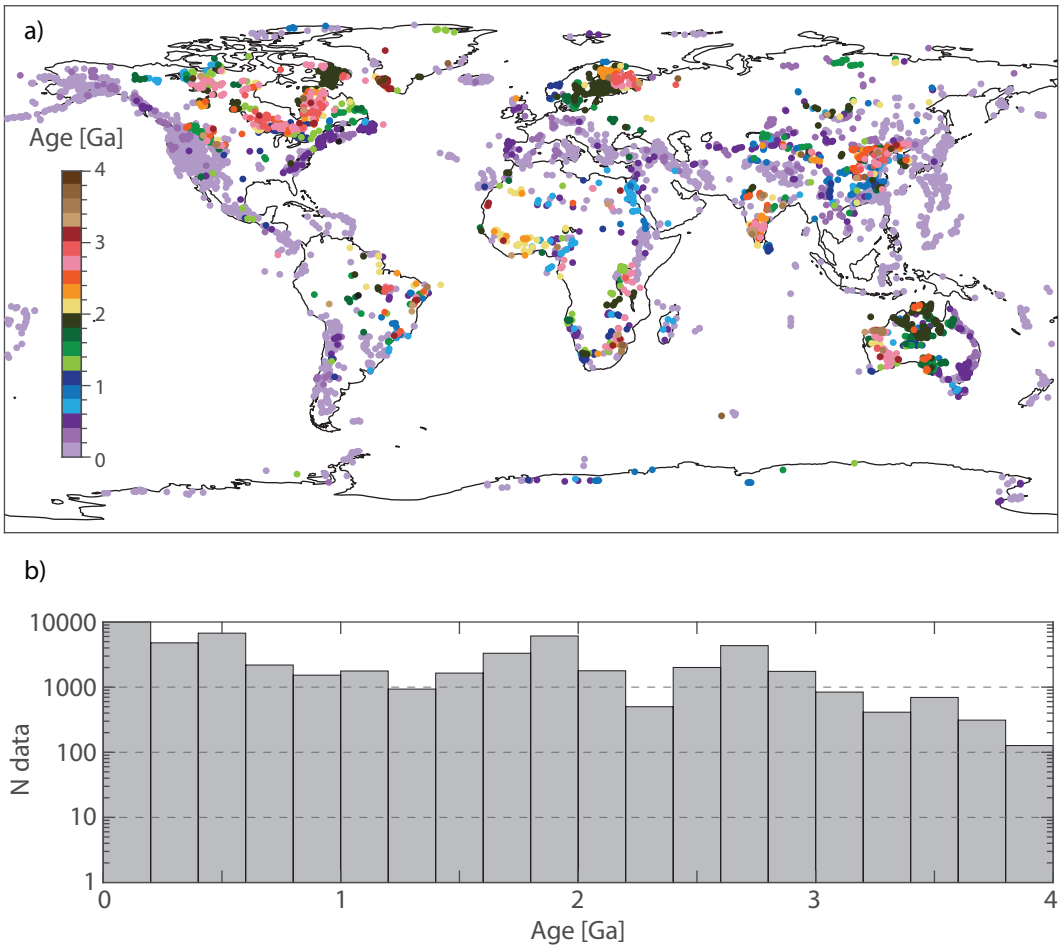

Figure 4.2: (a) Locations of all igneous and metamorphic heat production estimates utilized in this study. Points are coloured by age. (b) Temporal sampling of heat production data.

Our data set significantly expands on the current compilations, particularly for those with associated ages and heat producing element concentrations. As EarthChem is biased towards young and volcanic rocks, the improvement is most apparent among age bins >200 Ma and plutonic samples.

Table 4.1: Age distributions

Age range (Ma)	No. Data
0 – 200	34,034
200 – 400	4,787
400 – 600	6,741
600 – 800	2,187
800 – 1000	1,528
1000 – 1200	1,770
1200 – 1400	934
1400 – 1600	1,644
1600 – 1800	3,314
1800 – 2000	6,099
2000 – 2200	1,783
2200 – 2400	501
2400 – 2600	2,005
2600 – 2800	4,336
2800 – 3000	1,748
3000 – 3200	841
3200 – 3400	413
3400 – 3600	696
3600 – 3800	312
3800 – 4000	127
Total	75,800

4.4 Methods

4.4.1 Estimating Heat Production

Heat production can be estimated from the concentration of HPEs. We use the formulation and coefficients by Rybach (1988),

$$A(\mu\text{W m}^{-3}) = 10^{-5}\rho(9.52[C_{\text{U}}] + 2.56[C_{\text{Th}}] + 2.89[C_{\text{K}_2\text{O}}]), \tag{4.1}$$

where C_{U} and C_{Th} are the concentrations of uranium and thorium in parts per million (ppm) respectively, $C_{\text{K}_2\text{O}}$ is the concentration of K_2O in wt.%, and ρ is the density in kg m^{-3}.

4.4.2 Estimating Density

Since heat production requires density, and few samples within the global database include density measurements, we need a way to estimate density for the geochemical samples. Many studies simply assume densities but lack compositional information to develop more accurate estimates. To estimate density, we use major element compositions following the method of Hasterok et al. (2018). Compositions are first normalized on an anhydrous basis and then density is calculated for silicate-dominated igneous samples using

$$\rho = 2506 + 205\,\text{Fe}^* + 793\,\text{maficity} - 4.5\,\text{MALI}, \tag{4.2}$$

where

$$\begin{aligned} \text{Fe}^* \text{ (iron number)} &= C_{\text{FeO}_\text{T}}(C_{\text{FeO}_\text{T}} + C_{\text{MgO}})^{-1} \\ \text{MALI (modified alkali-lime index)} &= C_{\text{Na}_2\text{O}} + C_{\text{K}_2\text{O}} - C_{\text{CaO}} \\ \text{maficity} &= n_{\text{Fe}} + n_{\text{Mg}} + n_{\text{Ti}}, \end{aligned}$$

and n is the molar fraction (Frost et al., 2001; Clemens et al., 2011). Estimated average uncertainty in density is ±97 kg m^{-3}(1σ), translating to a heat production uncertainty for each sample of (~4%).

This density relationship is calibrated to igneous samples with density estimates (Haus and Pauk, 2010; Bédard et al., 2016; Barette et al., 2017; Slagstad, 2008). We consider these uncertainties acceptable and superior

to assuming a constant density for all samples, as is often the case. This method will likely overpredict densities for any volcanic samples that have porosity, since porosity is not included as a parameter. However, since porosity estimates are not included in the database, it would be impossible to correct for it in this current iteration. For the majority of other samples however, the predicted densities fall very close to typical assumed values e.g. ~2.75 g/cm^3 for granite samples. For further discussion on this density model fit, refer to Hasterok et al. (2018).

4.4.3 Correcting for radioactive decay

Heat production of bulk Earth decreases with time due to the radioactive decay of the heat producing isotopes. If we wish to observe any variations in heat production separate from this long-period decay influence, we must adjust each sample to its estimated heat production at formation.

Samples inherently host lower heat production at present than at the time of formation. We can estimate the heat production at the point of crystallization by applying a decay correction. By utilizing present-day abundances of the isotopes, in conjunction with their measured decay constants, we can recompute each sample's individual isotope concentrations (^{40}K, ^{235}U, ^{238}U and ^{232}Th) at the time of formation, and then recompute the heat production estimate using Equation 4.1.

Radioactive decay follows the following relationship:

$$A_t = A_0 \mathrm{e}^{-\lambda t}, \tag{4.3}$$

where A_t is the concentration of the HPE isotope at some time in the past at time t, A_0 is the HPE isotope concentration at present-day, λ is the decay constant for the HPE isotope, and t is the time to project back to. The decay constant it given by,

$$\lambda = \frac{ln(2)}{t_{1/2}}, \tag{4.4}$$

where λ is the decay constant, and $t_{1/2}$ is the half-life of the isotope.

Table 4.2: Half-life and present-day fractional abundance of heat producing elements

Isotope	Half-life (Ga)	Abundance
^{238}U	4.510	0.9928
^{235}U	0.713	0.00711
^{232}Th	13.90	1
^{40}K	1.230	0.000117

We recompute the ^{40}K, ^{252}Th, ^{238}U and ^{235}U isotopes in this manner for each individual sample. The present-day concentrations of each isotope are estimated from the given concentrations of the elements, multiplied by the average abundances of the isotopes.

This adjustment assumes other influences such as disequilibrium, or post-formation processes have not significantly altered the isotope ratios or concentrations since creation of the samples, at least on average for the bin distributions.

4.5 Temporal analysis

4.5.1 Unprocessed temporal trend

Previous studies, often for local regions, tend to plot different rock types, ages, and tectonic environments together on the same plot and ordered temporally to examine if there are any apparent trends with heat production and age. We have done similar in Figure 4.3 in 200 Ma age bins. Compared with previous models, our temporal sampling is at a much higher resolution. In past heat production–age studies, most authors utilize very coarse age resolutions (Jaupart and Mareschal, 2014; Artemieva et al., 2017), or ordered time-period data (Kukkonen and Lahtinen, 2001; Slagstad, 2008). This higher resolution may increase our ability to determine whether variations are smoothly varying or step changes. While Jaupart and Mareschal (2014) discussed heavily the variability of samples within any age group, such extended age intervals can give the impression either heat production varies simply over coarse temporal resolutions or that there are step changes corresponding to divisions in the geologic timescale instead of gradients (Morgan, 1985). This delineation of step

changes or smooth variations are important to help identify processes which may affect continental evolution. Our results using 200 Ma bins suggest the changes are generally smooth (also suggesting relatively low bias), but that there are variations that are not captured by the coarse resolutions of previous studies (Figure 4.1 and 4.2b). We observe significant variations in the global median heat production over the past 4 Ga. The median heat production varies between a max of ~2.52 in the 1600 to 1800 Ma interval, and minimum of ~0.15 in the 3000–3200 Ma interval.

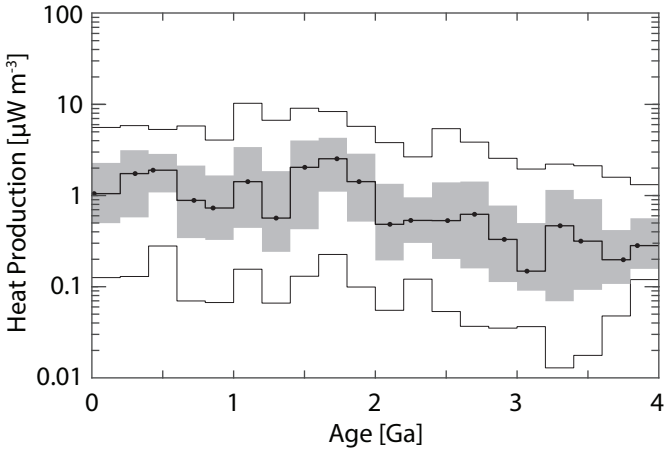

Figure 4.3: Raw, unprocessed heat production distributions presented in log-space. The shaded region depicts data within the 25 to 75 quartiles and the thin lines identifies the 5 and 95% quantiles. The data are divided into age intervals of 200 Ma to maintain a minimum of 100 samples within each division. Dots indicate median age and median heat production for data contained within each interval.

While it can be seen that older samples on average have less heat production (likely due to decay, but not quantified or validated in this figure), not much more information can be drawn from this. Spatial bias, lithology bias, and other influences are likely buried in this trend. In this study we work towards processing this information to decipher as much information as possible from these temporal trends.

4.5.2 Decay correction and silica distributions

Removing the influence of decay is the first step in deciphering heat production variations at formation. Figure 4.4a depicts the decay adjusted temporal trend for heat production based on the method in section 4.4.3.

The oldest Archean data increase ~0.5 log-units in heat production on average (Figure 4.3 vs. Figure 4.4a).

For the purposes of this study, 'felsic' and 'mafic' samples are taken to be greater and less than 60 wt.% SiO_2 respectively. Besides being commonly divided in this way, we also note a minimum in SiO_2 composition histograms at ~60 wt.% (Figure 4.4b), an observation often referred to as the 'Daly gap' (Daly, 1925). After decay adjustment, we observe the heat production at formation to be relatively flat through time at the longest wavelength, albeit with significant shorter temporal variations persisting. Median felsic heat production is 2.53 μW m^{-3}, and median mafic heat production is 0.61 μW m^{-3}. Figure 4.4b and c depict how silica distributions vary for each age bin, and there appears to be a correlation between relative mafic/felsic proportions and the observed heat production medians in the bins. This correlation is expected; there is a propensity for felsic material to be more enriched in heat producing elements than mafic material (Rybach and Buntebarth, 1984; Fountain, 1987; Hasterok and Webb, 2017). The exact magnitudes do not necessarily correlate; for example the lowest median silica bin does not correlate to the lowest heat production age interval, however the step-wise pattern of increasing and decreasing heat production compared to adjacent intervals does appear correlated.

The types of magmatism occurring within the continental crust are generally related to the tectonic processes operating at any given time. Some tectonic settings are more common during particular intervals of Earth's history. For example, mafic dike swarms are common during periods of supercontinent breakup, felsic magmatism is dominant during continent-continent collisions and arc magmatism during intervening periods (e.g. Hawkesworth et al., 2009, and references therein). Periods with varying dominant tectonic environments may perhaps lead to coarse variations in heat production signal, potentially as a product of a mafic/felsic bias in the preserved global rock record, or as varying enrichments of trace elements for similar major element composition samples. Felsic (intermediate) magmas are far more abundant in continental arcs than in island arcs (Lee and Bachmann, 2014), and these environments are more common during intervals of supercontinent amalgamation. Conversely during supercontinent breakup, extensive rift environments and associated mafic dike swarms

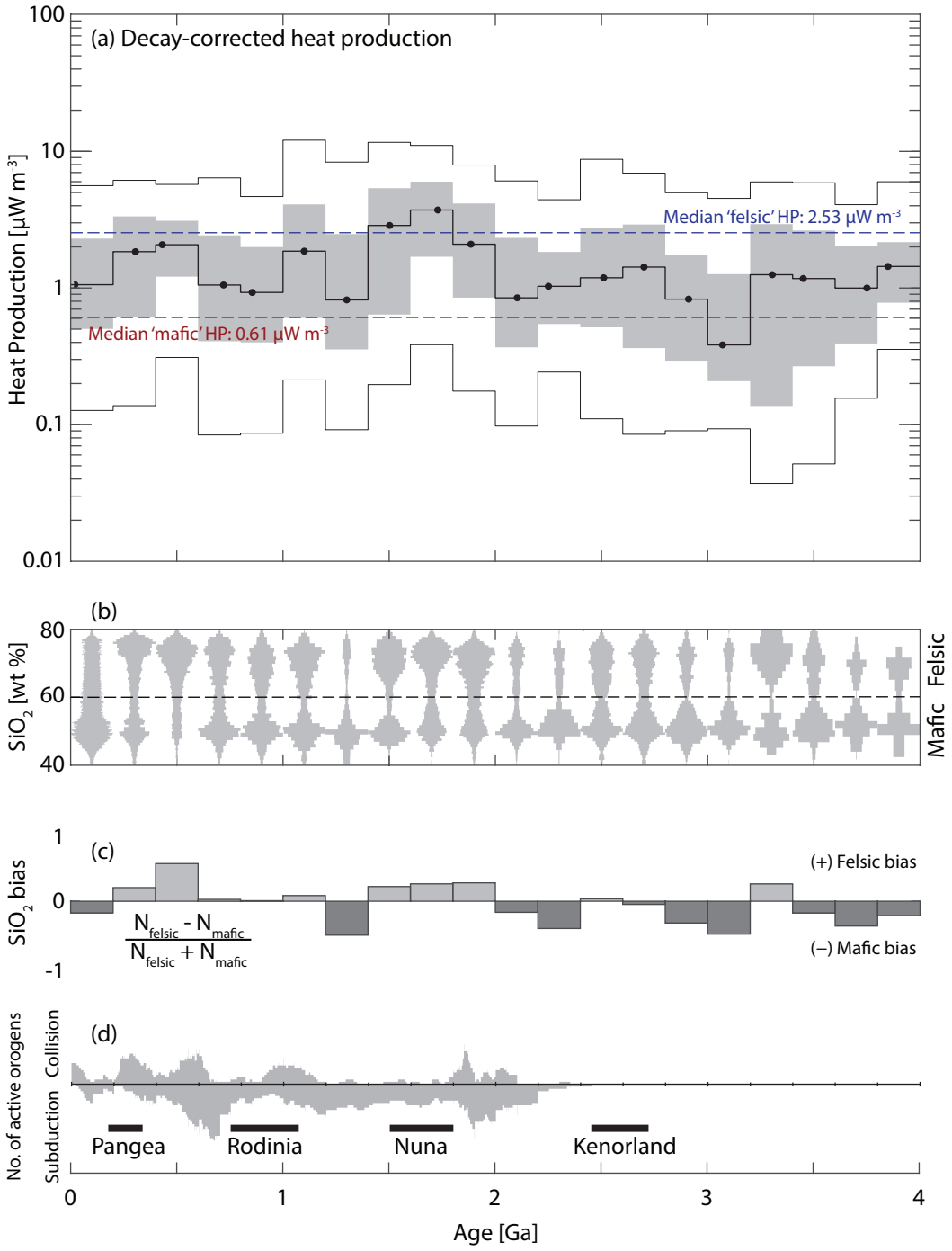

Figure 4.4: Heat production and composition of igneous rocks over the past 4 Ga. (a) Same as Figure 4.3, but the heat production has been adjusted for radioactive decay (Equation 4.3) (b) Variations in SiO_2 composition with age. Each 'Cloud-city' diagram is produced by constructing a histogram with respect to SiO_2 and mirroring it in order t emphasize the peaks and troughs in silica content within each age interval. (c) SiO_2 bias presented in a simple ratio bias plot for easier comparison to (b). (d) Supercontinents and orogenic activity data (Condie and Aster, 2013). The number of active collisional (above the line) and subduction orogens (below the line) active as as a function of time shaded in grey.

become more prevalent in the rock record (e.g. Worsley et al., 1984). Extensive flood basalts, increased mafic magmatic activity and continental dike swarms for example have also been utilised as potential evidence for one or more Late Archean supercontinents (Heaman, 1997; French et al., 2004).

While we do observe heat production variations that appear to correlate with shifts in felsic to mafic dominance (Figure 4.4 a,b and c), there appears to be little to no correlation with the supercontinent cycle and orogenic activity from Condie and Aster (2013). This correlation is not observed in either the heat production–age temporal record, contrary to the suggestions made by Artemieva et al. (2017), or the relative concentrations of felsic/mafic samples (Figure 4.4d). While it is possible such high frequency variations in composition related to orogenic cycles are aliased by the 200 Ma interval size, this issue is even more likely present in previous lower resolution studies (e.g. Artemieva et al., 2017).

The observed trends in the decay adjusted plot are still subject to significant sampling (lithologic) and spatial biases. As discussed previously, for example, incompatible heat producing elements are more likely to be concentrated in felsic lithologies than mafic samples, so merging all samples together will be heavily influenced by relative proportions of these rock types. Known spatial bias from previous literature may also obfuscate the temporal trends e.g. Proterozoic Australian rocks are known to be highly enriched in heat producing elements, which can be observed in the record at least from 1400–1800 Ma. We return to this in Section 4.5.4.

4.5.3 Sampling bias (lithological)

It is clear that lithological variability appears to dominate the temporal trends in heat production after decay adjustment, corroborating previous studies (e.g. Slagstad, 2008; Kukkonen and Lahtinen, 2001). To account for this variability, one may choose to analyse individual rock types separately to significantly reduce the variability due to lithology (e.g. Artemieva et al., 2017). Figure 4.5 presents the temporal trends of decay-corrected heat production for the four most prevalent rock types in our database.

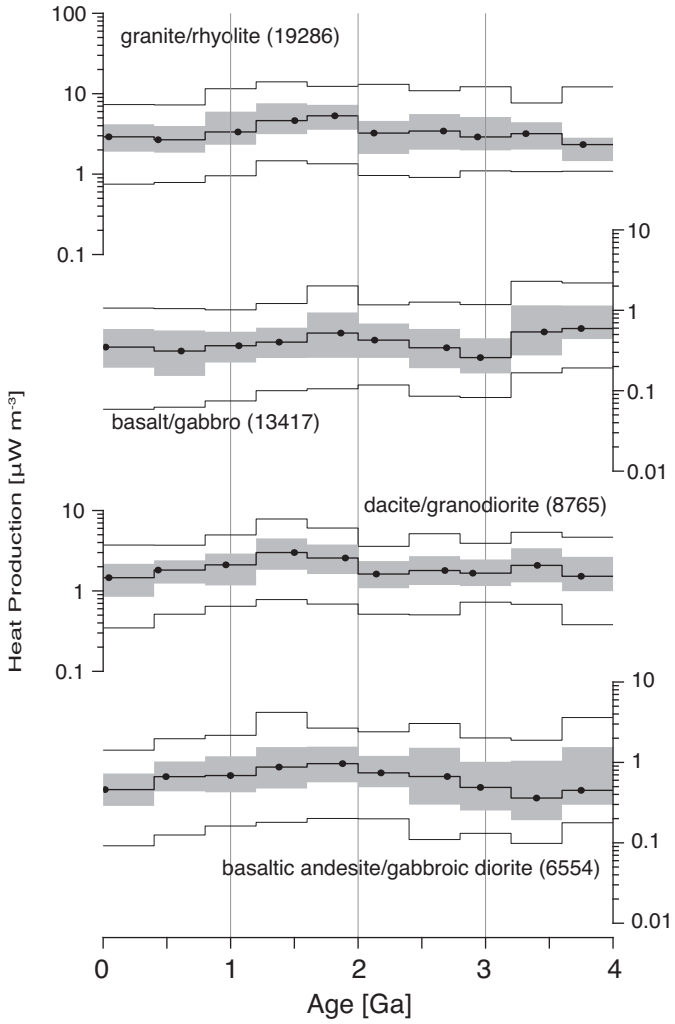

Figure 4.5: Heat production through time for the four most common rock types in the database. The lines and shading indicate the median and same quantiles as described in Figure 4.3.

From 3.2 to 0 Ga, nearly all rock types have similar long period heat production–age variations. From the Archean to Paleoproterozoic, heat production appears (relatively) constant, and there may be a minor step increase in heat production at ~2 Ga to ~1.2 Ga (Figure 4.5), and then decreasing again to a similar median to the rest of the set. One may suggest the timing of this increase is consistent with the formation of the supercontinent Nuna, however this is unclear since there is no apparent correlation to other supercontinent cycles. Other than these gross observations, it is difficult to interpret finer scale variations in these individual rock-type plots due to the many fewer samples in individual age bins (expanded here

to 400 Ma). Archean bins in particular suffer from poor sampling and strong spatial bias when observing any one rock type.

While observing individual rock types may be a reasonably valid method for damping the lithological influence, this restricts the data available analysis and as a result lowers temporal resolution of the data set. It is clear that there may be consistent long period trends across mafic and felsic ranges of rocks, albeit at different magnitudes. We seek a simple adjustment that allows all rocks (or at least the largest percentile rocks) to be compared on an equivalent scale for interpretation. One possible method removes gross lithological variations by adjusting compositions to a common silica content, removing the dominant effect of fractionation.

4.5.3.1 Silica normalization

Correlation between heat production and silica is generally considered weak because of large natural variability (Fountain, 1987; Kukkonen and Lahtinen, 2001; Artemieva et al., 2017). For example, Kukkonen and Lahtinen (2001) applied a linear fit between silica content and heat production and resolved a correlation coefficient (r-value) of 0.44 and 0.69 for plutonic and metavolcanic rocks, respectively. We calculate an r-value between SiO_2 and the log of heat production of 0.62 (r^2 value of 0.38) on this global data set, confirming the suggestion that this is a weak relationship. This weakness is due to the high natural variability within narrow silica bands. Heat production can vary by an order of magnitude or more within any silica interval. Values that sit above the median tend to be more alkali-rich (especially potassium), whereas lower values tend to be alkali-poor (Hasterok and Webb, 2017).

Despite the natural variability, there is a well resolved trend in median heat production and silica content (Figure 4.6a). Calculating the median log heat production in 2 wt.% SiO_2 bins resolves an r^2-value that is much higher than for the individual samples (weighted linear fit - $r^2 = 0.91$), suggesting the two are quite well correlated, on average, but that natural variability is high. There is some non-linear behaviour the tails i.e., for mafic samples with SiO_2 <46 wt.%, as well as highly felsic samples with SiO_2 >78 wt.%. If these tails are ignored, r^2 is as large as 0.96. Thus, for

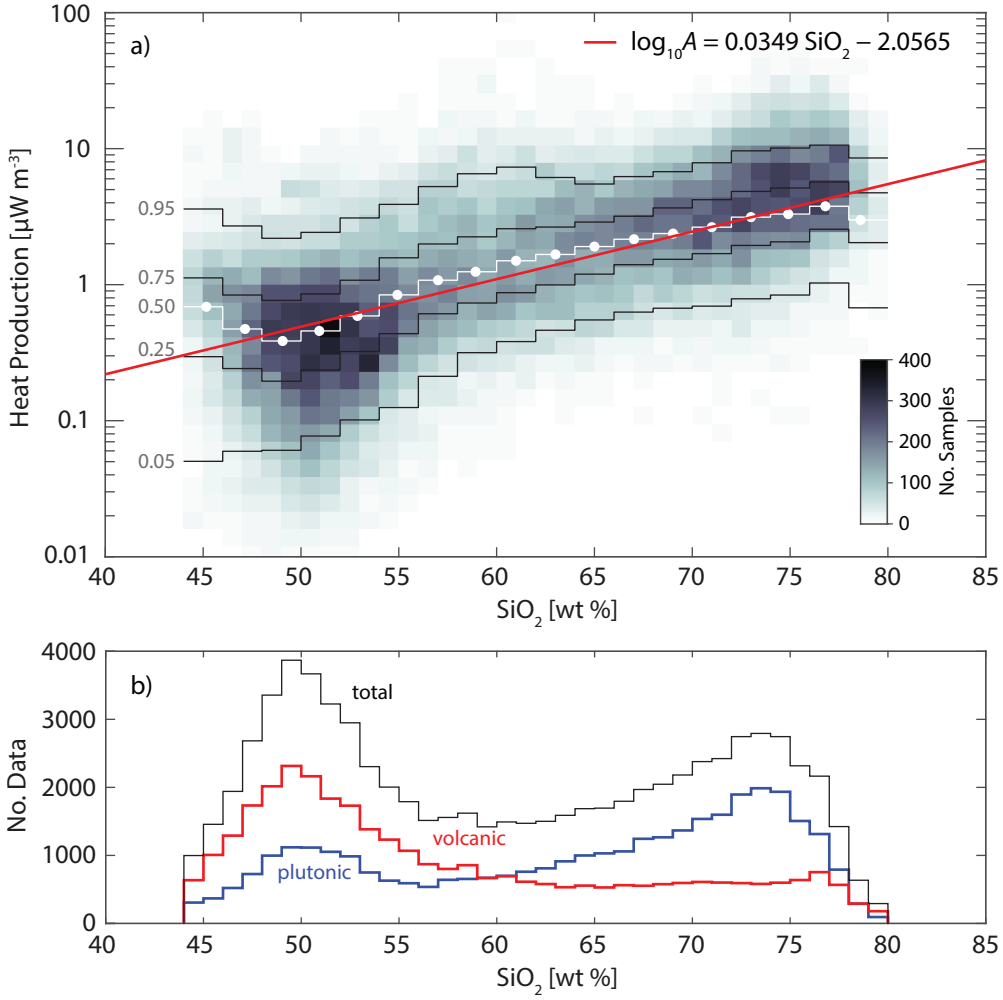

Figure 4.6: The relationship between SiO_2 and heat production. (a) The background 2-d histogram indicates the data frequency. The box and whisker plots identify the 0.05, 0.25, 0.75, 0.95 quantiles in SiO_2 bins of 2 wt.%. The points indicate the median SiO_2 and heat production of each respective bin. The red line is a model fit to the median SiO_2–heat production values. (b) The distribution of SiO_2 among all (black), plutonic (blue) and volcanic (red) samples.

the majority of rocks, a silica adjustment works very well as a means to directly compare heat production.

To remove the dominant lithological influence on the temporal heat production record, we produce a linear fit to the median heat production that is weighted by the number of samples per silica-bin. This weighting reduces the influence of the tails on the overall fit at the expense of a slightly lower

r^2 value (0.91), but should fit the bulk of the data much more reasonably. The weighted fit is given by,

$$\log_{10} A = 0.0349\, C_{SiO_2} - 2.0565, \tag{4.5}$$

where A is heat production in μW m^{-3} and C_{SiO_2} is the median SiO_2 concentration in wt.%. The RMSE (root mean square error) is 0.09 log-units.

Heat production estimates for individual samples with varying SiO_2 can now be normalized to a common SiO_2 by simply shifting the data up or down-slope using the relationship,

$$\log_{10} \bar{A}_i = \log_{10} A_i + 0.0349(\bar{C}_{SiO_2} - C_{SiO_2,\,i}), \tag{4.6}$$

where $\bar{A}_i$ is the heat production normalized to a reference SiO_2 concentration of $\bar{C}_{SiO_2}$.

The exact value of SiO_2 normalization is unimportant since it simply represents a shift of the data. This adjustment maintains the natural variability within each silica bin but shifts the distributions to comparable magnitudes. For example, a mafic sample that sits 0.5 log-units below the median at an SiO_2 of 50 wt.% will retain a similar position in the normalized distribution, ~0.5 log-units below the median heat production. We chose a value of 75 wt.% SiO_2 as the reference value.

4.5.3.2 Temporal plutonic and volcanic trends

Though some of our estimates are derived from drill cores and xenoliths, the vast majority of samples originate at the surface and therefore represent an estimate of the average surface heat production. However, in the analysis that follows, one must be careful equating samples collected at the surface with information about the surface alone. While volcanic rocks are surface samples, plutonic rocks originate from below the surface thus providing a vertical dimension, even if we are not certain at what depths they are derived from. In our analysis, we must examine the differences between plutonic and volcanic samples to potentially identify any coarse depth influence on heat production.

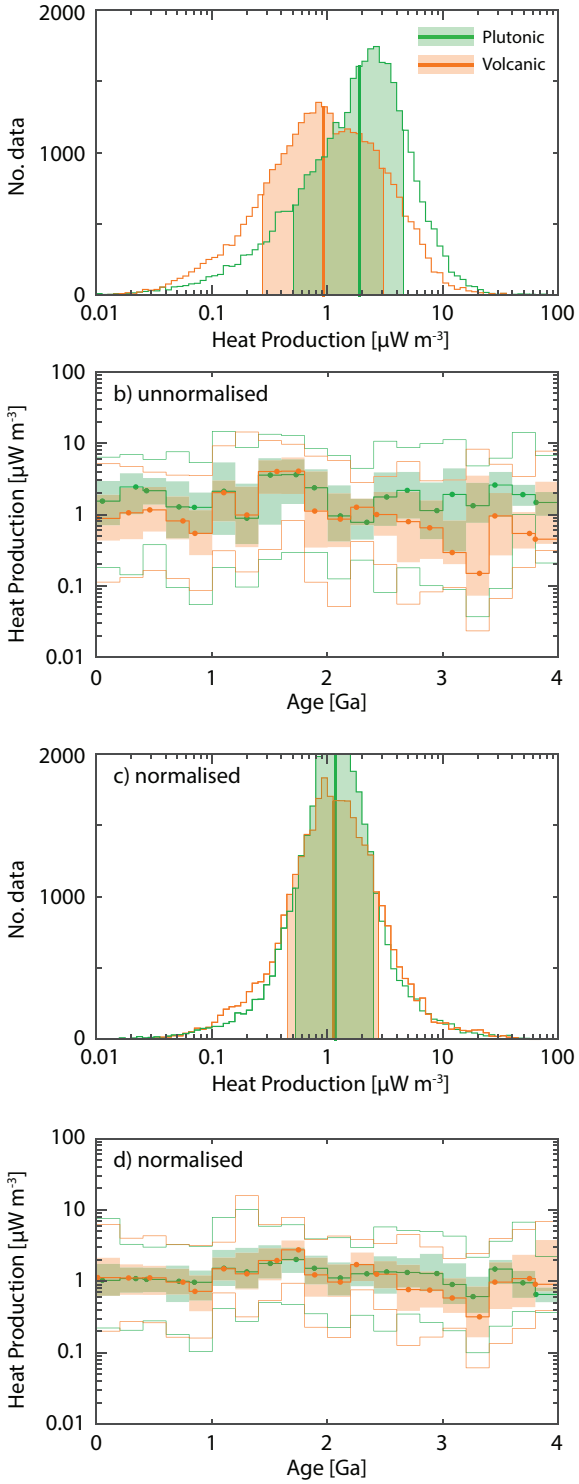

Figure 4.7: SiO_2 correction and its effect on plutonic and volcanic samples. (a) Plutonic (green) and volcanic (orange) heat production distributions before SiO_2 adjustment. (b) Plutonic and volcanic heat production trends through time before adjustment. (c) Heat production distributions normalized to 75 wt.% SiO_2. (d) Temporal variations in plutonic and volcanic heat production after SiO_2 normalization.

There is a dichotomy between plutonic and volcanic rocks (Figure 4.6b and Figure 4.7a) that presents the potential for both a compositional bias and difference in magnitude. There are some age bins for which the heat production of plutonic and volcanic rocks are similar, but for bins that differ, the plutonic heat production tends to be greater than the volcanic heat production (Figure 4.7b).

After normalizing for SiO_2, both sets have similar median values and variance, and are approximately log-normal (Figure 4.7c). The similarity in heat production for the majority of ages (Figure 4.7d) suggests that the raw plutonic and volcanic differences are dominated by the bias associated with SiO_2 content from each respective set. Furthermore, the similarity of the adjusted trends indicates that both plutonic and volcanic data can be analyzed together to produce a more robust temporal model. However, since both plutonic and volcanic data include mafic and felsic samples, the two sets are not compositionally independent.

4.5.3.3 Temporal mafic and felsic trends

Decay-adjusted felsic and mafic temporal trends appear to be correlated, separated by a relatively constant magnitude (Figure 4.8a and b). After silica normalization, the median heat production values for felsic and mafic samples are essentially coincident. A wider distribution among mafic samples persists after normalization (Figure 4.8c). Examination of the normalized heat production–age curves shows similar temporal trends between the two (Figure 4.8d). The correlation appears to break down within some intervals e.g. between 1.6-1.8, 3.2-3.4, and 3.8-4 Ga where sample numbers are lowest. As the two records are largely coincident post-SiO_2 adjustment, we choose to merge the two sets for the subsequent analyses. With the ability to adjust heat production to a common SiO_2 magnitude, it is now possible to examine global temporal variations free from the largest compositional influence resulting from fractionation.

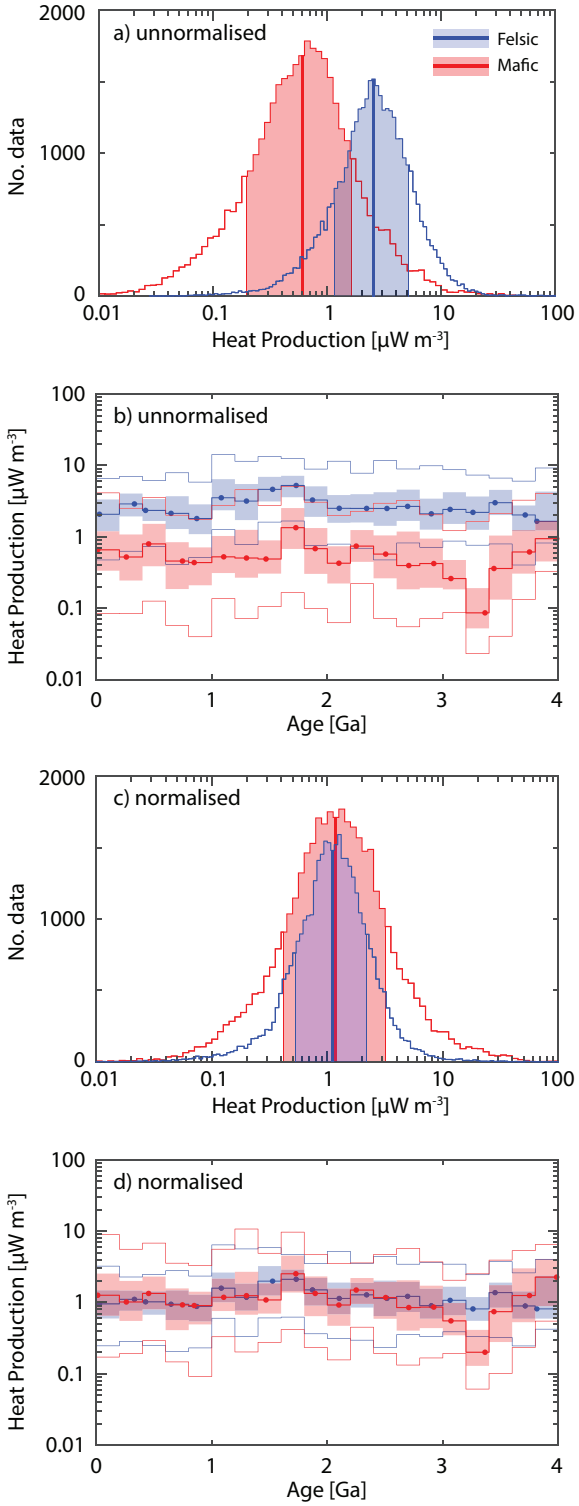

Figure 4.8: SiO_2 correction and effects on decay-corrected felsic and mafic samples. 'Mafic' samples are defined as those with ≤ 60 wt.% SiO_2 and 'felsic' samples >60 wt.% SiO_2. (a) Felsic (blue) and mafic (red) heat production distributions before SiO_2 adjustment. (b) Temporal felsic and mafic heat production (decay-corrected) before silica adjustment. (c) Heat production distributions normalized to 75 wt.% SiO_2 (d) Temporal variations in felsic and mafic heat production (decay-corrected) after SiO_2 normalization.

4.5.4 Sampling bias (spatial)

Silica normalisation removes the first-order component of spatial bias due to differences in lithology, though it will not remove biases related to trace element enrichment and/or depletion that may be attributed to the source or crustal contamination. The remaining spatial variations are, in general, relatively small (Table 4.3).

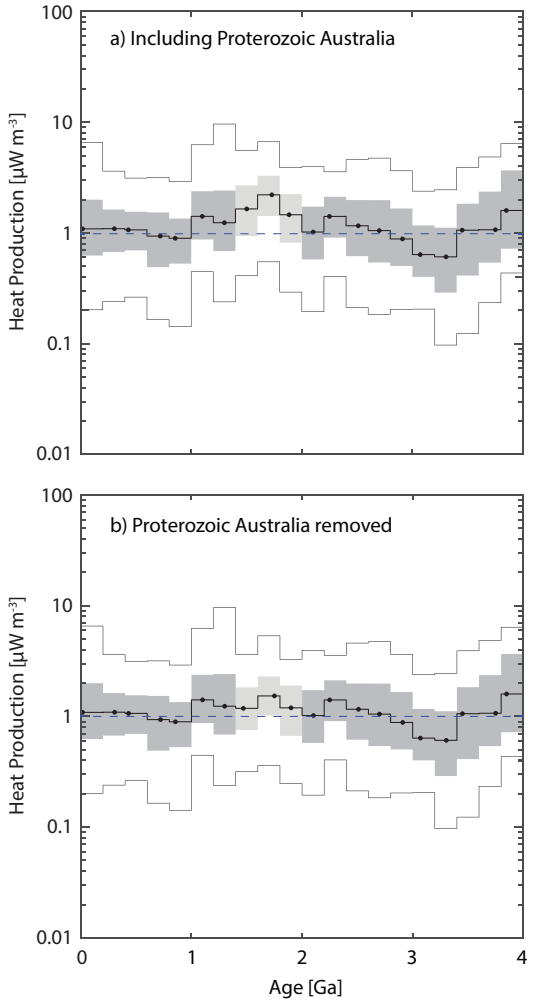

Figure 4.9: Decay- and SiO_2-corrected heat production through time. Dashed line denotes 1 μW m-3. a) all data, b) excluding Proterozoic Australia (1400–2000 Ma).

However there are some exceptions, including the oldest age intervals of ~≥3 Ga, where the amount of preserved crust is small, and the number of regions are limited. A peak also persists in heat production in the Meso-proterozoic to the late Paleoproterozoic (from ~1.4 to 2 Ga). This peak is

Table 4.3: Analysis of spatial bias among decay and SiO_2 normalized HP distributions by age interval [a]

Age bin (Ga)	Country	Country % of age bin	Median HP (Country) (μW m^{-3})	HP Quantiles (Elsewhere) (μW m^{-3})		
				0.25	0.5	0.75
0–0.2	US	47.51%	1.038	0.559	1.166	2.525
0.2–0.4	CN	16.61%	1.050	0.692	1.097	1.599
	AU	18.05%	1.273	0.612	1.013	1.614
	CA	21.47%	1.077	0.632	1.101	1.701
0.4–0.6	CA	51.92%	1.047	0.637	1.102	1.797
0.6–0.8	CN	21.54%	0.927	0.495	0.937	1.637
	EG	23.59%	0.783	0.484	1.040	1.739
0.8–1.0	CN	63.29%	0.815	0.611	1.074	1.574
1.0–1.2	AU	18.98%	1.670	0.848	1.375	2.356
	CA	19.83%	1.731	0.856	1.380	2.205
1.2–1.4	AU	19.59%	0.796	0.805	1.346	2.666
	CA	24.30%	1.042	0.769	1.348	3.067
1.4–1.6	CA	20.32%	1.001	1.074	1.822	3.051
	AU	39.78%	2.607	0.755	1.183	1.827
1.6–1.8	AU	66.66%	2.582	1.021	1.532	2.295
1.8–2.0	AU	27.58%	2.151	0.667	1.196	1.902
	FI	38.10%	1.190	0.892	1.663	2.480
2.2–2.4	CA	17.37%	1.175	0.955	1.501	2.228
	CN	27.54%	1.506	0.850	1.390	2.039
	IN	30.54%	1.520	0.884	1.389	2.071
2.4–2.6	FI	15.41%	1.364	0.572	1.095	2.005
	CN	46.33%	0.894	0.748	1.471	2.283
2.6–2.8	CA	35.77%	0.792	0.626	1.261	2.284
2.8–3.0	AU	16.59%	2.005	0.444	0.753	1.268
	GL	21.51%	0.654	0.543	0.998	1.855
	CA	39.65%	0.817	0.533	0.938	1.840
3.0–3.2	AU	16.88%	0.838	0.390	0.618	1.103
	GL	58.38%	0.551	0.507	0.906	1.584
3.2–3.4	AU	15.74%	1.049	0.254	0.551	0.972
	ZA	16.71%	0.455	0.292	0.715	1.179
	IN	39.23%	0.314	0.440	0.780	1.255
3.4–3.6	SZ	31.90%	0.442	0.747	1.428	2.084
	AU	45.83%	1.597	0.237	0.582	1.379
3.6–3.8	TF	16.99%	0.857	0.585	1.105	2.276
	GL	58.01%	0.972	0.685	1.184	2.738
3.8–4.0	CA	41.73%	2.557	0.603	0.797	2.373
	GL	54.33%	0.804	1.530	2.489	3.776

[a]Deviations of country median beyond the 0.25 or 0.75 quantiles of the "elsewhere" set highlighted in grey

attributed almost exclusively to the dominance of the high heat-producing felsic samples of the Australian data set. While Artemieva et al. (2017) attribute this peak to potential supercontinent cycle and plate velocities, it is clear from our analysis that this is just an artifact of spatial bias.

This irregularity is unsurprising, as the anomalous nature of the Australian Proterozoic samples is well documented in studies of heat flow, heat production and thermal isostasy (Morgan, 1985; Neumann et al., 2000; McLaren et al., 2003; Hasterok and Gard, 2016; Hasterok and Webb, 2017). While this region is generally considered anomalous, the Proterozoic terranes of Australia are spatially extensive and make up a significant fraction of the preserved crust from that time. Our data set contains ~2,000 Australian samples in the age range from 1.4-2 Ga, accounting for around half the samples in this interval. Removing the Australian Proterozoic samples in this interval brings the median heat production down to similar magnitudes of neighbouring ages (Figure 4.9a and b). We chose to remove the Australian Proterozoic samples, as they represent the largest deviation from the global means.

4.6 Discussion

Temporal variations in decay-corrected mafic and felsic heat production are very similar for the majority of Earth history, for both lithologically normalized and un-normalized distributions (Figure 4.8b and d), with the exception of some of the oldest intervals (≥3 Ga). This similarity is remarkable considering the diversity of sources and processes that create or alter the chemistry of a melt. Mafic melts are typically extracted from the mantle, whereas felsic melts are more complex, originating from fractionation of mafic melts or melting of the crust, both of which may incorporate variable amounts of metasedimentary material. The absence of a temporal lag between the mafic and felsic records implies that whatever process has led to this shared relationship must occur with a separation of no more than 200 Ma (the width of our age bins).

After the decay correction, silica adjustment, and removal of the Australian Proterozoic terranes, the distribution of heat production through

time exhibits shallow long-period variations (Figure 4.9b). These changes are similar or shallower in magnitude to the width of the inter-quartile range of natural variability, with the exception of a potential decrease from 4-3.2 Ga and a subsequent increase from 3.2-2.8 Ga. The downwards trend from 4-3.2 Ga is likely due to the divergence in felsic and mafic correlation discussed previously, where merging of the sets may not be valid (Figure 4.8d). These trends are only observed in the mafic samples, whereas the felsic samples appear relatively flat for the entire period from 4.0-2.8 Ga. Plutonic and volcanic rocks do not share this breakdown in correlation but are also are not compositionally independent.

4.6.1 Observed and expected Heat Production

Jaupart et al. (2016) discussed that crustal heat production appeared to show a clear trend of decrease with increasing age, and was able to be accounted for almost exclusively by decay. While we agree this flattens this first order variability of the heat production record, there is still more to this result that needs to be discussed, even after the lithological influence is normalised. In the Archean, heat production of the bulk silicate Earth was 3 to 4 times higher than the present-day due to decay alone. In a simplified sense, ignoring other known processes that may influence HPE distributions temporarily, one might expect samples from the Archean to contain 3 to 4 times as much heat production at formation as a result. If we project the present-day heat production distribution back into the past using the inverse of Equation 4.1, we expect an exponential decrease in heat production at formation from the Archean to present-day (Figure 4.10). The adjusted heat production record falls below this prediction, which we refer to as a deficit in old terranes (Figure 4.10). This deficit is as large as 0.5 log-units in the Early Archean. The comparison to this deficit is simply to acknowledge a decrease in heat production enrichment compared to present day conditions extrapolated to the past. Either the rock record is biased towards lower HP distributions and/or the HP distributions for similar lithologies have varied through time as a result of differing conditions in the past. Below we discuss the relevance of the aforementioned hypotheses that may contribute to variations in the temporal heat-production record to produce the observed deficit.

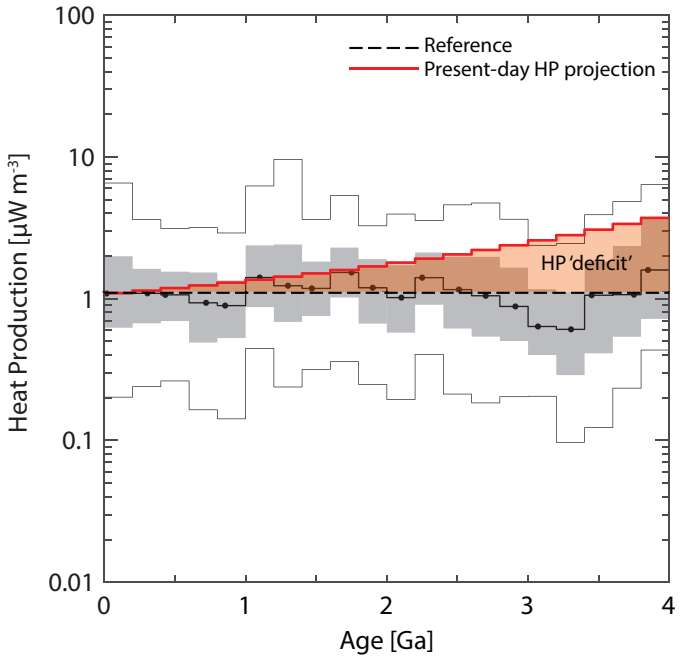

Figure 4.10: Present-day crystallization heat production distribution projected back into the past accounting for decay only (Density: 2.81 g/cm^3, K_2O: 2.19 wt.%, U: 1.61 ppm (99.28% ^{238}U, 0.711% ^{238}U), Th: 5.76 ppm). Assuming no other influences on HP distributions, we might expect the heat production at formation to be higher in the Archean than present-day due to the higher availability of heat producing isotopes. We do not observe this however; other influences must be responsible for the HP deficit observed in the record.

4.6.1.1 Shift in bulk crustal composition

There is clear evidence for a temporal shift in HPE concentrations for approximately uniform major element composition sedimentary and metasedimentary samples (McLennan et al., 1980). This shift is attributed to a shift in the composition of exposed crust from more mafic (lower Th and U) in the Archean, to more felsic (higher Th and U) towards the end of the Archean. Though we normalize for SiO_2, granites derived from more mafic sources are likely to have lower heat production than those with greater contributions from felsic and intermediate crust. Hence, the composition of the crust being reworked will have an influence on newly formed melts, raising the heat production by differing amounts depending upon the SiO_2 content of the crust. With time, the enrichment of U and Th may then indicate a shift from more mafic crust in the Archean, to more felsic crust in the late Archean, and maintained to present day.

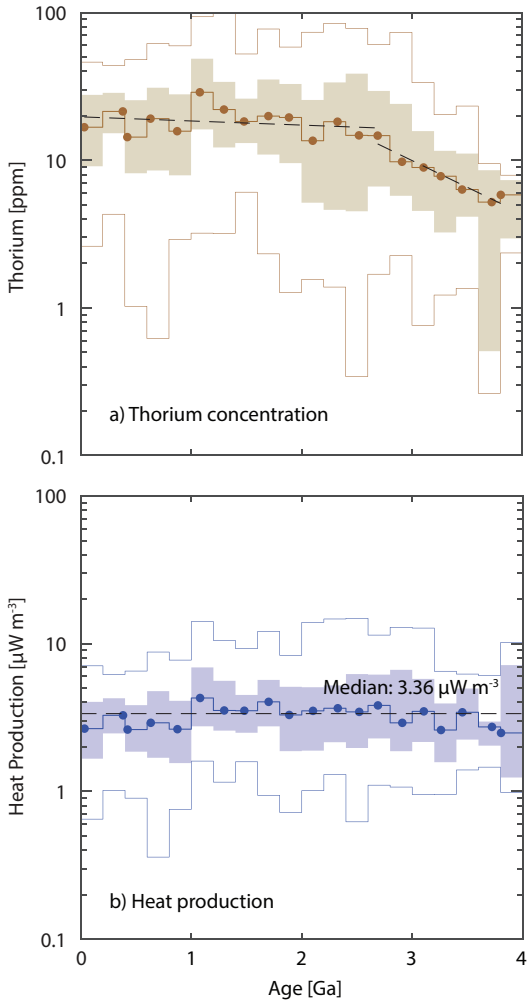

Figure 4.11: Temporal plots for 'granite' (TAS classification) restricted to between 72.1 and 75.97 wt.% SiO_2 (0.25 and 0.75 quantiles for SiO_2 concentration for 'granites'). a) Decay-adjusted thorium enrichment. The dashed lines represent the best fit to the median values for each bin between 0 to 2.8 Ga, and 2.8 to 4 Ga. There is a clear change in trend starting from ~2.8 Ga. b) Decay-adjusted heat production. Thorium enrichment (as well as uranium) increases from 4 Ga to ~2.8 Ga, and then remains relatively constant towards present day. Despite changing HPE enrichment, heat production at formation for these granites has been constant through time due to declining proportions of high heat producing ^{235}U.

Despite relatively constant heat production discussed in this manuscript, we also show a rapid increase in Th and U content from early Archean to ~2.7 Ga, and then a relatively constant Th value to present day (Figure 4.11). At first glance this may appear contradictory, as one might expect that an increase in heat producing element enrichment would be associated with an increase in heat production. However, this is easily resolved when analysing the decay adjustment. In the early earth, the

proportion of the isotope ^{235}U to ^{238}U was significantly higher than today due to the much shorter half life of ^{238}U (see Table 4.2). The decay of ^{235}U (~575 μW kg^{-1}) produces just over six times as much energy as that of the decay of ^{238}U (~91.7 μW kg^{-1}), and ~20 times that of ^{232}Th and ^{40}K (~25.6 and ~29.7 μW kg^{-1}, respectively) (Rybach, 1988). Thus, while total heat producing element enrichment was lower in the Archean, this was counterpoised by increased ^{235}U proportions. Thus, the heat production deficit identified in Figure 4.10 is the result of a shift in HPE enrichment, independent of lithology, and likely due at least in part to the shift in bulk crustal composition (McLennan and Taylor, 1980). However, other hypotheses must also be considered that might attribute to this alteration of HPE enrichment.

4.6.1.2 Crustal Reworking

In a simplified global crustal reworking model, it is assumed an increase in heat production in younger rocks should be observed. HPEs preferentially partition into melts during partial melting due to their incompatibility (e.g. Workman and Hart, 2005), so during consecutive events of crustal accretion, orogenesis and tectonic reworking one may expect differentiation of the continental crust to progressively increase. Nd and Hf isotopes both suggest that crustal and mantle reworking is an important process for crustal evolution and may account for a significant fraction of the present volume of the crust (Hawkesworth et al., 2019). Such processes could be assumed to increase on average during periods of supercontinent formation and breakup. As a result, in a simplified model, one may expect a general first order increase in heat production through time due to progressive reworking, with a second order variation correlated with periods of supercontinent formation and breakup (Figure 4.12).

The average heat production of igneous rocks appears to change on multiple temporal scales in our analyses. Most of the short period variations were removed through the compositional normalization. What remains are smoothly varying and long-period temporal differences that could potentially be considered within natural variability. Artemieva et al. (2017) suggested the pattern of heat production through time for a small set

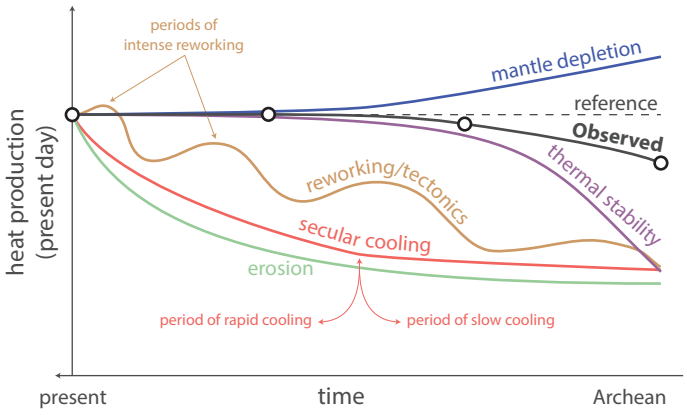

Figure 4.12: A conceptual diagram of expected deviations in HP observed at present-day (not decay-adjusted) for different aged rocks due to time-varying global processes. Due to decay alone, we would expect all rocks to look the same at present day (reference line) assuming all other processes and conditions are unchanged. We instead observe a roughly exponential decrease with time (solid black line). After decay correction this observed line is approximately flat (Figure 4.9b). This flat trend must result from other external influences lowering the 'reference' decay-only Earth curve to the observed curve.

of granites was correlated with estimated plate velocities from Korenaga (2013). However, we find no correlation to the decay-corrected, nor silica normalized temporal heat production models (Figure 4.4a and 4.9b, respectively). Similarly, we do not observe a correlation with these estimated plate velocities for the unprocessed granite data or even similar temporal trends of heat production as Artemieva et al. (2017) (Figure 4.5a).

Within our silica and decay adjusted temporal signal, we observe no apparent periodic correlation to supercontinent formation or break up, and no systematic increase through time in heat production. Interestingly, mafic and felsic temporal trends track each other almost coincidentally (Figure 4.8d). If partial melting and assimilation of older heat production into younger rocks was occurring on a global scale in the crust, and if the sources of mafic melts have remained relatively constant through time, we might expect a divergence in the mafic and felsic samples temporally, increasing towards the present. Additionally, modern felsic samples, in particular, are expected to be more enriched in HPEs relative to the oldest Archean samples after decay adjustment. While we observe greater enrichment in the present, the long term trend does not fit the expected response of reworking. It is possible enrichment due to this reworking argument may have limited potential to redistribute HPEs. With each in-

stance of successive partial melting, the ability to redistribute meaningful amounts of trace elements plummets rapidly. In general, there may be only one or two instances of HPE redistribution associated with partial melting, but even melting may not redistribute HPEs in any meaningful way unless significant amounts of water are reintroduced (Alessio et al., 2018).

Surprisingly, our results suggest that global variations in dominance of geodynamic processes have little influence on relative heat production enrichment for similar rock types. Instead, it is likely that these processes impart a quasi-periodic signal on the median volumes of different compositions of melts through time, rather than the heat production of the individual compositions themselves e.g. periods of more intense and voluminous mafic magmatism may be associated with certain temporally dominant geodynamic environments. However, such an influence could only be observed prior to SiO_2 normalization and would then, in turn, likely be heavily masked by compositional sampling bias. Prior to the adjustment for SiO_2 there could potentially be a weak correlation to troughs and peaks of heat production to supercontinent cycle, but there is large uncertainty as a result of the compositional influences. Deciding how to differentiate whether a certain rock type was more pervasive during a time interval, or if it's merely the result of oversampling of a particular rock type in that time period is difficult to distinguish from the database alone.

4.6.1.3 Secular Cooling and Melt Fractions

Earth's internal temperatures have reduced through time, a function of secular cooling with primordial heat loss and the decrease of HPE due to radioactive decay. Evidence of this cooling has been observed in the decline in relative abundance of komatiites (Nisbet et al., 1993), studies of mantle potential temperatures from MORB's (Abbott et al., 1994), xenon isotope data (Coltice et al., 2009), and continental basaltic geochemistry (Keller and Schoene, 2012). These studies suggest that Archean mantle temperatures were on the order of 100-200°C hotter than present-day. Processes such as crustal diapirism, formed by the process of sagduction (Goodwin and Smith, 1980), a unique feature of the Archean, also suggests a hotter

and more ductile crust (Mareschal and West, 1980). Similarly, high and intermediate thermal gradients in the continental crust were also perhaps more common in the past (Brown and Johnson, 2018).

Existing thermal evolution models suggest an increase in temperatures in the first 1-1.5 Ga of Earth history, and then cooling towards present at an increasing exponential rate (Labrosse and Jaupart, 2007; Herzberg et al., 2010; Condie et al., 2016). Greater temperatures in the mantle and crust in the past might suggest that higher degrees of partial melting were present, and thus one may hypothesize a signal in the heat production record as a result. As previously discussed, HPEs preferentially partition into the melt phase during partial melting (e.g. Workman and Hart, 2005), and thus higher melt fractions on average may produce lower heat producing melt products. Thus, if there exists a partial melting signal associated with cooling rates, we may expect a general increase in heat production towards the present, with most rapid variation closest to present-day due to more rapid cooling (Labrosse and Jaupart, 2007; Condie et al., 2016; Herzberg et al., 2010) (Figure 4.12).

While there may be a slight decrease in heat production from 1 Ga to present-day (Figure 4.10), the trend appears to be within the natural variability of the distribution and is hard to distinguish with any certainty. It is also expected that if this was a temperature/partial melting influence, the median at 1 Ga should persist further into the past, however the period from 1-2 Ga has much the same median as the present-day age interval. It appears unlikely that secular cooling has exerted a significant influence on the heat production–age record from these results.

4.6.1.4 Mantle Depletion

The formation of the continental crust has depleted the mantle of incompatible elements. While the rate of continental growth and rates of recycling are still debated (Belousova et al., 2010; Condie and Aster, 2010; Armstrong et al., 1981; Goodwin, 1996; Pujol et al., 2013), mantle depletion should result in a decrease in heat production of progressively younger rocks extracted from the products of mantle melting (Figure 4.12), assuming other influences such as degree of mantle melting were constant. Thus,

we may expect depletion should cause a surplus of heat production in the early Earth rather than the deficit observed. Among the better constrained portion of the temporal heat production curve (<3.4 Ga), we observe no surplus pattern in heat production (Figure 4.9b). It is possible most of the continental crustal growth occurs >3.4 Ga, where there appears to be a rapid decrease in heat production of mafic samples (Figure 4.8d), divergent to the relatively flat trend in the felsic samples. For example, Campbell (2003) suggests that at ~3 Ga, ~75% of the present-day continental mass already existed. However, the relatively few sites from which these data are drawn makes it difficult to interpret these changes with great confidence (Figure 4.8d). It is also possible such a signal might be offset or altered by subduction enrichment, especially at continental margins with high erosion rates (e.g. Scholl and von Huene, 2007).

4.6.1.5 Erosional Influence

Modern orogens may be eroded with time, exposing deeper and presumably more intermediate to mafic rocks (e.g. Christensen and Mooney, 1995; Rudnick and Gao, 2003). Thus, it is reasonable to assume there is also a compositional influence on the vertical heat production distribution. Vitorello and Pollack (1980) suggested an impact on the heat production record may be observed due to this erosional influence; subsequent to formation and mountain building, surface heat production may approach an equilibrium at an exponential rate after a few hundred million years.

The global signal expected from erosion is, at least on a global scale, an increase in the proportion of felsic rocks exposed towards the present with an associated increase in median heat production (Figure 4.12). Such variations may be hard to distinguish when observing a global data set; as the largest component of this influence is likely compositionally entwined (increasing maficity with depth), we may have effectively removed its impact with the silica normalization. Thus, we do not preclude the existence of an erosional influence for local regions, but there appears to be no systematic decrease in silica or heat production in the global data set within the first 200-500 My in the pre-silica correction data sets (Figure 4.4a,b).

For most stable continental regions, the upper crustal rocks (~10 km) are responsible for the majority of the bulk crustal radiogenic component of surface heat flow (McLennan and Taylor, 1996). As HPEs are highly incompatible, they will be preferentially enriched during partial melting and crustal growth. The exact nature of the vertical distribution is unique to any location and sometimes highly variable, dependent on complex histories of crustal growth, accretion, deformation and tectonic reworking (e.g. Brady et al., 2006; He et al., 2008; Ketcham, 2006). The lack of an erosional signal in the globally averaged rock record may also be attributed in part to this complexity. As volcanic and plutonic samples are so similar after silica adjustment (Figure 4.7), this suggests that depth of emplacement has a minor influence on HPE concentrations once lithology is accounted for, at least on a globally averaged scale.

4.6.1.6 Thermal Stability and Selective Preservation

Morgan (1985) suggested that the early earth heat production record may not represent the true global distribution of the time due to a selective preservation bias (discussed in more detail in Section 4.2.6). Lithosphere with lower heat production will house lower geotherms and will be internally cooler than regions with higher heat production and similar mantle heat flow contributions. As a result, these low heat producing regions are less susceptible to orogenic reworking and have a higher probability of stabilization and survival in the Archean record (see also Sandiford et al., 2002). This influence does not preclude higher heat producing rocks existing in these older time intervals or being preserved in some locations. Instead, Morgan (1985) hypothesizes that, in general, high heat producing regions will be statistically less likely to survive in the geologic record resulting in a decrease in the average preserved heat relative to the true heat production distribution. Delineating a quantifiable thermal stability derived preservation model from the other processes discussed however is almost impossible.

Although heat production appears to be relatively constant through time for similar major element compositions, the concentrations of HPE's were lower in the Archean. This result seems well described by the bulk com-

position shift in exposed terrains, as discussed previously. The oldest sediments should also preserve a record of the samples at the surface at this time, even if the sources themselves have disappeared through thermally driven tectonism or reworking. The sedimentary record from McLennan and Taylor (1980) presents similar results compared to the trends in the igneous/metaigneous sample set here (Figure 4.11), suggesting that our data set may not be biased towards lower heat production compared to the true distribution of the time. However, the sedimentary record utilised within their study is not entirely immune from this hypothesis either. Samples from these oldest time periods are metamorphosed, carried to various depths within the crustal column, and thus also vulnerable to thermal instability. Thus, we do not believe that the sedimentary result entirely precludes an existence of a thermal preservation influence on the record either. Is the more mafic Archean crust we observe today a natural consequence of growth of the crust and continental crust, or is it at least in part a consequence of being more thermally stable than more felsic crust? If it is the later, what is the degree to which felsic crust has been destroyed, and was there a time in Earth's history where mafic crust was also largely unstable due to high radioactivity, i.e., in the earliest Archean or Hadean?

4.6.2 Implications for the continental crust

There are three major implications one can draw from the heat production analysis performed in this study: (1) a shift in the crustal composition appears to have enhanced enrichment in heat producing elements for similar major element composition samples up to to the Archean-Proterozoic boundary; (2) Thermal stability may perhaps provide a complimentary chemical bias in the rock record; and (3) a correlation between mafic/felsic and plutonic/volcanic heat production allows us to draw inferences about the vertical distribution of HPEs in the crust.

Changes in thermal stability through time has the potential not only to affect the heat production distribution preserved in the geologic record, but also the chemical nature of the crust that is correlated with these low heat producing regions. This selective preservation of crust has the potential to bias towards more mafic and less alkali (especially K) compositions than

likely existed at the time. If valid, our models of chemical evolution of the Earth would need to be modified to take into account the potential for thermally influenced selective-preservation. The deficit in HPE enrichment is quite large in the early Earth with respect to the present, however, this model assumes that the present-day distribution is the appropriate metric from which to judge this deficit. It is likely the majority of this deficit may be accounted for by the shift in crustal composition from mafic to more felsic and intermediate compositions up to ~2.7 Ga, but thermal preservation may also play an additional role.

Average heat production has been shown to follow an exponential relationship with respect to estimated P-wave velocities (Hasterok and Webb, 2017), which suggests that there is a relationship between mafic and felsic heat production in individual terranes. Although our model is global, the correlation between mafic and felsic temporal records implies that such a connection may occur for many time periods as well. Therefore, regions with high upper crustal heat production may be expected to also have high lower crustal heat production. Many general crustal heat production models often assume a common lower crustal heat production while allowing upper crustal heat production to vary (Chapman, 1986; Artemieva and Mooney, 2001; Hasterok and Chapman, 2011). As a result, these generalized geotherm models may over- or under-estimate temperatures in the lithosphere. The result may not be very large within the crust due to relatively low heat production of mafic rocks, but it could still have a significant effect on mantle temperatures and thermal estimates of lithospheric thickness. Therefore, when modelling the thermal state of the lithosphere it is advisable to take into account the age distribution of the lithosphere as well as the correlative nature of heat production.

While we have not delved into discussions about heat flow, our model undoubtedly has implications for such variations. Archean terrains are old and often more predominantly mafic, which accounts largely for their lower heat flow. However, Archean samples have been shown to have particularly low enrichments of heat producing elements even once adjusted for decay, compared to modern samples (Figure 4.11). While their heat production at formation would have been similar to present day samples, over the course of time their heat production dropped more rapidly than present day sam-

ples due to lower enrichments of HPEs and the decreasing proportion of ^{235}U to ^{238}U. Thus, due to extensive decay, lower average silica concentrations, and particularly low enrichment of HPEs compared to modern day equivalents, present day heat flow in these regions is uncharacteristically low.

We are not attempting to explain the decrease in surface heat flow in the past, although our model undoubtedly has implications for such variations, but must be combined with knowledge of dominant lithology and depth distribution of heat production as well.

4.7 Concluding remarks

Correcting for the decay removes a long-term trend that described the first-order decrease in heat production with age as suggested by (Jaupart and Mareschal, 2014). The decay-corrected pattern suggests a quasi-periodic variation in heat production that can be linked to lithology. This lithological influence is the largest source of variability and can be removed by in large by normalizing for SiO_2.

After correcting for gross lithological changes and radioactive decay, a deficit in heat production remains compared to modern day sample projections. A number of hypotheses have been proposed to account for heat production variations through time:

1. A shift in the bulk composition of the crust, evidenced by various studies (e.g. Taylor and McLennan, 1985; Condie, 1993; Dhuime et al., 2015; Tang et al., 2016, and references therein), and discussed with respect to heat producing element enrichment in sediments by McLennan and Taylor (1980). Our results seem closely aligned with the sedimentary record, and appears to provide further evidence for a shift in bulk composition of the crust rapidly altering heat producing element enrichments for similar major element composition samples. The total heat generated by uranium drops drastically due to a significant drop in the proportion of ^{235}U compared to ^{238}U, which leads to the heat production record not appearing to correlate with this HPE in-

crease, and instead remaining relatively constant. We consider this hypothesis to be the best explanation for the observed, relatively constant temporal heat production signal at formation after correction for gross lithology and decay.

2. We do not find a clear correlation with the super-continent cycle or modelled plate velocities as suggested by Artemieva et al. (2017), either before or after SiO_2 normalization and decay adjustment. Secular cooling and mantle depletion are also not clearly expressed in the SiO_2 normalized heat production model.

3. Contrary to the heat flow based model by Vitorello and Pollack (1980), we do not observe a clear decrease in heat production with time due to any evident erosional influences in either the distribution of samples in silica space or heat production as deeper rocks are exhumed. Our model does not rule out the potential for local erosional influences on heat production, only that erosion is not a significant influence on secular variations in global heat production.

4. Selective preservation due to thermal stability, as discussed by Morgan (1985), may impart an additional heat production deficit (greatest in the Archean and increasing to a steady-state as Earth cools). Regions with high heat production may not have been stable in the early Earth as the crust in high heat producing regions would be hot and weak, making them susceptible to destructive plate forces. As a result, a selective bias could be created for regions with low heat producing elements. This selective bias could raise interesting questions about the chemical nature of regions that were unable to survive this period and their influence on the chemical evolution of the continental crust. Quantifying this influence is difficult however, and would contribute in conjunction, or perhaps control in part, the hypothesis of a shift in bulk composition.

This study has implications for improving heat production distribution estimates, particularly when providing initial constraints on poorly understood regions. Magmatic age, and dominant lithological type in silica space can provide two independent constraints for bounding heat production estimates of large-scale provinces. Adjusting for decay and lithological

influence appears to remove the majority of the temporal heat production distribution variations. More robust constraints on crustal heat production, temperature, and heat loss are thus possible, particularly for poorly understood terranes where simply assuming continental averages is often the case. Although these correlations are weak when considering individual rock samples and geological suites, their strength lies in providing initial constraints on heat production for thermal estimates at large scales.

4.8 Acknowledgements

We would like to thank the following for providing datasets and/or personal compilations: D. Champion (GA), D. Claeson (SGU), T. Slagstad (NGU), and H. Furness. Peter Johnson provided a collection of papers with data for the Arabian-Nubian Shield. M. Gard is supported by an Australian Government Research Training Program Scholarship.

We would like to thank Roberta Rudnick for her thorough review which helped immensely in improving this manuscript. Additionally, thank you to the two anonymous reviewers whose comments assisted in clarifying some content.

CHAPTER

FIVE

A GLOBAL CURIE DEPTH MODEL UTILISING THE EQUIVALENT SOURCE MAGNETIC DIPOLE METHOD

Gard M.[12], Hasterok D.[13]

[1]School of Physical Sciences,
University of Adelaide, Adelaide, Australia
[2]Geoscience Australia,
Canberra, Australia
[3]Mawson Geoscience Centre,
University of Adelaide, Adelaide, Australia

Published in *Physics of the Earth and Planetary Interiors*
https://doi.org/10.1016/j.pepi.2021.106672

Statement of Authorship

Title of Paper	A global Curie depth model utilising the equivalent source magnetic dipole method
Publication Status	☑ Published ☐ Accepted for Publication ☐ Submitted for Publication ☐ Unpublished and Unsubmitted w ork w ritten in manuscript style
Publication Details	Gard, M., Hasterok, D., 2021. A global Curie depth model utilising the equivalent source magnetic dipole method. Physics of the Earth and Planetary Interiors, 313, 106672. doi: 10.1016/j.pepi.2021.106672

Principal Author

Name of Principal Author (Candidate)	Matthew Gard		
Contribution to the Paper	Conception of ideas Programming, visualisation, and modelling Data interpretation Manuscript writing		
Overall percentage (%)	90		
Certification:	This paper reports on original research I conducted during the period of my Higher Degree by Research candidature and is not subject to any obligations or contractual agreements with a third party that would constrain its inclusion in this thesis. I am the primary author of this paper.		
Signature		Date	02/06/2021

Co-Author Contributions

By signing the Statement of Authorship, each author certifies that:

i. the candidate's stated contribution to the publication is accurate (as detailed above);

ii. permission is granted for the candidate in include the publication in the thesis; and

iii. the sum of all co-author contributions is equal to 100% less the candidate's stated contribution.

Name of Co-Author	Derrick Hasterok		
Contribution to the Paper	Supervised and aided data interpretation Manuscript editing and feedback		
Signature		Date	5/5/21

Abstract

The depth to the Curie isotherm provides a snapshot into the deep thermal conditions of the crust, which helps constrain models of thermally controlled physical properties and processes. In this study, we present an updated global Curie depth model by employing the equivalent source dipole method to fit the lithospheric magnetic field model LCS-1 from spherical harmonic degree 16 to 100. In addition to the new field mode, we utilize all three vector components and include a laterally variable magnetic susceptibility model. We also employ an improved thermal model, TC1, to supplement the degree 1 to 15 components that are otherwise contaminated by the core field. Our new Curie depth model differs by as much as ±20 km relative to previous models, with the largest differences arising from the low order thermal model and variable susceptibility. Key differences are found in central Africa due to application of a variable susceptibility model, and shield regions, but continents with poor constraints such as Antarctica require additional improvement. This new Curie depth model shows good agreement with continental heat flow observations, and provides further evidence that Curie depth estimates may be used to constrain evaluations of the thermal state of the continental lithosphere, especially in regions with sparse or surface contaminated heat flow observations.

5.1 Introduction

The thermal state of the lithosphere has implications for a diverse range of processes and physical parameters such as lithospheric strength (e.g. Jiménez-Díaz et al., 2012), can define potential regions of geothermal prospectivity (e.g. Hojat et al., 2016), and the dynamics and stability of ice sheets (e.g. Pattyn, 2010). Heat flow data are often spatially sparse, and are not always representative of the deep crustal thermal state, as heat flow is sensitive to near-surface influences such as hydrothermal circulation, thermal refraction, and the lateral distribution of heat producing elements. Thus, deep thermal crustal constraints derived from temperature-sensitive proxies are not only useful in regions with little to no direct thermal infor-

mation, but also aid in regions where this heat flow data is available. One way we can produce deep thermal models of the crust and lithosphere is via geophysical proxies such as magnetics.

It is well documented that, in general, there is a relation between surface heat flow and the depth to the bottom of the magnetized layer (e.g. Mayhew, 1982; Okubo and Matsunaga, 1994). As the depth to this layer in the continental crust is generally thermal in origin, this result is not surprising. In this article, we present an updated model for global Curie depths using the equivalent source magnetic dipole (ESMD) method (Dyment and Arkani-Hamed, 1998b) (as previously applied by e.g. Purucker et al., 2002; Fox-Maule et al., 2005, 2009; Hojat et al., 2016). There are four major contributors to the variance between the latest ESMD derived global magnetic crust thickness estimates from Fox-Maule et al. (2009) and the model presented here:

1. an improved satellite lithospheric field model (LCS-1, Olsen et al. (2017));

2. utilisation of a hybrid initial magnetic crustal thickness model built from TC1 (Artemieva, 2006), 3SMAC (Nataf and Ricard, 1996), and a Moho depth estimate from Szwillus et al. (2019);

3. the inclusion of the third vector component in the forward model (longitudinal component, ϕ); and

4. the application of a laterally variable magnetic susceptibility model (modified from Purucker et al., 2002; Hemant, 2003).

The global Curie depth solution resolved in this article matches the magnetic field model synthesised at 300 km altitude and shows reasonable correlation with observed surface heat flow. These results provide further evidence that Curie depth estimates are sensitive to the thermal state for large amounts of the continental lithosphere, and can help constrain temperature and heat flow estimates, especially in regions with sparse or surface contaminated heat flow observations.

5.2 Background

Most of the internal magnetic field of the Earth is generated in the core, with a smaller contribution sourced from induced and remanent magnetization within the crust (see Hulot et al., 2015, and references therein). Although several orders of magnitude weaker when compared to the core field, the magnetic anomalies resulting from the crust can still be identified from satellite magnetic measurements (e.g. Maus et al., 2002, and references therein).

Magnetisation of the crust resulting from the alignment of magnetic dipoles in susceptible rocks by the core field is known as induced magnetization, and depends on the strength of the inducing field, the magnetic susceptibility, and most importantly for this study, the thickness of the magnetized layer (Dyment and Arkani-Hamed, 1998b; Purucker et al., 2002). It is from this induced crustal magnetic signature that the maximum depth of magnetization can be inferred.

Conversely, remanent magnetization is relic permanent magnetization that exists irrespective of a present inducing field (Dyment and Arkani-Hamed, 1998a; Kent et al., 1978). One of the largest examples of remanent magnetism is the magnetic striping along oceanic spreading centres, whereby molten rock cools through its Curie temperature, and the orientation of the Earth's core field at the time of formation is locked in as a permanent magnetic field (e.g. Macdonald and Holcombe, 1978; Le Pichon and Heirtzler, 1968; Ramana et al., 2001). Though also present in the continental crust, its pattern is mostly indiscernible due to large variance in petrology, age and formation conditions and is generally considered to be dominated by the induced field for the majority of continental regions (Maus and Haak, 2002). When locally present, it can often be significantly greater in strength than the induced magnetization and must at least be considered during interpretations (See Thébault, 2010, for a full summary). More extreme examples of such continental remanent magnetisation include the Bangui magnetic anomaly of central Africa (Regan and Marsh, 1982) and the Kursk magnetic Anomaly in western Russia (Taylor and Frawley, 1987).

Above the Curie temperature, magnetic material loses its ferromagnetic properties and becomes functionally non-magnetic (Wasilewski and Mayhew, 1992). The Curie temperature is unique and ranges dramatically for different magnetic minerals. Magnetite is generally considered the dominant magnetic mineral in the crust, and has a Curie temperature of close to 580 ℃ (e.g. Clark and Emerson, 1991; Langel and Hinze, 1998). While the depth to the bottom of magnetisation can be associated with the magnetite Curie isotherm, this is not always the case. The magnetization of mantle rocks are commonly assumed to be relatively low (Wasilewski and Mayhew, 1992). In regions where the Curie isotherm extends past the depth to the bottom of the crust, it thus follows that the depth of magnetization will be largely bounded by this lithological layer rather than thermal constraints (Figure 5.1). Regions do exist where magnetization may be present in the mantle, such as the production of magnetite through serpentinization at subduction zones (e.g. The Cascadia convergent margin, Blakely et al., 2005), or potentially via diffusive exsolution within both olivine and pyroxene in colder geotherm environments (e.g. the Kamchatka arc, Ferré et al., 2013). The magnitude of expected anomalies discussed in Ferré et al. (2013) are generally below the noise level of satellite magnetic data (Burton-Johnson et al., 2020), however the tectonic history should indeed be considered when interpreting results from these magnetic based methods.

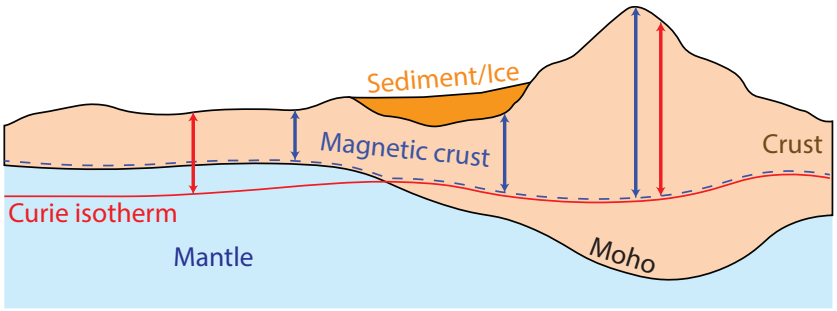

Figure 5.1: The relationship between Curie depth and the magnetic crust. The depth to magnetisation is generally thermally bounded in regions where the Curie isotherm is shallower than the Moho, and lithologically controlled when not. Sedimentary basins are generally very low in contribution to the magnetic signature and are excluded in this analysis.

Global Curie depth estimates have been developed through different methodologies, such as the equivalent source magnetic dipole method (e.g. Pu-

rucker et al., 2002; Fox-Maule et al., 2009) or via fractal magnetization (e.g. Li et al., 2017) which conducts the inversion for the magnetic signal in the frequency domain. Both methodologies suffer from differing assumptions and limitations: the ESMD method must make assumptions on magnetic susceptibility distributions across continental and oceanic regions, and the fractal process is constrained by other limitations such as selection of window size which has a direct result of maximum resolvable Curie depth and often fixed fractal scaling factors.

5.3 Method

We utilise the equivalent source magnetic dipole (ESMD) method for estimating the depth to magnetisation. The ESMD method is described in detail by Dyment and Arkani-Hamed (1998b); Fox-Maule et al. (2009). Put simply, the Earth's crust is discretised into a number of approximately equidistant regions, with each region containing a dipole that is representative of the vertical integration of induced magnetization for that crustal volume. An initial magnetic crustal thickness estimate at each of these locations is modified, and consequently the magnetic moment of each dipole, such that a modelled induced magnetic field at some altitude closely resembles an observed magnetic field model.

5.3.1 Dipole, observation points, and the synthesized 'observed' fields

Dipole positions, $\bar{r}_j$, are selected using an Inverse Snyder Equal-Area Projection Aperture 3 Hexagon discrete global grid (ISEA3H, Sahr et al., 2003). The ISEA3H represents an approximately equidistant grid spacing, thus giving equal weight spatially for the forward modelling procedure. A typical latitude/longitude grid would have higher density of points at the polar regions compared to the equator, and disproportionately bias the forward modelling procedure to over fit these areas. We utilise 21,872 dipoles, with a mean inter-dipole distance of 156 km. Magnetic field data is synthesized at observation points, $\bar{r}_i$, matching the dipole positions but

offset in altitude by 300 km. An example of the density of dipole positions for a region around Australia can be seen in Figure 5.2a.

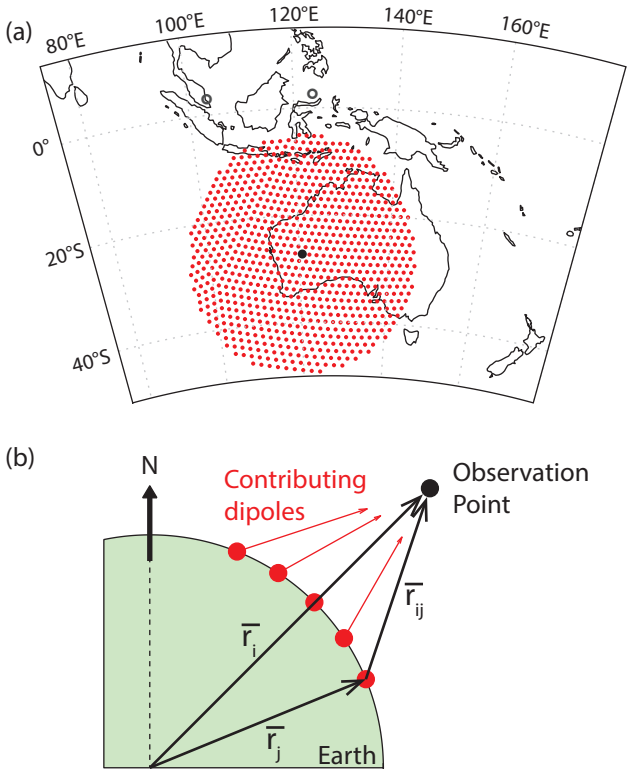

Figure 5.2: Visual illustration of the computational scheme used to estimate the magnetic field at a point using ESMD. a) Map view of an observation point (black) surrounded by dipole locations (<2500 km) used for the calculation. b) Cross-section showing altitude of observation point relative to dipole locations. $\bar{r}_i$ is the vector from the centre of the Earth to the observation point, $\bar{r}_j$ the vector to the dipole position, and $\bar{r}_{ij}$ the vector between them.

We utilise the LCS-1 magnetic field model (Olsen et al., 2017), a lithospheric magnetic field model from spherical harmonic degrees 16 to 185. LCS-1 makes use of a substantially larger data set than previous iterations of satellite derived lithospheric field model; it is derived from magnetic gradient data of a combination of the CHAMP and SWARM satellite missions. By using Swarm N-S and E-W gradient data, a significant reduction in variances compared to a CHAMP-only model is possible (Olsen et al., 2017). LCS-1 presents a number of improvements over previous satellite models, not just isolated to the expansion to higher spherical harmonic degrees. The use of gradient data improves signal-to-noise ratio which permits inclusion of data from periods of increased geomagnetic activity

and is less correlated in time which enables a higher data sampling rate. Generally large-scale magnetic field contributions are removed through pre-processing using an a priori model and line levelling which also removes part of the lithospheric signal. By using gradient data, Olsen et al. (2017) also removed the necessity to conduct orbit-to-orbit high-pass filtering or line levelling. Additionally, the availability of E-W gradient data from the Swarm satellite data should also assist in noise reduction in the E-W component of the field model in comparison to a CHAMP N-S gradient or field data derived data set (see Figure 6d in Olsen et al. (2017)).

Alternative models such as EMAG2 (Maus et al., 2009), or WDMAM2 (Lesur et al., 2016) provide exceptional magnetic anomaly detail in many continental and oceanic regions, but are built using a range of data sets with differing resolutions, grids, and high variance in detail across different continents. Contrasts in grid spacing and resolution between regions with high-quality near-surface data and satellite models can result in artificial structures in the final Curie depth model, and thus we have chosen to utilise a globally consistent resolution satellite model instead. WDMAM2 and LCS-1 show similar anomalies and amplitudes at matching truncation, but in regions where near-surface data is sparse or non-existent the new LCS-1 satellite model provides improvements (Olsen et al., 2017). Additionally, high resolution variations in the lithospheric magnetic signature are unlikely to be derived from deep thermal anomalies, which is the focus of this article.

We compute the three vector components of the 'observed' lithospheric magnetic field of the observation points (i.e., the radial (r), colatitudinal (θ), and longitudinal (ϕ) vector components) at an altitude of 300 km using spherical harmonic degree 16–100. We chose to truncate the model at degree 100 as the level of detail from spherical harmonic degree 100 to 185 was beyond the resolution of our dipole positions, and thus contributed little to the final solution, and additionally saved on computational time.

As discussed in Section 5.2, only the induced component of the lithospheric magnetisation depends on the thickness of the magnetized layer, and thus we must ideally isolate the induced field from the observed lithospheric magnetic field. To this end, we remove a remanent magnetic field model for the oceans produced by Dyment and Arkani-Hamed (1998a) and Purucker

and Dyment (2000). Such a model does not exist for the continents as it's pattern in continental material are much less systematic as discussed above. Our 'observed' lithospheric induced magnetic field model is illustrated in Figure 5.3.

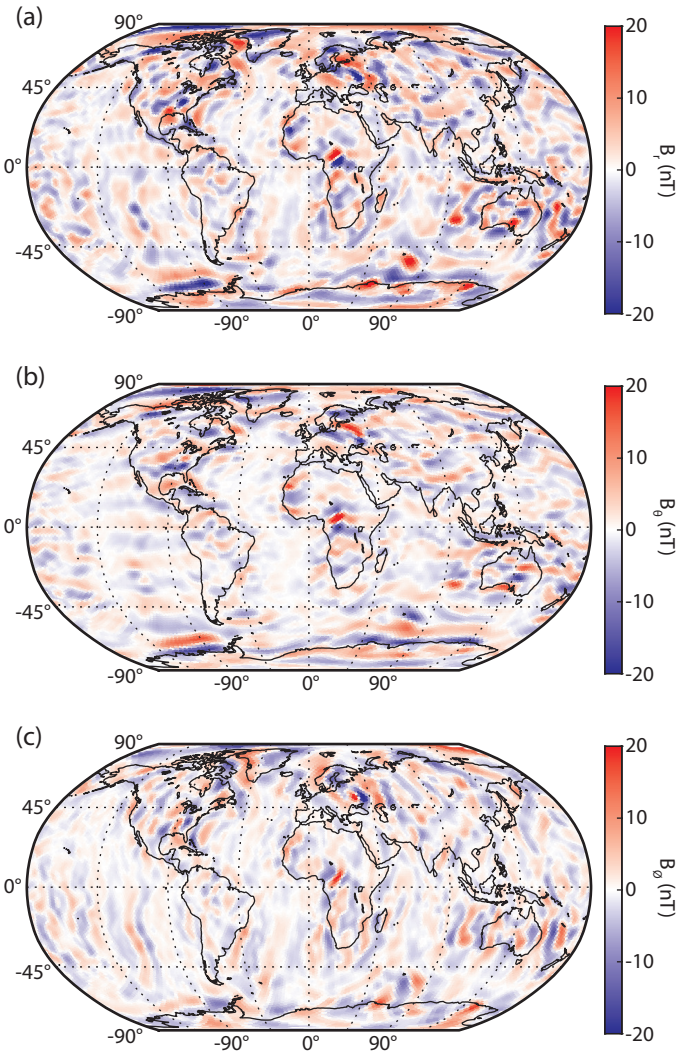

Figure 5.3: The LCS-1 magnetic field model components with the remanent oceanic field model removed: a) radial component, r; b) colatitudinal component, θ; and c) longitudinal component, ϕ

The inducing field, i.e. Earth's core field, is well described by various magnetic field models. For our purposes we utilise the CHAOS-6 magnetic field model (Finlay et al., 2016) from spherical harmonic degree 1 through 15 (CHAOS-6-x5, epoch 2018.1) and synthesize the induced field at each dipole location following methodology of Dyment and Arkani-

Hamed (1998b). We utilise a forward modelling procedure requiring an initial estimate of the magnetic crustal thickness, and improve the high order estimate (spherical harmonic degree 16–100) via iteration.

5.3.2 Long-wavelength supplement for magnetic crustal thickness

A crude separation of magnetic field sources (e.g., core and lithospheric contribution) at spherical harmonic degrees 15–16 can be accomplished through satellite derived magnetic field models. However, the long-wavelength magnetic crustal field cannot be distinguished from the core field from spherical harmonic degrees 1–15, and is thus set to 0. This limitation necessitates an initial estimate for the magnetic thickness (for spherical harmonic degree 1–15). In our case, we have used a hybrid model of the TC1 thermal model (Artemieva, 2006) for continental regions excluding Antarctica, the thermal model of 3SMAC (Nataf and Ricard, 1996) for the oceans and Antarctic continent. We synthesized a 580 ℃ isotherm from an extrapolation from the TC1 1300 ℃ $1^\circ \times 1^\circ$ model. It is likely, for many regions of the continental crust, that this model will be a sufficiently accurate estimate of the long-wavelength Curie isotherm field. This model is derived from relationships of tectonothermal ages of lithospheric terranes and a compilation of borehole heat flow measurements, as well as supplementation with xenolith P-T array and electrical conductivity data for the upper mantle. As detailed earlier, in general the depth to the bottom of magnetisation can be considered to be the 580 ℃ isotherm or the depth to the Moho, whichever is shallower. Thus the TC1/3SMAC thermal model was modified to be bounded by the Moho depth model of Szwillus et al. (2019) (see Figure 5.4b for the relative spatial contributions of each model), and the elevations from CRUST1.0 (Laske et al., 2012).

We prefer the TC1 model over the 3SMAC thermal estimate in most continental regions (used in Purucker et al., 2002; Fox-Maule et al., 2005, 2009; Hojat et al., 2016) as the 3SMAC model is a more simple plate thickness/age model applied to the crust. TC1 is systematically warmer than 3SMAC for most of the cratons. Plate thicknesses derived from seismic tomography tend to be larger than estimates produced by xenolith

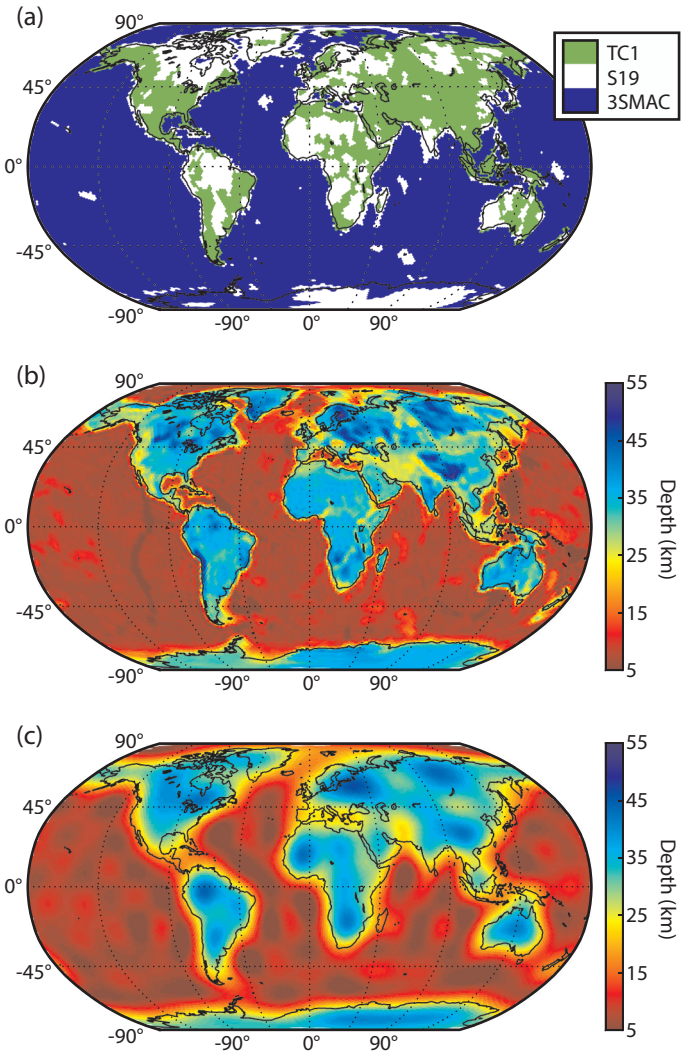

Figure 5.4: Constructing the spherical harmonic degree 1–15 initial Curie depth supplement model. a) Spatial diagram of the relative contributions from each model. TC1 (Artemieva, 2006)), 3SMAC (Nataf and Ricard, 1996), and S19 (Szwillus et al., 2019), b) TC1/3SMAC thermal model bounded by the Szwillus et al. (2019) Moho depth model, c) Spherical harmonic degrees 1–15 of the model in a).

thermobarometry (e.g. Hasterok and Chapman, 2011), which results in shallower Curie depths. On the whole, TC1 is a more robust estimate of the thermal structure, though there are still some poorly constrained areas. For example, the Tibetan plateau is likely a shallower Curie depth than TC1 suggests as evidenced by regionally extensive mid-crustal conductors at approximately 20 km depth (e.g. Sun et al., 2019; Unsworth et al., 2004). Conversely, in the Australian region the Archean Yilgarn and Pilbara Cratons likely exhibit a deeper Curie isotherm depth. However, Canada and North America appear much more in-line with expectations in TC1 as

opposed to 3SMAC, as is Siberia, North China and West Africa and the Congo area. Constraints on the thermal estimate for the Antarctic continent are borderline non-existent in the TC1 model. 3SMAC estimates for the Antarctic continent are more in-line with modern estimates of Curie depth (e.g. Martos et al., 2017), but in reality the signature would be far more heterogeneous than 3SMAC depicts. Nevertheless, we have chosen to utilise the 3SMAC model rather than TC1 for Antarctica. We also prefer using thermal models over crustal thickness models (e.g. CRUST1.0, Laske et al. (2012)) as crustal thickness is not necessarily correlated with the Curie isotherm depth.

5.3.2.1 Magnetic susceptibility

One of the largest assumptions in the ESMD method is the selection of a magnetic susceptibility model. Lithospheric magnetic field anomalies can be the product of variations in magnetic crustal thickness, or petrological variations resulting in changes of magnetic susceptibility (Purucker and Whaler, 2007). In truth, both parameters contribute in varying magnitudes and thus any solution is inherently non-unique. Assumptions of the relative dominance of these two parameters, or the application of assumed distributions or models for one of these parameters to obtain a unique solution is often required (e.g. Purucker et al., 2002; Hemant and Maus, 2005).

Although there is large heterogeneity in magnetic susceptibilities of different rocks, the typical compositions of continental and oceanic regions are largely coincidental, with a minor weighting towards higher susceptibility values for oceanic material due to greater proportions of elements such as iron, magnesium and titanium (Clark and Emerson, 1991). Some studies (e.g. Counil et al., 1991; Purucker et al., 2002; Fox-Maule et al., 2005; Purucker and Ishihara, 2005; Purucker et al., 2007; Fox-Maule et al., 2009; Rajaram et al., 2009; Thébault, 2010; Hojat et al., 2016; Lei et al., 2018; Jiao and Lei, 2019) make an assumption that the average susceptibility for these dipole positions, which are quite coarsely distributed, can be approximated crudely by a single isotropic estimate for continents and oceans. Conversely, other studies indicate lateral variations in magnetic

susceptibility are significant to the lithospheric magnetic field signature and should not be estimated with isotropic estimates. One such model of crustal magnetic susceptibility is that of Hemant (2003), which generated a vertically integrated magnetic susceptibility model based on seismic data, rock samples and geological domain maps. The approach of Hemant (2003) has a number of attractive features, and accounts for some of the magnetic features that are clearly not correlated with magnetic crustal thickness that a simple continental/oceanic model does not (Thébault and Vervelidou, 2015) (notable examples include regions of central Africa).

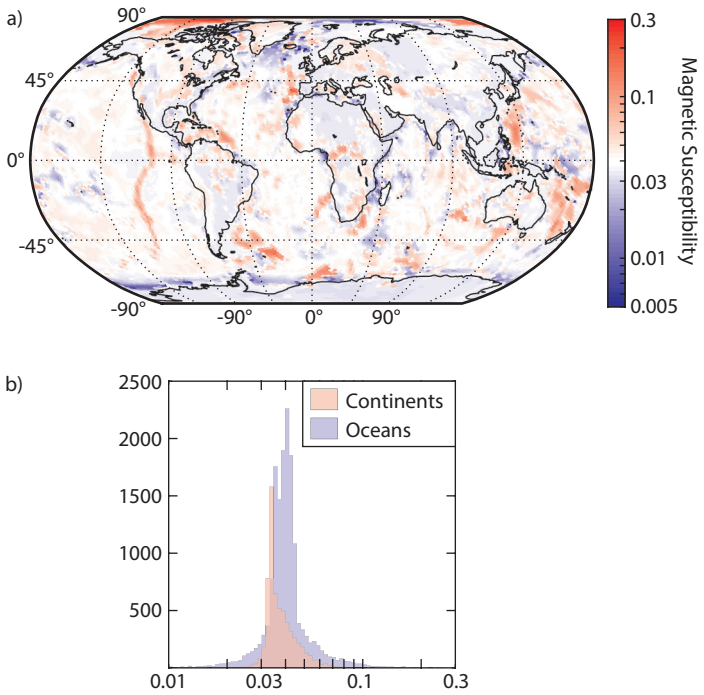

Figure 5.5: Magnetic susceptibility model utilised, modified from Hemant (2003) and Purucker et al. (2002). a) Spatial distributions. b) Histogram of continental and oceanic susceptibilities.

Nevertheless, the model of Hemant (2003) still contains a large number of broadband assumptions, and under-predicts the magnitude of a number of anomalies (Thébault et al., 2009). Thébault et al. (2009) suggest other world susceptibility distributions such as Purucker et al. (2002), may lead to their predictions falling within expected bounds of magnitudes for continents and oceanic anomalies, but that the Hemant and Maus (2005) model is a far better spatially variable estimate, and closer matches pre-

dicted magnetic field features. Thus, we seek a compromise whereby we use the mean continental and oceanic estimates akin to those often used in literature (e.g. Counil et al., 1991; Purucker et al., 2002; Fox-Maule et al., 2005; Purucker and Ishihara, 2005; Purucker et al., 2007; Fox-Maule et al., 2009; Rajaram et al., 2009; Thébault, 2010; Hojat et al., 2016; Lei et al., 2018; Jiao and Lei, 2019), but with the variation model from Hemant (2003) for the continents and oceans applied around this (Figure 5.5). We delineate oceanic and continental regions by the masking of continental borders in conjunction with bathymetry shallower than 800 m from ETOPO2 (National Geophysical Data Center, 2006). This spatially variable susceptibility model will ideally dampen the influence of magnetic susceptibility on the result such that remaining variations are dominantly a function of magnetic crustal thickness. The susceptibility model used here was generated from the vertically integrated susceptibility model (VIS) of Hemant (2003), divided by the crustal thickness model of 3SMAC (Nataf and Ricard, 1996). We find this susceptibility model produces satisfactory results, and permits crude interpretation of variances between different geological provinces due to magnetic susceptibility.

Vertical variations in magnetic susceptibility are not considered, as these likely only influence very small horizontal scales i.e. above spherical harmonic degree 650 (Langel and Hinze, 1998; Thébault and Vervelidou, 2015). Sedimentary basins were additionally not considered as a source of magnetisation (i.e. magnetic susceptibility set to 0).

5.3.3 Forward modelling of the magnetic thickness

From an initial magnetic crustal thickness estimate, the magnetic moment of each dipole is calculated, which in turn is used to synthesize a model for the vector components of induced magnetism (following the method of Dyment and Arkani-Hamed (1998b)).

From the initial magnetic crustal thickness model, the magnetic moment of each dipole is calculated which is used to synthesize the vector components of the model of induced magnetism as a result of these magnetization depths (following the method of Dyment and Arkani-Hamed (1998b)). A spherical harmonic expansion of the synthesized induced field from the

dipoles is made, and the terms below degree 16 are set to 0 to high-pass filter the magnetization model. The modelled induced magnetic field from the magnetic crustal thickness estimate is then compared to the 'observed' induced magnetic field model (LCS-1, with the oceanic remanent field model removed). If the difference between the modelled and observed magnetic field vector components is larger than a specified tolerance, an adjustment to the previous magnetic crustal thickness estimate is applied.

$$\Delta\bar{\mathbf{B}} = \bar{\mathbf{B}}_{\mathbf{obs}} - \bar{\mathbf{B}}_{\mathbf{model}} \tag{5.1}$$

$$\Delta\bar{\mathbf{B}} = \mathbf{G}\Delta\mathbf{m_j} \tag{5.2}$$

where $\bar{\mathbf{B}}_{\mathbf{obs}}$ is the lithospheric magnetic field model (Figure 5.3), $\bar{\mathbf{B}}_{\mathbf{model}}$ is the magnetic field produced by the magnetic crustal thickness estimate, $\mathbf{G}$ is a matrix related to the negative gradient of the magnetic potential of the dipole located at the observation points (see Fox-Maule et al. (2009)), and $\mathbf{m_j}$ is the magnetic moment of a dipole at observation point r_j.

Rather than constructing a $\mathbf{G}$ matrix that constitutes the influence of the entire set of global dipoles, we use a sparse version of the $\mathbf{G}$ matrix whereby only dipoles within a 2500 km radius are considered (Figure 5.2a) (See equations in Dyment and Arkani-Hamed, 1998b; Fox-Maule et al., 2009). This sparse matrix reduces the computational resources significantly, and dipoles outside a 2,500 km radius of the observation point are not major contributors to the magnetic field observed. We solve the system of linear equations using the conjugate gradient least-squares method. $\Delta\mathbf{h_j}$, which is directly proportional to $\Delta\mathbf{m_j}$ (See Fox-Maule et al., 2009, for equations), is then added directly to the previous estimate of $\mathbf{h_j}$, where $\mathbf{h_j}$ represents the estimated Curie depth. The process is repeated until the difference between the observed and modelled induced magnetic field vectors converges to within a specified tolerance; in our case, when the root mean square error for each vector component is below 0.05 nT. This tolerance was selected as it represents the energy carried by spherical harmonic degree 100 of the lithospheric field model, and more extensive iterations to refine the model beyond this point did not produce large improvements in the model and began to over-fit and amplify noise.

5.4 Global Curie depth model

Our updated magnetic crustal thickness model is presented in Figure 5.6a. We have recreated the model of Fox-Maule et al. (2009) using the MF5/CHAOS1 magnetic field model, two vector components (radial and co-latitudinal), and the initial magnetic crustal thickness derived from the crustal thickness and thermal estimates from 3SMAC (Nataf and Ricard, 1996) for comparison (Figure 5.7a). The differences between our preferred model and the model of Fox-Maule et al. (2009) can be seen in Figure 5.6b. These variations can be significant, with a number of continental areas exhibiting differences on the order of ±20 km.

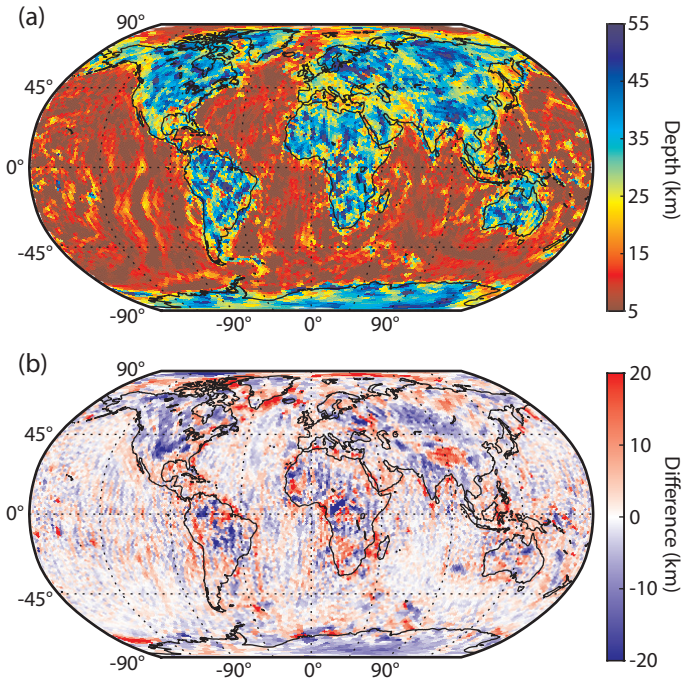

Figure 5.6: Updated ESMD derived global Curie depth model. a) Curie depth estimate of this article, consistent with the lithospheric magnetic field model LCS-1. b) Difference between the recreation of the Fox-Maule et al. (2009) model in Figure 5.7a and our model (i.e. subtracting the model of Fox-Maule et al. (2009) from our new model).

There are four major contributors to the variance between the previous model of Fox-Maule et al. (2009) and the model presented here:

1. Improvements due to utilisation of a newer satellite field model (LCS1, Olsen et al. (2017));

2. Variance due to a different initial magnetic crustal thickness model (and subsequently the inclusion of it's long-wavelength values in the final model);
3. the inclusion of the third vector component (ϕ); and
4. application of a variable magnetic susceptibility model.

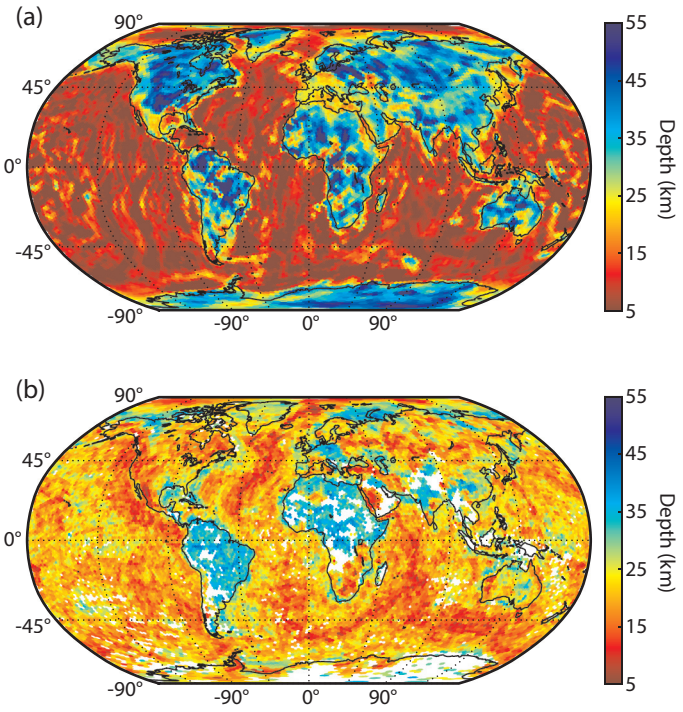

Figure 5.7: Global Curie depth models. a) Recreation of the Fox-Maule et al. (2009) model. b) Curie depth estimate of Li et al. (2017).

The largest contribution to the long-wavelength difference between our new model and the model of Fox-Maule et al. (2009) is due to the difference in long-wavelength Curie depth estimate. As discussed in Section 5.3.1, magnetic field models permit the crude separation of the core and lithospheric magnetic field sources, but the long-wavelength magnetic crustal field cannot be distinguished from the core field from spherical harmonic degrees 1–15, thus requiring an estimate from an additional source. Here we have utilised the hybrid TC1 thermal model of Artemieva (2006) and 3SMAC (Nataf and Ricard, 1996), bounded by the Moho estimates of Szwillus et al. (2019) as described in Section 5.3.2. Figure 5.4c depicts the low order contribution that remains in our final Curie depth model from

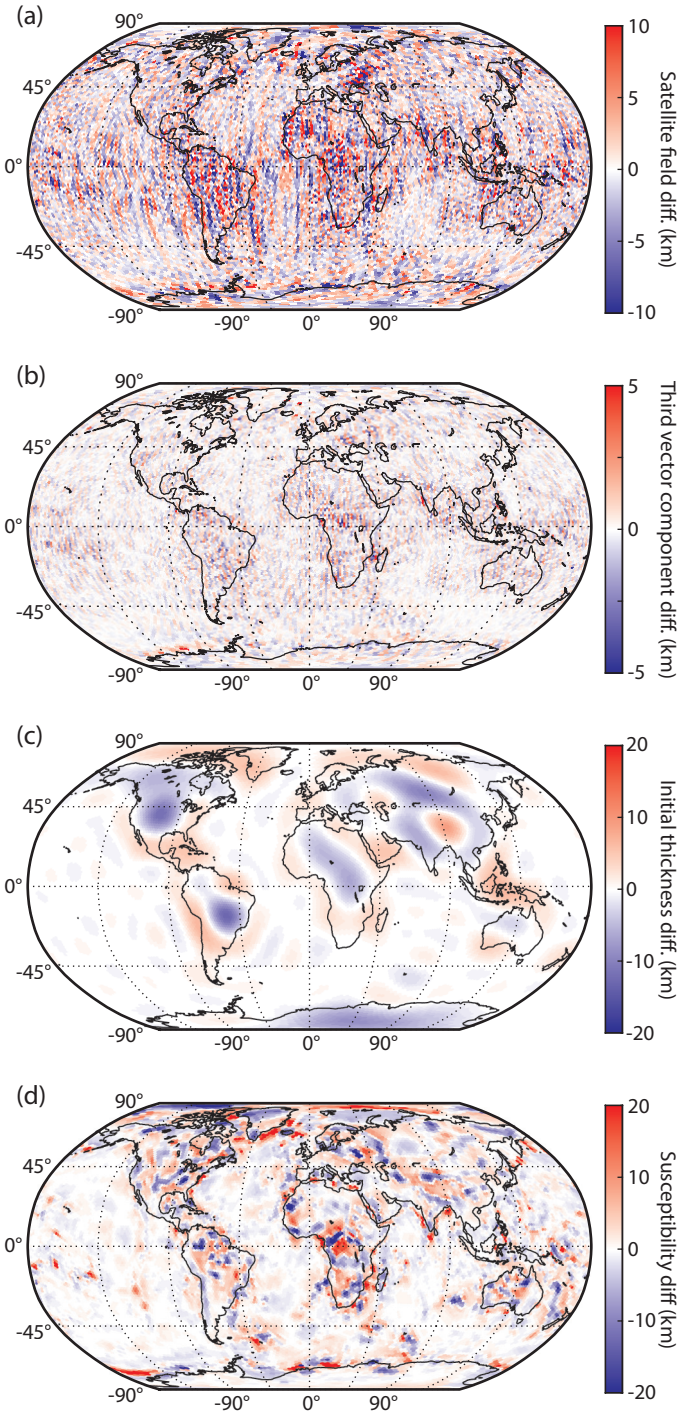

Figure 5.8: Variations in Curie depth estimate from the previous model of Fox-Maule et al. (2009) as a result of individual parameter changes. a) Differing satellite field model (LCS-1 vs MF5/CHAOS1) b) Two vs. three vector component solution c) Hybrid long-wavelength model of this article vs. 3SMAC only (spherical harmonic degrees 1–15) d) Magnetic susceptibility changes compared to Fox-Maule et al. (2009). A suite of models were calculated varying only one parameter at a time, and all differences are calculated by subtracting the old method from the new.

the initial estimate, and Figure 5.8c the difference between the 3SMAC thermally bounded estimate used in Fox-Maule et al. (2009) at these same spherical harmonic degrees. It can clearly be observed that this long-wavelength difference is present in the final model, with largest variance in North America, eastern south America and China (Figure 5.6b).

The influence of the magnetic susceptibility model applied is also of large significance; it's fingerprint evident in the final model (Figure 5.6b). Sharp contrasts in susceptibility estimates, such as central Africa and offshore Greenland (Figure 5.5a), are clearly visible in the final Curie depth estimates with variations. The Curie depth variations due to the spatially variable susceptibility model as opposed to the constant oceanic and continental values selected by Fox-Maule et al. (2009) are depicted in Figure 5.8d. The susceptibility model applied has dampened a number of sharp contrasts once associated with magnetic crustal thickness in Fox-Maule et al. (2009), particularly in central Africa.

Non-trivial improvements are also observed through utilisation of the LCS-1 magnetic field model as opposed to MF5. Suspicious stripes are present in the comparison figures of Figures 5.6c and 5.8a. These are present irrespective of inclusion of the E-W component in the modelling solution, and we suggest these are artefacts present in the MF5 magnetic model due to along-track noise, improved upon in LCS-1. This led to some anomalies presenting as more N-S trending in the previous Curie depth solution using this methodology in the previous global model of Fox-Maule et al. (2009).

To a lesser degree, enhancements have also been gained by utilising the longitudinal (ϕ) component of the magnetic field. This improvement contributes around 3.5% variation (1σ) on average globally between the two and three component solution (Figure 5.8b). Regions where one of the other components are zero show the most improvement due to the extra vector constraint. Additionally, minor oscillations observed along the magnetic equator in (Fox-Maule et al., 2009) appears to have been minimised further.

5.4.1 Comparison of Curie depth and heat flow

As the Curie depth is thermal in origin for large swathes of the continental crust, it is reasonable to expect a crude relationship between Curie depth estimates and measured heat flow. In Figure 5.9, we average the observed continental heat flow compilation from Lucazeau (2019) within each dipole surface area. These heat flow values are directly compared to the Curie depth estimate for continental regions (Figure 5.10a). Isotherms are constructed using exponentially decreasing heat production with a scale depth of 8 km, and varying thermal parameters to simulate crudely the expected natural scatter for continental regions.

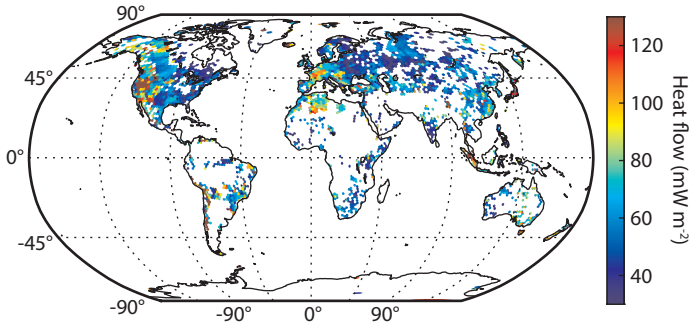

Figure 5.9: Heat flow data from Lucazeau (2019) averaged within each dipole area.

Obviously this comparison has a significant degree of variance. Thermal parameters such as heat production and thermal conductivity are able to vary significantly as depicted in Figure 5.10, but other near surface influences such as hydrothermal circulation, poor spatial sampling of heat flow, variances in the assumed parameters of the Curie depth modelling procedure, regions of lithologically bounded depth to magnetisation vs thermally controlled etc. all add to the observed scatter of the fit. Nevertheless, we show good agreement with the expected shape of average correlation between heat flow and Curie depth estimates (Figure 5.10a). We also show a tighter clustering of the Curie depth-heat flow estimates of the previous ESMD derived global Curie depth model of Fox-Maule et al. (2009) (Figure 5.10b).

An alternative global Curie depth model is also compared; the fractal magnetization model by Li et al. (2017) (Figure 5.7b). Li et al. (2017) show

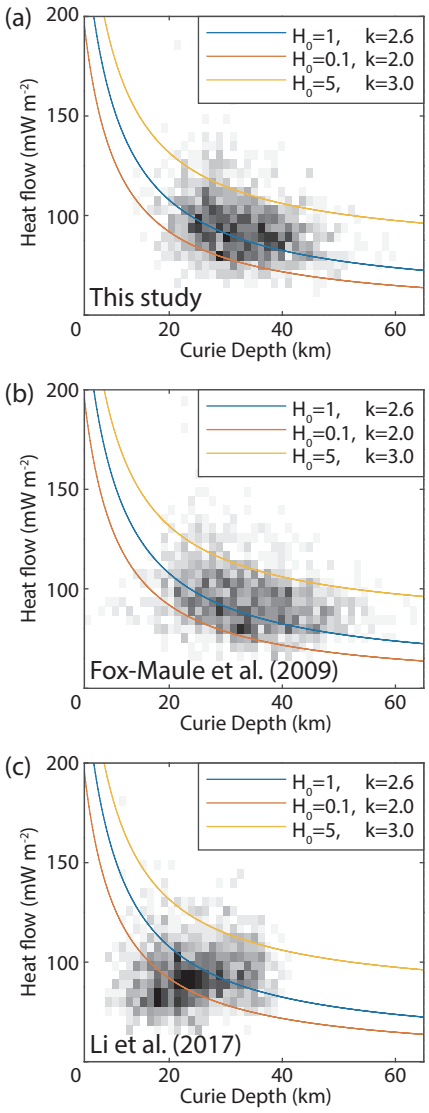

Figure 5.10: Comparison of Curie depth estimates against measured continental heat flow compilation of Lucazeau (2019). a) This study, b) the model of Fox-Maule et al. (2009), c) the model of Li et al. (2017). Curves in a), b) and c) depict expected heat flow for a Curie depth estimate when assigned simple thermal parameters denoted on graph. Thermal Conductivity (k) applied is constant for the crustal column, and heat production (H_0) denotes the surface heat production with an exponentially decreasing curve with depth, with scale depth of 8 km.

an excellent correlation to oceanic age, topography, and mid-ocean ridges, more-so than our Curie estimate where this information is not entirely clear. However, the average magnitude of their Curie depth estimates for the oceans are generally in excess of oceanic crustal thickness estimates. There is also a systematic difference in magnitude of Curie depth's across the globe, with those derived from the ESMD method in this article, and similarly for Fox-Maule et al. (2009), generally being deeper than the model of Li et al. (2017), and showing markedly higher intensity variations in intra-continental areas.

Unfortunately Li et al. (2017) do not provide an uncertainty estimate and it is hard to assess our variance in relation to their model. While we estimate relatively large uncertainties (Section 5.4.2), some long-wavelength trends of the Li et al. (2017) model (Figure 5.7b) show large anomalies with respect to thermal models and heat flow observations (Figure 5.9) (e.g. Artemieva, 2006; Lucazeau, 2019). Some stark examples include South-East Africa and Western Australia where heat flow is quite low, but the Curie depth estimate for both of these locations is very shallow. Conversely, Eastern Australia is markedly warmer than Western Australia from the heat flow data. Additionally Eastern South America, Ontario and Quebec in Canada, much of Europe including Germany, and Russia show seemingly better correlations with observed heat flow data.

The most obvious explanation for such stark mean variations between the ESMD method and the method of Li et al. (2017) is that our long-wavelength supplement model may perhaps account for the systematic variation, despite being well correlated with estimates from heat flow and thermal models such as 3SMAC and TC1. Thus, we have also compared just the higher frequency variations of Li et al. (2017) and our model (Figure 5.11a and b, respectively). While our model shows higher intensity variations at these shorter wavelengths, we also observe a number of similar features with that of Li et al. (2017). For example, south-eastern Africa is much similar than the long-wavelength comparison, and North America shows similar perturbations across the continent. However, many regions still exist with stark variations including Australia, Antarctica and Germany that are clearly not just a simple by-product of the long-wavelength supplement model.

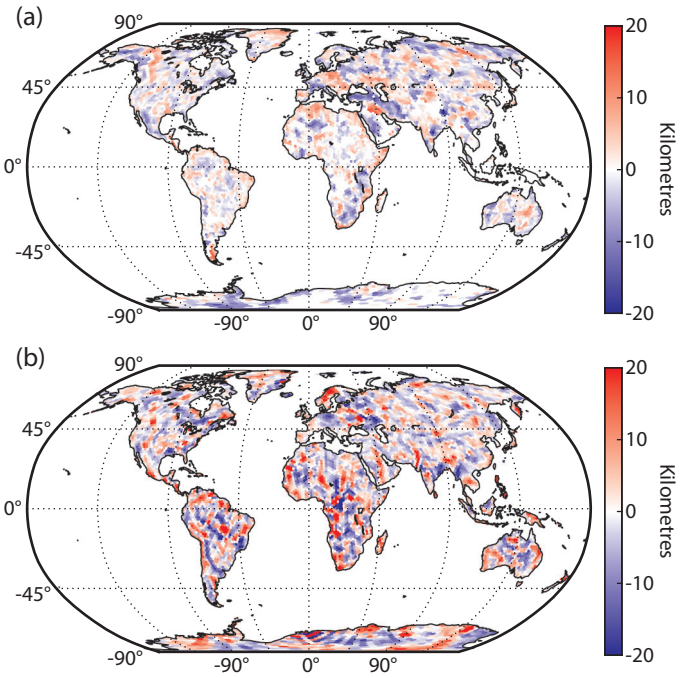

Figure 5.11: Comparison of only the short wavelength variations of the Curie depth result with Li et al. (2017). a) Li et al. (2017), b) This study.

5.4.2 Deficiencies, uncertainty estimates, and future work

As we have utilised a lithospheric field model, any uncertainties in its derivation propagate directly into the uncertainty of our Curie depth estimate. Assuming comparisons of models produced via different lithospheric field models is an indicator of uncertainty; we observe variance (1σ) of 5.82%, 10.55%, 11.37% respectively when utilising the lithospheric field models MF7, WDMAM and LCS-1. We suggest the use of a more conservative estimate of 15%, and this additionally is more in-line with previous discussions of lithospheric field model uncertainties (Lowes and Olsen, 2004; Fox-Maule et al., 2009).

While we have removed a remanent magnetic field model for the oceans, we have not done so for the continents as no reliable model currently exists. Where applicable, this remanent magnetism may have significant influence on the lithospheric magnetic field observed. Some studies indicate that the majority of magnetic lithospheric field anomalies globally can likely be attributed to induced rather than remanent magnetism in the continents (Counil et al., 1991; Maus and Haak, 2002). Quantifying the uncertainty

due to this parameter is rather ambiguous, so we defer to previous estimates of uncertainty related to continental remanent magnetism of around 20% (Fox-Maule et al., 2009).

Based on the variance ranges of the Hemant (2003) model for magnetic susceptibility, we observe an uncertainty of ±15.5% for continents and oceans separately. However, we acknowledge that solutions of magnetic crustal thickness vs. magnetic susceptibility are inherently non-unique, and that our final Curie estimate is proportional to the a priori susceptibility model applied. We estimate a more generous upper bound of around 25%, and appreciate that in some regions this can be easily exceeded (See Figure 5.8d). It is our hope that the variation model modified from Purucker et al. (2002) and Hemant (2003) has helped to at least dampen the effects of susceptibility variations, and appears to be the case from Figure 5.6a and b.

An initial estimate for the magnetic thickness is required to supplement the long-wavelength (spherical harmonic degree 1–15) of the Curie depth solution. The lowest order terms of our initial magnetic crustal thickness estimate are thus directly transferred to our final result. The contribution to the final magnetic crustal thickness model that will persist through modelling is presented in Figure 5.4c i.e., spherical harmonic degrees 1–15 of the spherical harmonic expansion of the Moho bounded TC1 model in Figure 5.4a. As the longest-wavelength solution is controlled entirely as a result of the initial model fed into the process, it constitutes the largest variance. We believe the hybrid model of TC1 (Artemieva, 2006) and 3SMAC (Nataf and Ricard, 1996) constrained by the Moho depths of Szwillus et al. (2019) constitutes a more modern and improved long-wavelength model than the 3SMAC estimate alone, which has fallen out of favour in recent years in some seismic studies (e.g. Xing and Beghein, 2015). That being said, regions still exist where this combined model appears to not perform well; the Antarctic continent being a notable example. Uncertainty in the long-wavelength model is directly translated into the final Curie solution. While the Moho uncertainty in general is relatively low for many of the higher resolution continental regions (4 km), TC1 constitutes over 66% of the continental long-wavelength solutions. 3SMAC and TC1 differ on the order of ±10.5% (1σ) for continental regions, and we

suggest this gives an indication of the uncertainty in the long-wavelength model. Fox-Maule et al. (2009) estimate an uncertainty on the order of 7% due to the initial long-wavelength mode, but this seems too small given the variance between 3SMAC and TC1.

Although we have produced an absolute value for Curie depth in this article, it is proposed that the short-wavelength solutions which are ultimately the target of the modelling process presented here are the most applicable result (Figure 5.11c). Employing the high-wavelength solutions of magnetic crustal thickness in conjunction with independent long-wavelength estimates of the thermal state of the crust, for example thermal isostasy or seismic tomography, may yield a more holistic thermal result. Additionally, utilising other data sets such as geochemistry may assist in restricting thermal parameters to more appropriate regional values if wanting to estimate heat flow from these Curie depth solutions. The variance about expected generalised heat flow-Curie depth relationship depicted in Figure 5.10b is the result of many factors, including Curie depth estimation uncertainty, potential existence of meaningful continental remanence, major lithological variations, and regions where the depth to the bottom of magnetisation may not correlate with the Curie isotherm at all, such as at depths below the Moho or where lithological boundaries define sharp contrasts in magnetisation. Such models are the focus of future work. Despite all this, our modelling produces a magnetic crustal thickness estimate that is consistent with the lithospheric magnetic anomalies of the magnetic field model LCS-1, as well as providing a reasonable fit to expected thermal correlations.

Work to reconcile large variations in mean magnetic crustal thickness between different methodologies must be addressed. It is unclear why the model of Li et al. (2017) and the methodology of Purucker et al. (2002) can produce such large variations in mean magnetic crustal thickness. The methodology of Li et al. (2017) seems to resolve spatial variations in the oceans well in regard to age and spreading rate expectations, but some regions of the continents show some very questionable Curie estimates when compared to heat flow data. By removing the long-wavelength supplement field from our model it appears to reduce variations between the model we

have presented here and the model of Li et al. (2017) for some regions such as North America, but regions such as Australia still show stark contrasts.

As a result of the high degree of variance in thermal parameters we have decided that the calculation of a global heat flow model is beyond the scope of this article. While studies of global heat loss may justify a need for globally averaged thermal parameters, care must be taken when utilising the results of these studies for localised regions. Heat production can vary significantly on very small spatial scales (Hasterok and Webb, 2017; Gard et al., 2019c,b; Hasterok et al., 2018), and lead to dramatically different heat flow estimates for the same Curie depth estimate. Thus for localised heat flow estimates, it is highly suggested that other data sets be utilised to help constrain these parameters. For example, geochemical sample properties, basement geology knowledge, existing heat flow measurements, temperature profiles, and other geophysical proxies may be used to constrain temperature such as seismic velocity and thermal isostasy. This will be explored in a future study.

5.5 Concluding remarks

We have produced an updated global Curie depth estimate utilising the equivalent source magnetic dipole (Purucker et al., 2002; Fox-Maule et al., 2009). Results show variations up to ±20 km in contrast to the previous global estimate derived via ESMD methods by Fox-Maule et al. (2009). Utilisation of a hybrid initial magnetic crustal thickness model built from TC1 (Artemieva, 2006), 3SMAC (Nataf and Ricard, 1996), and a Moho depth estimate from Szwillus et al. (2019), as well as the laterally variable magnetic susceptibility model modified from Hemant (2003) and Purucker et al. (2002) dominate the variations. Differences are also associated with the improved satellite lithospheric field model (LCS-1, Olsen et al. (2017)) which refined along track noise present in the previous iterations of this method, as well as the inclusion of the third vector component in the forward model. Regions such as central Africa show the most improvement due to application of the variable susceptibility model, but continents with poor constraints such as Antarctica require further work. Curie depth estimations share a crude pattern to the previous iteration of Fox-Maule et al.

(2009), but show large differences in the mean estimates with respect to the fractal methods of Li et al. (2017). The results of this article match both the LCS-1 lithospheric magnetic field model at 300 km altitude, as well as being consistent with observed surface heat flow. This model provides further evidence that Curie depth estimates are sensitive to the thermal state for large amounts of the continental lithosphere, and may be used to help constrain temperature and heat flow estimates, especially in regions with sparse or surface contaminated heat flow observations.

5.6 Acknowledgements

We would like to thank Liejun Wang for his comments on the article, and two anonymous reviewers for their comprehensive suggestions that markedly improved the article structure. A number of scripts were adapted from codes from Simons and Dahlen (2006), and Frederik Simons provided helpful communications. Additionally, thank you to Azadeh Hojat, Bernhard Steinberger and Nils Olsen for providing assistance with data sets. The support of Geoscience Australia is gratefully acknowledged.

M. Gard was supported by an Australian Government Research Training Program Scholarship. This research was supported partially by the Australian Government through the Australian Research Council's Discovery Projects funding scheme (project DP180104074).

CHAPTER

SIX

ANTARCTIC HEAT FLOW ESTIMATES DERIVED FROM GEOPHYSICAL PROXIES: THERMAL PARAMETER ESTIMATES AND UNCERTAINTIES

Gard M.[12], Hasterok D.[13]

[1]School of Physical Sciences,
University of Adelaide, Adelaide, Australia
[2]Geoscience Australia,
Canberra, Australia
[3]Mawson Geoscience Centre,
University of Adelaide, Adelaide, Australia

Unsubmitted manuscript format

Statement of Authorship

Title of Paper	Analysis of Antarctic heat flow estimates derived from geophysical proxies: Thermal parameter estimates and uncertainties
Publication Status	☐ Published ☐ Accepted for Publication ☐ Submitted for Publication ☑ Unpublished and Unsubmitted w ork w ritten in manuscript style
Publication Details	

Principal Author

Name of Principal Author (Candidate)	Matthew Gard		
Contribution to the Paper	Conception of ideas Collated data Programming, visualisation, and modelling Data interpretation Manuscript writing		
Overall percentage (%)	90		
Certification:	This paper reports on original research I conducted during the period of my Higher Degree by Research candidature and is not subject to any obligations or contractual agreements with a third party that would constrain its inclusion in this thesis. I am the primary author of this paper.		
Signature		Date	02/06/2021

Co-Author Contributions

By signing the Statement of Authorship, each author certifies that:

i. the candidate's stated contribution to the publication is accurate (as detailed above);

ii. permission is granted for the candidate in include the publication in the thesis; and

iii. the sum of all co-author contributions is equal to 100% less the candidate's stated contribution.

Name of Co-Author	Derrick Hasterok		
Contribution to the Paper	Assistance with programming and modelling Supervised and aided data interpretation Manuscript editing and feedback		
Signature		Date	5/5/21

Abstract

Estimating surface heat flow from geophysical proxies typically requires application of generalised vertical thermal parameter models of the crust. Disparities in thermal parameters applied in different studies can magnify variances in final heat flow solutions, even when the isotherms estimated from geophysical proxies show many similarities. This is of particular importance to the Antarctic continent to produce meaningful ice sheet and glacial models. In this study, I propose new generalised models for heat production and thermal conductivity based on global information sourced from geochemistry, and guided by global scale continental studies, with uncertainties associated with this model are estimated via a Monte Carlo solution. The uncertainty model produced shows around 20% increase over that published in some previous models. Around 40-50% of independent heat flow estimates are satisfied within uncertainty, and 90% of lake derived heat flow minimums are exceeded. Mean misfit of the median heat flow produced in this study to independent heat flow estimates show residuals of 0.71 mW m^{-2} and standard deviation of 27.68 mW m^{-2}. Uncertainty distributions are approximately log-normal or log-logisitic, closer resembling heat flow distributions observed globally, compared to Gaussian statistics presented in previous studies. I show that applying generalised global parameters provides a reasonable fit to the Antarctic continent and provides a way of estimating uncertainty in a region with poor basement geology constraints.

6.1 Introduction

As the Antarctic continent hosts the largest single mass of ice on the planet, the current and future stability of the ice-sheets has been a focal topic in studies involving climate change and future sea level rise. Therefore, it is critical that we understand the basal thermal inputs into the Antarctic ice sheet for estimating and modelling ice sheet dynamics and stability. Heat flux from the crust and mantle can impact basal ice temperatures; consequently influencing a number of mechanical and physical properties including degree of basal sliding, distribution of sub-glacial lakes

and basal melt-water, along with the ice-sheet mass balance (Pollard et al., 2005; Van Liefferinge and Pattyn, 2013; Schroeder et al., 2014). Although essential for a number of modelling procedures, the heat flow into the base of the ice sheet is poorly constrained. Direct measurements of heat flux in Antarctica are extremely limited (e.g. Fisher et al. (2015)), and those that do exist have yet to reach bedrock, largely a function of the difficulty in penetrating the extensive ice cover. Consequently, the primary source for continent and regional scale heat flow estimates for the Antarctic continent are through various geological and geophysical proxies. Some examples include ice temperature profiles (Engelhardt, 2004), geological sampling and glacial moraine testing (Carson et al. (2014); Goodge (2018)), previously conjugate terrane studies (Pollett et al., 2019), satellite and airborne magnetic-derived estimates (Fox-Maule et al., 2005; Purucker, 2013; Martos et al., 2017), and estimates based on seismic velocities and tomography (Shapiro and Ritzwoller, 2004; An et al., 2015). Estimates from geophysical proxies are routinely used in studies related to ice sheet dynamics (e.g. Pattyn, 2010; Van Liefferinge et al., 2018).

It is often noted that the geophysical proxy derived estimates show variance in mean values at large scales, and high spatial variability at smaller scales (see Burton-Johnson et al. (2020) for a review of current Antarctic heat flow models). The disparities create issues when attempting to determine uncertainties in models derived from these heat flow estimates. Van Liefferinge and Pattyn (2013), for example, average the heat flow estimates available due to the large variability between the models. A number of these models require estimates of continental thermal parameters such as the vertical thermal conductivity and radiogenic heat production profiles through the crust, which imparts further discrepancies in final heat flow estimates. The differences in these thermal models can be considerable, often obscuring variations due to modelling procedures.

I have selected four commonly cited heat flux models derived from geophysical proxy methods for the Antarctic continent to discuss:

1. the Curie depth (Equivalent source magnetic dipole method) derived heat flux estimate of Fox-Maule et al. (2005),

2. the Curie depth (Equivalent source magnetic dipole method) derived heat flux estimate of Purucker (2013) (updated from Fox-Maule et al., 2009),

3. the seismic velocity relationship of An et al. (2015), and

4. the Curie depth (De-fractal spectral method) derived heat flux estimate of Martos et al. (2017).

In this study, I compare and discuss the selection of continental thermal parameters used in a number of existing heat flux models for Antarctica that are derived from geophysical proxies, and instead propose generalised models based on global geochemistry and continental studies. Uncertainty in the heat flow maps derived from these models is estimated using the Monte Carlo method.

6.2 Background

Owing to the distinct lack of subglacial bedrock information for the majority of Antarctica, the primary methods of continental-scale heat flux estimates have involved the use of geophysical proxies such as active and passive seismics, gravity, and geomagnetics.

The Curie depth is the depth at which magnetic material loses its ferromagnetic properties and becomes functionally non-magnetic, considered generally to be about 580 ℃ if magnetite is the dominant magnetic mineral (e.g. Wasilewski and Mayhew, 1992; Clark and Emerson, 1991; Langel and Hinze, 1998). A number of studies have demonstrated that there is a relationship between surface heat flux and the depth to the bottom of the magnetised layer, particularly for the continents (e.g. Mayhew, 1982; Okubo and Matsunaga, 1994; Purucker et al., 2002). Magnetic-derived estimates use satellite, aeromagnetic and/or near-surface data to estimate the depth to the bottom of the magnetic crust, and then typically apply a thermal parameter model to estimate crustal temperatures and surface heat flow. Two methods are common, both of which have been used to estimate the Curie depth in Antarctica; the equivalent source magnetic dipole

(ESMD) method employed by Fox-Maule et al. (2005) (and later by Fox-Maule et al. (2009)/ Purucker (2013)), and the defractal spectral method applied by (Martos et al., 2017) (Figure 6.1 a, b and d respectively).

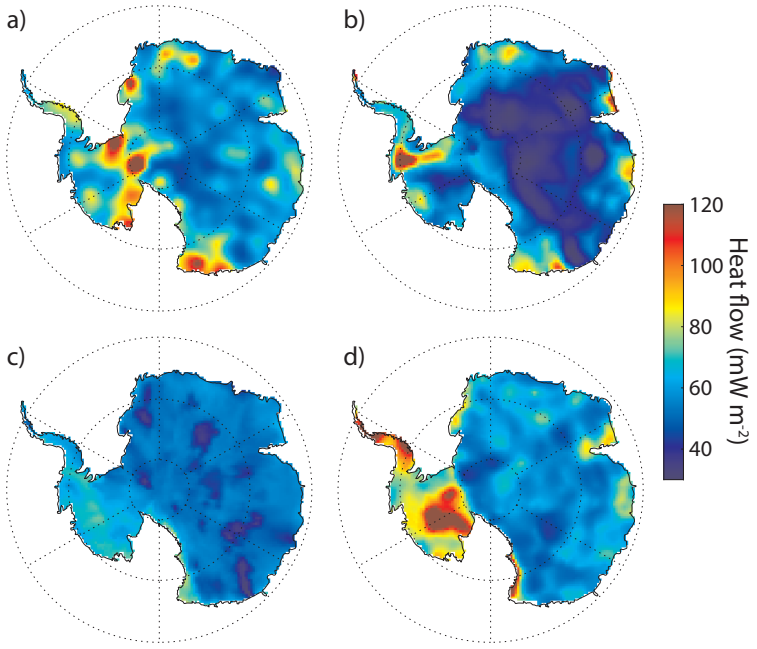

Figure 6.1: Antarctic heat flow models examined in this study: a) Satellite-derived Curie depth model by Fox-Maule et al. (2005), b) Satellite-derived Curie depth model by Fox-Maule et al. (2009)/Purucker (2013), c) Seismic model of An et al. (2015), d) Aeromagnetic and satellite-derived Curie depth model from Martos et al. (2017).

Alternatively, seismic velocity relationships have been used to estimate temperatures in the upper mantle. An et al. (2015) estimated upper mantle temperatures utilising a similar method to Goes et al. (2000), whereby shear wave velocities are transformed into temperature estimates through knowledge of mantle mineral properties and forward modelling. Crustal temperatures are estimated using the seismically-derived mantle temperatures as anchors along with assumed thermal properties of the crust (Figure 6.1c).

The proxies discussed give an estimate for temperature at depth that requires extrapolation to the surface. The variance in heat flux estimates derived from these methods has been the topic of discussion in recent years (e.g. Burton-Johnson et al., 2020), and is often noted in studies of the cryosphere where estimates of heat flow are most pertinent (e.g. Van Li-

efferinge et al., 2018). While these models show a general consensus of warmer geotherms in the West Antarctic compared to the East, the estimated heat flow values can vary significantly at all spatial scales across the continent (Figure 6.1). All of the models predict a continental average heat flux around 50-70 mW m^{-2}; however, local variations exceed 100 mW m^{-2} for all model combinations, and some even up to 170 mW m^{-2}. Fox-Maule et al. (2005) and Martos et al. (2017) models show the most agreeable magnitudes in general across West and East Antarctica. However, the model from Martos et al. (2017) shows some exceptionally high heat flux values in the Ross Ice Shelf region (up to 240 mW m^{-2}) (Figure 6.1d). Conversely, An et al. (2015) predicts a model mostly devoid of sharp anomalies in heat flux, but emulates the general trend of warmer West Antarctic values, albeit at lower magnitudes. The model of Fox-Maule et al. (2009)/Purucker (2013) shows a much colder East Antarctic than the other models and exhibits sharp contrasts in heat flux values near a number of its edges (Figure 6.1c).

While the methodology for determination of the isotherm depths is often complex, the extrapolation to generate a surface heat flow value is often not addressed satisfactorily. The vertical distribution, magnitudes and uncertainty windows for thermal parameters can have significant variance when looking at global data sets. The question arises; is the variance observed in the heat flow estimates of Antarctica a result of large deviations in estimated depth to the isotherms calculated from the geophysical proxy methods, or is it an artificial byproduct of the selection of thermal parameters for the continent? A simple way to remove the influence of assigned thermal parameters to the crust is to compare the depth to the isotherm estimate directly. For most of the models discussed here, this constitutes the Curie depth. In the case of the seismically derived model of An et al. (2015), this isotherm estimate is based in the upper mantle, and as such the depth to the Curie isotherm in this case will be partially contaminated by the thermal parameters applied to the lower crust. However, as the lower crustal thermal parameters applied in the An et al. (2015) model are quite small, their influence is minor.

The differences in the long wavelength heat flow models are not always reflected in the Curie depth estimates from each of these studies (Figure 6.2).

For example, although Fox-Maule et al. (2009) depict broadly similar Curie depth models to that of their previous model (Fox-Maule et al., 2005) and the more recent model by Martos et al. (2017) (Figure 6.2), there exists stark contrasts in the heat flow estimates produced, particularly for East Antarctica (Figure 6.1). The model of An et al. (2015) also exhibits some of the shallowest Curie depth estimates, which would lead one to expect it might also have one of the warmest heat flux estimates when a generalised continental crust model is applied. In fact, the opposite is true (Figure 6.1c). It is clear even from these simple comparisons that the selection of thermal parameters applied to these models has had a marked influence on the final estimates of surface heat flow.

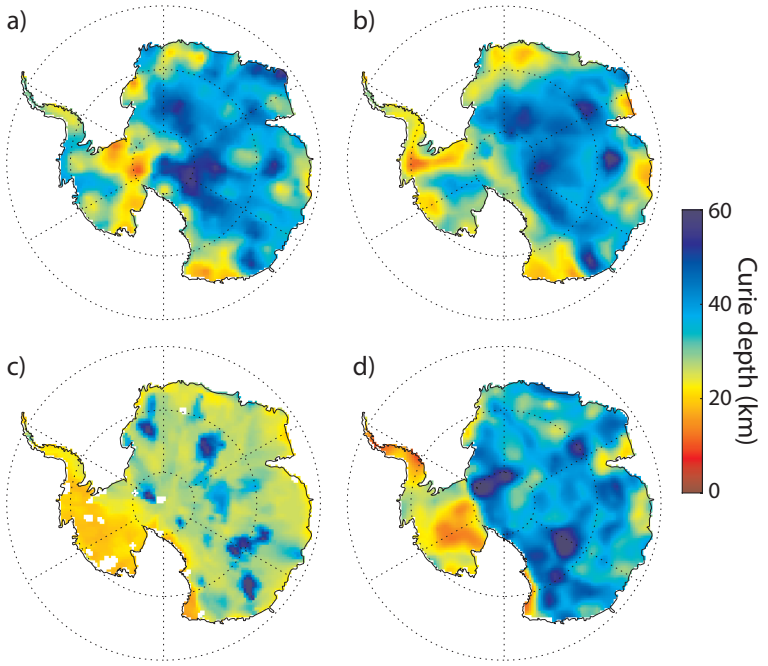

Figure 6.2: Estimates to the depth to the Curie isotherm: a) Fox-Maule et al. (2005), b) Fox-Maule et al. (2009)/Purucker (2013), c) An et al. (2015), d) Martos et al. (2017).

6.2.1 Comparison of crustal thermal parameters

To estimate surface heat flow from a proxy-derived temperature at depth requires application of a thermal parameter model to the crust. Most studies apply a generalised heat production and thermal conductivity profile based on continental averages and studies from the literature (e.g.

Pinet and Jaupart, 1987; Clauser and Huenges, 1995; Rudnick and Fountain, 1995; Artemieva and Mooney, 2001; Kukkonen and Lahtinen, 2001; Artemieva, 2006; Hasterok and Chapman, 2011). Generally studies make use of the steady-state 1-D heat conduction equation with a number of common assumptions including no lateral variations in thermal parameters, such that;

$$K\frac{\partial^2 T(z)}{\partial z^2} = -A(z) \tag{6.1}$$

and,

$$q(z) = -K\frac{\partial T(z)}{\partial z} \tag{6.2}$$

where q is the heat flow, K is the thermal conductivity, T is temperature, A is the heat production, and z depth.

I apply each of the thermal models summarised in this article to a synthetic example to demonstrate their variability, particularly with depth. In this scenario, the surface is denoted as $Z_0 = 0$ km, a Curie depth of $Z_c = 30$ km, and upper, middle and lower crustal thicknesses of 10 km (Figure 6.3).

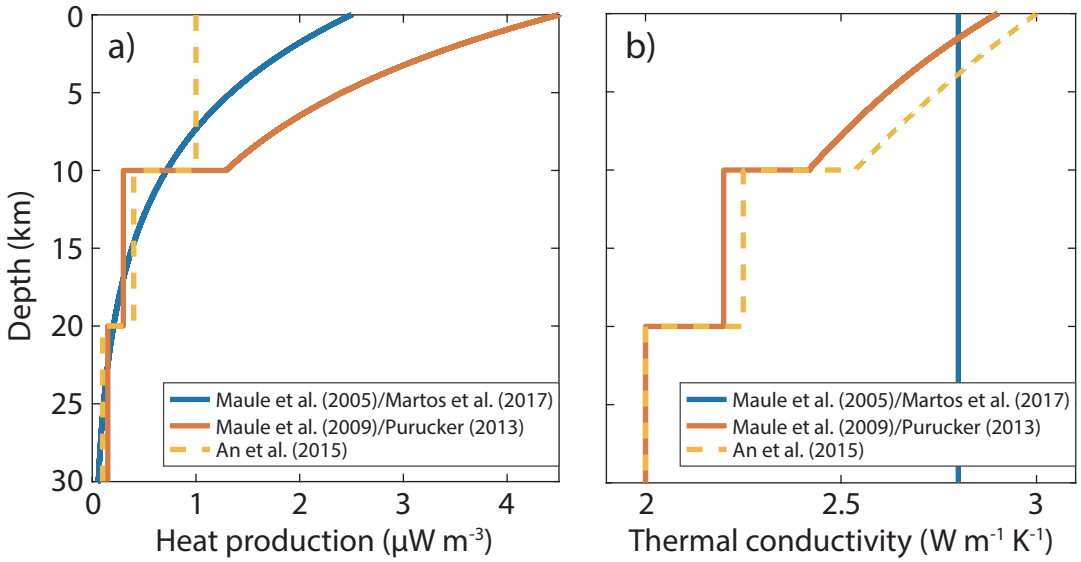

Figure 6.3: a) Heat production models with depth in a synthetic crust scenario; Upper, middle, and lower crust are set to 10km, Curie depth/Moho depth of 30km. Fox-Maule et al. (2009)/Purucker (2013) set upper crustal heat production to much higher distributions than An et al. (2015) and Martos et al. (2017). b) Thermal conductivity profiles of the various Antarctic models applied to the same synthetic depth model for comparison. Martos et al. (2017) and Fox-Maule et al. (2005) apply a much simpler constant thermal conductivity model.

Popularised by Lachenbruch (1970), the exponentially decreasing heat production with depth is now a common representation used in literature for crustal thermal models. Fox-Maule et al. (2005) and Martos et al. (2017) make use of this model with identical parameters; a scale depth of 8 km, surface heat production of 2.5 μW m^{-3}, and a fixed thermal conductivity profile of 2.8 W m^{-1}K^{-1}(Figure 6.3a). In the case of Fox-Maule et al. (2005), the heat production parameters were selected based on studies such as Sandiford and McLaren (2002). Thermal conductivity was then selected to force the average continental surface heat flow value of Antarctica to around 65 mW m^{-2}, in-line with the global average heat flow estimates from Pollack et al. (1993), and lied within the broad range of 1.5-3.5 W m^{-1}K^{-1}for most rocks described in Clauser and Huenges (1995). Justifications for the selection of the thermal parameters from Martos et al. (2017) is not particularly clear. The authors detail optimization of the parameters due to a number of input data sets; ice temperature profiles, ice balance studies etc. but ultimately use identical values of that of Fox-Maule et al. (2005) for thermal conductivity, heat production and scale depth.

Alternatively, layered models were used in the later model of Fox-Maule et al. (2009), as well as the seismic derived surface heat flow estimate of An et al. (2015). These models provide an arguably more realistic geometry, with similarly decreasing radiogenic heat production with depth. As thermal conductivity is well understood to be inversely proportional to temperature (Clauser and Huenges, 1995), both the model of Fox-Maule et al. (2009) and An et al. (2015) apply a temperature sensitive thermal conductivity profile in the upper crust that is solved iteratively. Additionally, a decreasing thermal conductivity profile with deeper crustal sections is applied (Figure 6.3b). At depth, most rocks converge to around 2-2.5 W m^{-1}K^{-1} thermal conductivity (see Goes et al. (2020) for a summary).

There are considerable differences in the heat production models used by the heat flow studies of Antarctica, especially in the upper crust (Figure 6.3a). While Fox-Maule et al. (2009) constitutes the highest upper crustal heat production estimate by a reasonable margin, this result is not surprising considering calibration was done with respect to the Australian

continent. It is well understood that regions of central and southern Australia exhibit anomalously high heat production concentrations (at least two or three times the global average) with respect to similar aged global terranes (Neumann et al., 2000; McLaren et al., 2003). Although Australia was once a conjugate terrane with Antarctica, and some of the higher heat producing regions may persist into East Antarctica (Pollett et al., 2019), it is unlikely to be representative of East Antarctica as a whole. Other conjugate terranes, such as southern India, show low heat flow and crustal radiogenic heat (e.g. Gupta et al., 1991).

Fox-Maule et al. (2009) and An et al. (2015) share very similar vertical thermal conductivity models, including a temperature dependent model for the upper crust that is solved for iteratively. Conversely, Fox-Maule et al. (2005) and Martos et al. (2017) use a simpler model whereby a single value is applied for all depth slices of the crust. A constant value of thermal conductivity of 2.8 W $m^{-1}K^{-1}$across the continent seems rather high, particularly when extrapolated to the lower crust where it typically converges to values of around 2-2.5 W $m^{-1}K^{-1}$(Clauser and Huenges, 1995; Whittington et al., 2009; Goes et al., 2020).

In regions such as Antarctica where sub-surface geology and vertical structure is largely a mystery owing to the extent and thickness of the ice sheets, these assumptions of laterally fixed parameter models and crude continental average models can be justified, however the quantification and acknowledgement of the significant uncertainty associated with them must be clearly defined. As can be observed in Figure 6.4a, average heat production models show reasonable variance in the literature. Each of the studies discussed above cite differing sources and studies for their justifications of selection of thermal parameters. These non-trivial variations imparts a direct influence that further exacerbates variations of the final heat flow solutions of the models discussed above. Accurate quantification of the uncertainty is just as important if not more so than the model itself (Burton-Johnson et al., 2020).

6.2.2 Summary of thermal parameter uncertainty estimates from Antarctic models

Discussion and quantification of uncertainty associated with the selection of thermal parameters varies appreciably between different publications.

The seismic velocity model of An et al. (2015) frames their brief discussion of uncertainty in terms of their estimated LAB depth and the variance in terms of temperature. Discussion on the variability of thermal parameters is unfortunately limited in the context of surface heat flow.

Fox-Maule et al. (2005, 2009) apply broad uncertainties to the thermal parameters (around 10-15% for thermal conductivity, and 40 to 60% for heat production), and do not compute a spatially variable estimate of thermal parameter or total uncertainty in their heat flow model.

The most in depth uncertainty analysis of the geophysical proxy heat flow models is provided by Martos et al. (2017), whereby they calculate a laterally variable uncertainty estimate in a more numerical manner. By assuming variables are independent, they estimated uncertainty in the heat flow related to the selection of thermal parameters by way of the uncertainty propagation equation, i.e.;

$$\Delta q_{s,thermal} = \sqrt{\left(\frac{\partial q_s}{\partial K}\Delta K\right)^2 + \left(\frac{\partial q_s}{\partial h_r}\Delta h_r\right)^2} \tag{6.3}$$

where Δh_r is the scale depth of an exponential heat production model and is set to 3 km, and uncertainty due to the thermal conductivity terms (i.e. $\frac{\partial q_s}{\partial K}\Delta K$) is set to a fixed value of 10 mW m^{-2} (estimated from Fox-Maule et al. (2005)). Other uncertainties such as those associated with constant temperature surface and Curie isotherm boundaries are ignored as their influence is assumed to be small.

While the uncertainty model of Martos et al. (2017) constitutes a more involved attempt of assessment of uncertainty over some previous models, I believe this underestimates the uncertainties in the heat flow estimate. The most glaring deficiency is the exclusion of the surface heat production term (H_0) from the uncertainty propagation equation. This parameter is

independent of the h_r estimate, and arguably more important than the h_r term in terms of the vertically integrated heat production profile. By using a fixed H_0 value they have significantly restricted the permissible heat production profiles, and vertical radiogenic heat variability is only permitted in a small band (Figure 6.4b). Additionally, the thermal conductivity model used by Fox-Maule et al. (2005) and Martos et al. (2017) likely significantly over estimates lower crustal conductivities, and uncertainty due to the estimate is generalised to a simple constant term of 10 mW m^{-2}.

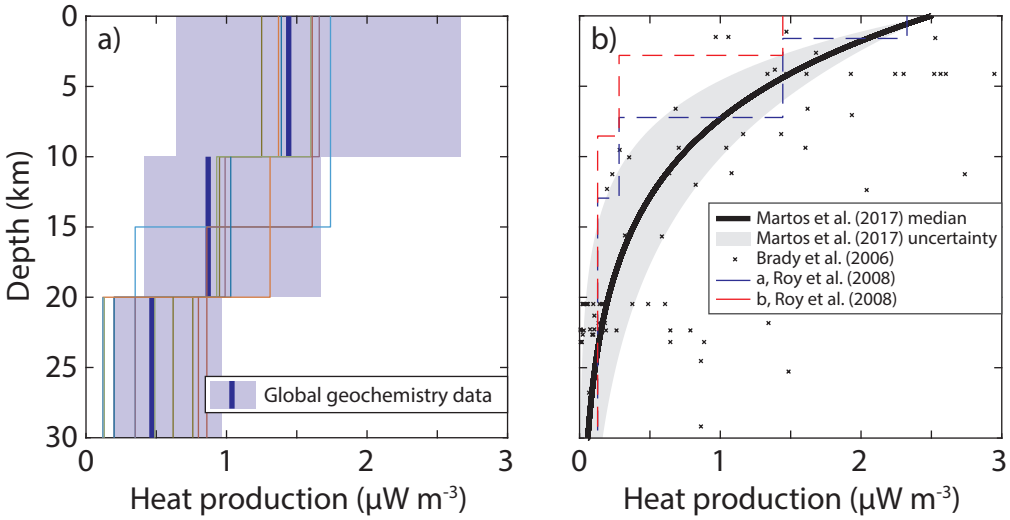

Figure 6.4: Comparison of vertical models for heat production. Thin lines with depth are various crustal models for heat production of average continental crust compiled in Goes et al. (2020). See Goes et al. (2020) Table S2 for a full summary. a) Blue shaded regions are uncertainty windows (1-σ) for granodiorite, diorite and gabbroic diorite for the upper, middle and lower crust respectively. Dark blue thick lines are the median for each synthetic layer. Derived from global whole-rock geochemical data from Gard et al. (2019b). b) Shaded region is uncertainty band for the heat production model published by Martos et al. (2017), with black line marking the median model. Cross points mark the heat production with depth from the Sierra Nevada Batholith as seen in Brady et al. (2006) rescaled to a Moho depth of 30km, and dashed lines represent vertical heat production profiles from Roy et al. (2008) for the Closepet Batholith.

When projecting a simplified model to a region of poor geological knowledge, as is required in regions such as Antarctica, it is very important that the large uncertainty associated with the model selection is adequately defined. For most continental regions, upper crustal rocks have a higher heat production relative to the bulk crust. This general decrease in heat production with depth is inferred through heat flow and heat production

observations, whereby the total radiogenic crustal contribution would exceed the observed surface heat flow if extrapolated to depth (Mareschal and Jaupart, 2013), as well as through bulk compositional crustal studies (e.g. Rudnick and Gao, 2003). As heat producing elements are highly incompatible, they may be redistributed via partial melting (Perry et al., 2006), or via processes such as tectonic redistribution (Sandiford and McLaren, 2002) or hydrothermal alteration by groundwater (Gosnold, 1987). The vertical profile of heat production through the crust at any location is a function of it's unique tectonic and magmatic history, and as such cannot be easily described or predicted with any high confidence (e.g. Ketcham, 2006).

For much of this article, I draw comparisons to the uncertainty estimates of Martos et al. (2017). This is not to be critical of the model provided, but because it is one of the only models to conduct a laterally variable uncertainty estimate.

6.3 Methods

I propose a new generalised layered model guided by continental average studies from literature and constrained by whole-rock geochemical data. Associated uncertainties are then estimated using the Monte Carlo method.

A multitude of studies have attempted to estimate average continental crust compositions (Goes et al., 2000, Table S2), and a number of these have been plotted using our synthetic crustal parameters used previously to compare the thermal models (Figure 6.4a). Ideally, any vertical profile model that is applied under the pretense of 'continental average composition' would roughly fall in-line with these models. Although variability exists, a loose commonality exists between the various models whereby the average upper crust is of granodiorite composition, the middle crust of dioritic composition, and the lower crust of diorite/gabbroic diorite composition (Goes et al., 2020). It is from these equivalent rock types that I estimate our heat production uncertainty windows using global geochemical data.

6.3.1 Heat Production

Under the presumption of 'average continental crust', I can analyse the variability of heat production for each of these rock types by looking at global compilations. Gard et al. (2019b) collated 1,022,092 global whole-rock geochemical samples including major and trace element concentrations, isotopic ratios, and location information, in conjunction with physical property estimates computed on a major element normalized version of the geochemical data. Radiogenic heat production shows large variability within rock types, for example, granodiorite exhibits a range of heat production from 0.6 to 2.6 μW m^{-3}, diorite from 0.4 to 1.6 μW m^{-3}, and gabbroic diorite from 0.2 to 0.96 μW m^{-3} (1σ). These windows of uncertainty are depicted in Figure 6.4a for upper, middle and lower crust, respectively. I use these ranges for rock type variability as an approximation of the uncertainty in each of the layer radiogenic heat production estimates, under the assumption the crustal column is of 'average' continental composition. For the Antarctic continent I use the crustal thickness model of Pappa et al. (2019), with upper, middle and lower crustal depths crudely estimated as equal partitions of this thickness model (See Figure 6.5 for further details).

Figure 6.4b depicts a few observed vertical profiles; measurements of heat production from exposed terranes and estimated depths in the Sierra Nevada Batholith by Brady et al. (2006), and two 'representative' crustal columns constructed by Roy et al. (2008) for the Closepet Batholith. These examples give an idea of the considerable variability possible in the vertical stratification of radiogenic heat production.

6.3.2 Thermal conductivity

To get a rough idea of the variability in thermal conductivity of upper crustal continental samples, one can look at the global heat flow database from Hasterok (2010). While the conductivity associated with heat flow estimates are a mix of inferred and measured, the distributions of these can give an idea of the range of variability that might be expected in the Antarctic continent without a priori information. Figure 6.6 depicts this

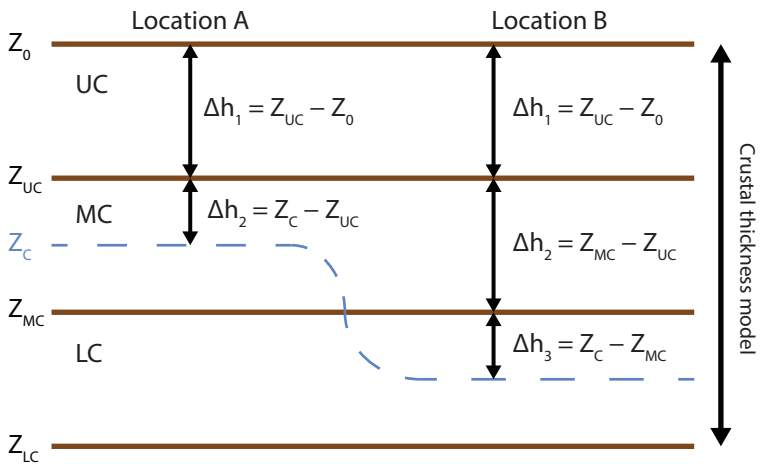

Figure 6.5: Schematic of Crustal thickness model for estimating heat producing layer thicknesses. The selected crustal thickness model (Pappa et al., 2019) is divided equally into three layers; a simple upper, middle and lower crustal model where Z_0, Z_{UC}, Z_{MC} and Z_{LC} are the surface, and the bottom of the upper, middle and lower crust, respectively. The relative contribution from each of these approximated layers to the modelled surface heat flow is based on the Curie depth model's intersection with these layers (Z_C). For example, Location A's Curie depth estimate intersects the middle crust. As such, the surface heat flow estimates are derived as a function of the vertical integration of the heat production down to this point (the total of the upper crust, within Δh_1, a partial contribution from the middle crust, within Δh_2, and no contribution from the lower crust). Conversely, at Location B the Curie depth estimate intersects the lower crust, and thus the lower crustal heat production model partially contributes to the heat flow estimate according to the interval defined by Δh_3. In both cases, the heat flow estimate is additionally constrained by the estimate of the Curie depth and temperature.

distribution. The range of thermal conductivities, as well as the median value, seem offset from previous discussions of crustal and upper continental thermal conductivities (e.g. Clauser and Huenges, 1995). I suggest that this thermal conductivity set is likely biased as a result of sedimentary basin measurements. Thermal conductivity is a function of quartz content, porosity and fluid content, as well as temperature and pressure. These factors show highest variability in near surface sedimentary samples and would not be representative of the crust as a whole. Studies of thermal conductivity at depth show that at higher temperatures most rocks converge to values around 1.5–2.5 W $m^{-1}K^{-1}$ (e.g. Vosteen and Schellschmidt, 2003). Estimates for upper crustal conductivity are also highly variable, but a recent study by Goes et al. (2000) suggests the average composition is likely granodioritic and that an average surface thermal conductivity

of around 2.7 W $m^{-1}K^{-1}$ may be a reasonable estimate, converging to 2–2.5 W $m^{-1}K^{-1}$ at the base of the lower crust for most rock types.

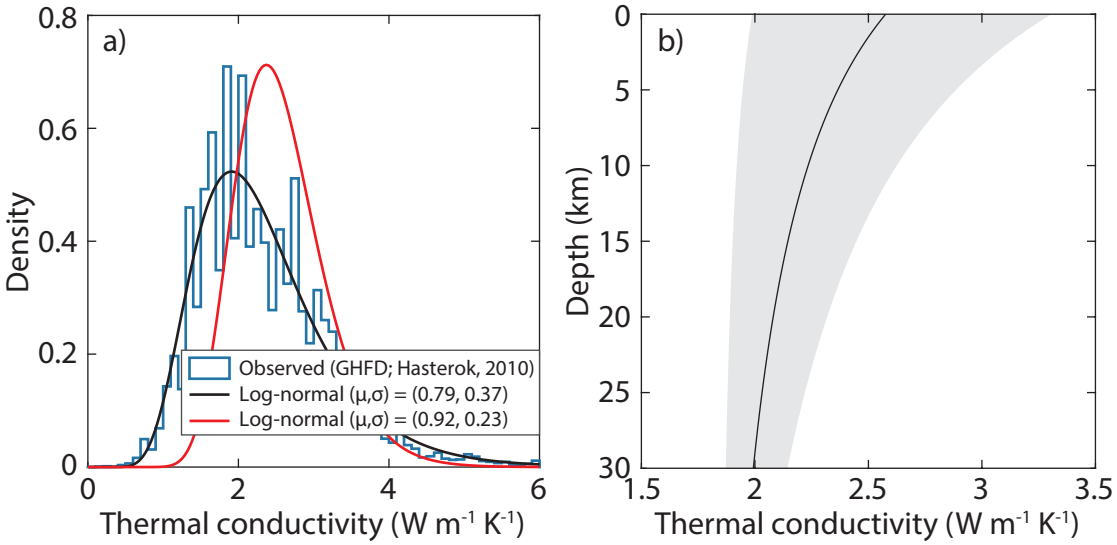

Figure 6.6: a) Thermal conductivity data and estimates from a global heat flow database (Hasterok, 2010). Black curve denotes the log-normal best fit to the data, and the red curve our synthetic estimate of a better fit for continental igneous uncertainty (Refer to Section 6.3.2). b) Synthetic example of thermal conductivity with depth for an example temperature profile from 0-400 °C with the conductivity-temperature model of Sekiguchi (1984) applied to a starting surface thermal conductivity k_0 derived from the red curve in a).

I make use of a synthetic model for surface thermal conductivity (k_0) derived from the adjusted thermal conductivity log-normal model from Figure 6.6a. These are then projected to depth using the thermal conductivity-depth model of Sekiguchi (1984), as shown by Lee and Deming (1998) to provide a reasonable estimate for igneous rocks;

$$k(z) = k_a p + \left(\frac{T_0 T_m}{T_m - T_0}\right)(k_0 - k_{ap})\left(\frac{1}{T(z)} - \frac{1}{T_m}\right), \tag{6.4}$$

where T_0 is the temperature at the surface (set to 298K), and k_{ap} and T_m is the thermal conductivity and temperature at 'the assumed point' (set as 1.8418 W $m^{-1}K^{-1}$ and 1473 K respectively as suggested by Sekiguchi (1984)), and $T(z)$ the temperature profile in Kelvin.

As this model is dependent on the temperature profile, I solve for the thermal conductivity model and temperature profile iteratively from a starting

guess until the maximum difference in temperature profile from one iteration to the next converges to below 10^{-5} K. Figure 6.6b depicts the uncertainty and median thermal conductivity with depth in our synthetic scenario of a Curie depth of 30 km.

6.3.3 Monte Carlo input parameters

For the estimate of radiogenic heat production variability, I generate kernel density functions for each rock type of granodiorite, diorite, and gabbroic diorite for the upper, middle and lower crust respectively from Figure 6.4. The synthetic thermal conductivity variability model discussed in Section 6.3.2 randomly samples for k_0 and iteratively solves a vertical thermal conductivity profile consistent with temperature, and I also permit the surface temperature (T_0) and Curie temperature (T_c) to vary with a Gaussian distribution with standard deviation of ±15 ℃ . Curie depth uncertainty estimates provided by Martos et al. (2017) are also included as Gaussian uncertainties for each Curie point. For each data point, 100 layers through the crust are used and 10^5 random samples from the distributions defined above.

6.4 Results and Discussion

The 0.159, 0.5 and 0.841 quantiles of the heat flow models produced via Monte Carlo simulation can be observed in Figure 6.7. I estimate a mean heat flow of 64.72 mW m^{-2}, with lower and upper bounds of heat flow of 52.94 and 80.84 mW m^{-2}, respectively. The most notable differences to the model of Martos et al. (2017) (Figure 6.1d) are the smoother transition between the divide of East and West Antarctica, the heat flow of both the West Antarctic rift and region adjacent to Victoria Land and the Ross ice shelf show values not quite as extreme, and East Antarctica has a minor increase heat flow estimates in general.

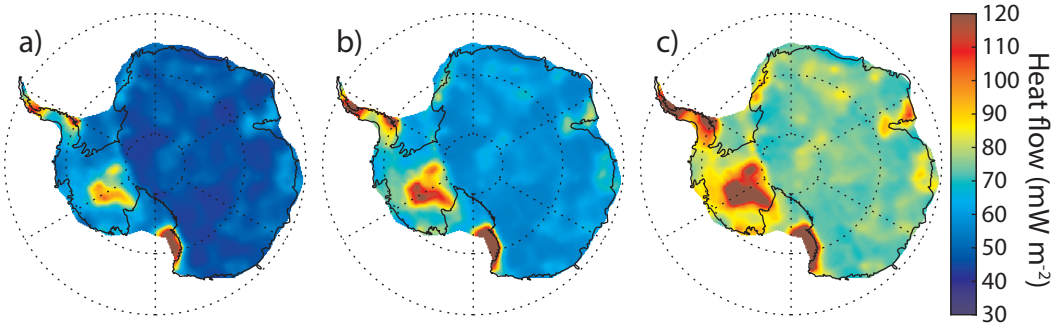

Figure 6.7: Estimated heat flow and uncertainty from Monte Carlo assessment using global estimates of heat production and thermal conductivity distributions. a) 0.159 quantile, b) Median , and c) upper 0.841 quantile produced via a Monte Carlo solution.

6.4.1 Model comparison and uncertainty

The uncertainty estimate of Martos et al. (2017) is much more involved than previous Antarctic heat flow models. Nevertheless, some deficiencies in the uncertainty propagation equation used are evident. First, surface heat production is ignored, which has a critical influence on the exponential heat production model used, restricting the uncertainty band to a very tight region (shaded region of Figure 6.4b). Additionally, by using the uncertainty propagation in the form presented in Equation 6.3, the uncertainty is presented as Gaussian. Heat flow is inherently non-Gaussian; non-linearity of heat production distribution and the steady-state heat flow equation mean that heat flow is closer in shape to a log-normal or log-logistic distribution. The uncertainty model presented in this paper is derived from much more robust estimates on the continental average compositions and the variability associated with those rock types from the geochemical database of Gard et al. (2019b). Additionally, by making use of the Monte Carlo method, and distributions for the radiogenic heat production and thermal conductivity as observed globally, our heat flow uncertainty estimates are also non-Gaussian, with the distribution of heat flow looking approximately log-normal. I estimate a mean increase in uncertainty over that which was proposed by Martos et al. (2017) of around 20–25% for much of the Antarctic continent. Not only is the uncertainty greater on average, but the distribution of the uncertainty in heat flow from the Monte Carlo model is also closer to the distributions observed in surface heat flow, i.e., similar in shape to a log-normal or log-logisitic

distribution, rather than Gaussian uncertainty models that have been used in previous models (Figure 6.8).

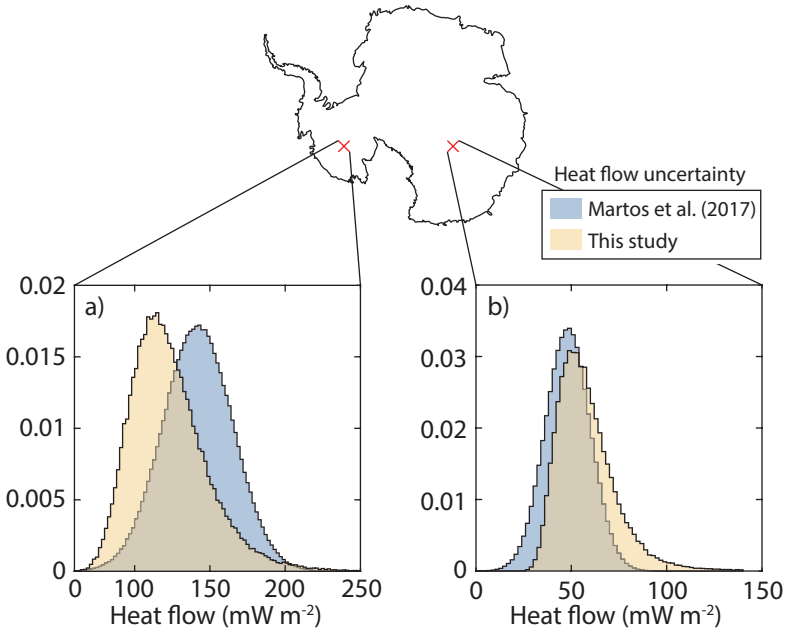

Figure 6.8: Comparison of heat flow uncertainty distributions of this study and that of Martos et al. (2017). a) A point selected in West Antarctica, and b) a point from East Antarctica. Note the resemblance to a log-normal or log-logistic distribution produced from this study, compared to the Gaussian model of Martos et al. (2017).

A considerable caveat to the modelling presented here, and one that is normally not discussed, is the fact that all of our uncertainties estimated here are under the strict assumption that the entire continent of Antarctica is of average composition, i.e., equal thicknesses of granodiorite, diorite, and gabbroic diorite for the upper, middle and lower crust respectively. While I have included large uncertainty windows for these, the assumption of an average rock type is still a large assumption considering the complexity of tectonic histories and lithologies at local, regional and continental scales. The uncertainty due to variability of rock type laterally and with depth is likely considerable, and extremely difficult to quantify numerically. No single place in the world is likely to follow the average vertical stratification applied in our model, or any of the other models in literature. Some examples of vertical radiogenic heat production profiles are depicted in Figure 6.4b. Additionally, not only is the strict rock type of the layers a source of uncertainty, but also the geometry of the layers. There is no

evidence-based reason to assign three equal layers; most regions have a complex vertical structure consisting of numerous geologically distinct layers, which ultimately adds a considerable amount of uncertainty that is extremely difficult to quantify numerically.

6.4.2 Validation to independent heat flow estimates

While direct heat flow estimates are considerably lacking due to the extensive ice cover, other methods exists for constraining heat flow in Antarctica. Recently, Guimarães et al. (2020) compiled the heat flows reported in Martos et al. (2017), additional estimates derived from the 'Magmatic Heat Budget (MHB)' method of Vieira and Hamza (2019) whereby known volcanic regions are used to loosely constrain heat flow, and minimum heat flow estimates for basal melting for regions of known subglacial lakes following the method of Robin (1955)(Figure 6.9a, b and c respectively).

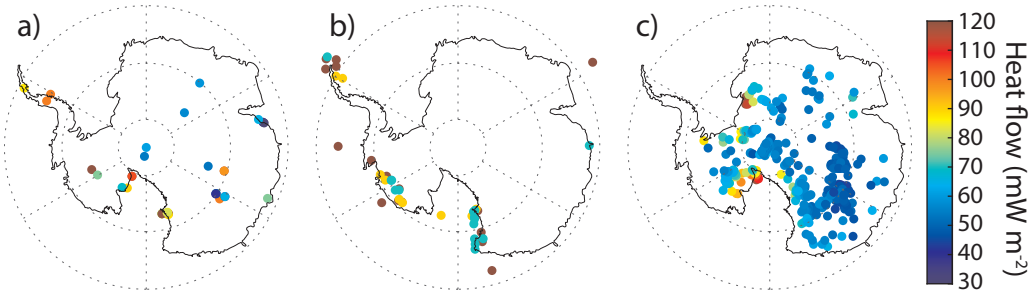

Figure 6.9: Independent heat flow estimates compiled in Guimarães et al. (2020). a) Previously compiled heat flow as found in Martos et al. (2017), b) Heat flow estimates derived from the Magmatic Heat Budget (MHB) method of Vieira and Hamza (2019), c) Minimum heat flow based on lake locations and the method of Robin (1955).

I compare these independent heat flow estimates to the results produced in this study; if uncertainty windows between the independently estimated heat flow estimates overlap with the heat flow model uncertainty model produced in this study they are considered 'satisfied'. In the case of lakes, if any of the uncertainty window of our estimated heat flow lies above the estimated minimum lake heat flow then it is also considered satisfied. Our results indicate that 47.2% of the heat flow data compiled in Martos et al. (2017) is satisfied, versus 41.67% by the Martos et al. (2017) heat flow model. For lakes, 91.22% of the lake locations show estimated heat flow in

excess of the minimum lake heat flow compiled in Guimarães et al. (2020), compared with 85.37% by the Martos et al. (2017) thermal parameter model. The MHB derived estimates show an equal measure of fit of 48.39% for both thermal parameter models.

I also produce a more typical residual plot of the misfits to the independent heat flow estimates compiled in Guimarães et al. (2020) in Figure 6.10. Without any calibrations or modifications, our median heat flow model exhibits a mean misfit of only 0.71 mW m^{-2}, and standard deviation of 27.68 mW m^{-2}. As the crustal models were not calibrated to Antarctic specific data this result is somewhat surprising. The model generated via Monte Carlo simulation from global data sets performs at least as good, if not better, than some previous models that in some cases are calibrated. The main purpose of these models was to emphasise the variability and scatter that is possible (as observed in Figure 6.10) and that uncertainties should be represented by non-Gaussian models (Figure 6.8).

There is a slight positive bias in the misfit as a number of the independent heat flow estimates are from minimum lake heat flow models, as discussed in Section 6.4.2.

6.4.3 Continent-wide calibration considerations

Arguments have been made for calibration of thermal parameters at the continental scale, but calibrations at this scale must be considered carefully. Fox-Maule et al. (2009) used the Australian continent Curie depth estimate, and heat flow data, to calibrate their thermal parameter model which they then applied to the Antarctic continent. Conversely, Martos et al. (2017) suggested calibration directly with an undefined subset of the heat flow data in Antarctica.

One should be hesitant in conducting a calibration for an entire continent based on a handful of data points. Geological terranes can change drastically across a continent, leading to changes in heat production across several orders of magnitude. Age and lithology heavily dominate radioactive element enrichment (e.g. Slagstad, 2008; Kukkonen and Lahtinen, 2001; Gard et al., 2019c), but even if the basement age and lithology of Antarc-

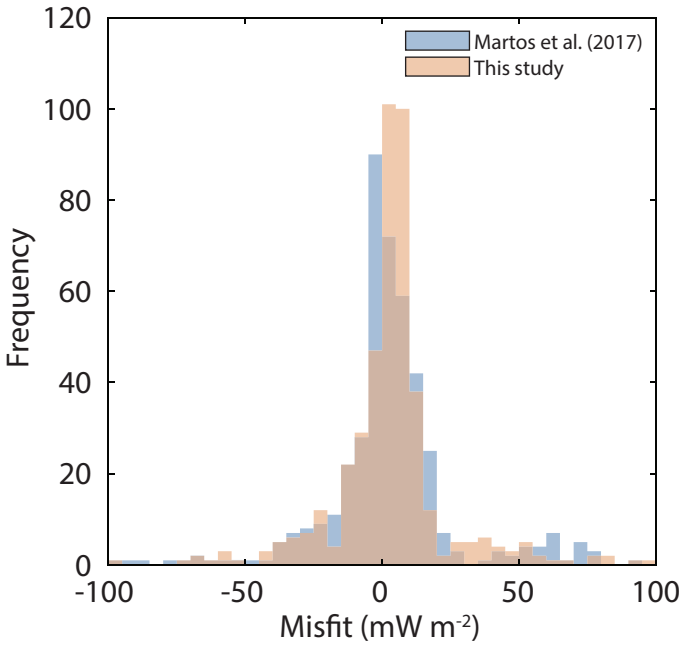

Figure 6.10: Residuals of estimated heat flow to the heat flow compiled in Guimarães et al. (2020). Blue depicts the heat flow misfits for Martos et al. (2017) with a mean of 2.95, median of 1.50 and std. dev. 31.1 mW m^{-2} respectively. In red, the heat flow misfit of our uncalibrated model with mean 0.76, median 3.24 and std. dev. of 27.72 mW m^{-2}.

tica was known in detail, the uncertainty in a heat production estimate would likely still be considerable, and any calibrations highly spatially biased. While calibration may be very useful in smaller regions or in regions with high data density, particularly if it is known that the basement geology might share common characteristics across the mapping area, application across an entire continent is contentious as large degrees of variability can be present at all spatial scales. In an ideal world, a robust model including vertical and lateral stratigraphy and extensive sampling of heat production would be conducted, similar to the adjoint inversion in southeastern Australia by Mather et al. (2019). However due to the significant deficiencies in knowledge of basement geology in Antarctica, this is not possible at the present time.

As geological terrane information in Antarctica is substantially lacking in comparison to other continents, simplified models are a necessity to generate thermal models across the continent. However, some partitioning can be justified from our current knowledge. Martos et al. (2017) themselves identify that West and East Antarctica are tectonically and geologically

very distinct enough to model their Curie depth separately for each region. In this scenario, if an author wished to apply a calibration, it might be suggested a separation of the calibration of thermal parameters for West and East Antarctica should also be applied.

Additionally, the exact nature of the calibration methods was not disclosed for either Fox-Maule et al. (2009) or Martos et al. (2017). In the case of Fox-Maule et al. (2009) this is of particular importance as the multi-layer nature of their model makes solutions incredibly non-unique due to the large range of parameters to be co-estimated from the heat flow fit in Australia. As a result this optimisation is not reproducible. Heat flow is also non-Gaussian, thus a simple minimisation of the residuals across the full range of heat flow may not weight the model fit in a proportional manner.

Martos et al. (2017) quote thermal parameter values of identical nature to that of Fox-Maule et al. (2005), who simply forced the Antarctic continent to a mean heat flow estimate of 65 mW m^{-2} to bring it in line with the global continental average heat flux of Pollack et al. (1993). As the reduced data set used in the calibration is not disclosed, the exact nature of the calibration fit or if any was actually applied is hard to discern. Attempts were made to construct a minimisation approach using percentage error, absolute variances, and minimisation of weighted residuals from the observed heat flow values published in Martos et al. (2017), but I was unable to reproduce the standard deviations and mean quoted in the manuscript, and the optimised thermal parameters did not match the parameters used by Fox-Maule et al. (2005). Calibration methodology should be disclosed in future manuscripts and the exact data points used in the calibration, with justifications for each, are necessary due to the subjective nature of the selection and minimisation process.

6.4.4 Other heat flow estimates

Other models exist for the Antarctic continent that do not, or at least not directly, make assumptions about thermal parameter distributions across the continent. One recent example is Shen et al. (2020), who calibrated a relationship for seismic velocity and geothermal heat flow in the continental

United States. This relationship was then applied to an improved resolution seismic model of the Antarctic continent. The major assumption in the methodology of Shen et al. (2020) is that results in the United States are directly comparable to correlations in the Antarctic continent. Correlations between upper mantle structure and average crustal composition are bundled together in this methodology, which indirectly includes assumptions that thermal parameter vertical distributions of the continental United States and Antarctica are similar. When compared to independent heat flow estimates, the model of Shen et al. (2020) appears to underestimate large regions including the West Antarctic Rift. An earlier model by Shapiro and Ritzwoller (2004) used broadly similar methodologies to Shen et al. (2020), albeit at a far lower resolution due to the seismic data available at the time. Shapiro and Ritzwoller (2004) calibrated their model based on global data sets and produced systematically higher heat flow results that are seemingly more in-line with the independent heat flow estimates. Future studies that calibrate physical characteristics to heat flow in regions external to Antarctica may benefit from using terranes that share tectonic histories, rather than entire continents, where possible.

Some of the most encouraging foundations for future heat flow estimates in Antarctica are those produced from multiple observables, such as the models of Lösing et al. (2020) and Stål et al. (2021). By combining the magnetic and seismic estimates for Curie depth and LAB temperature respectively, Lösing et al. (2020) were able to invert for a laterally variable model of surface heat flow and thermal parameters such as thermal conductivity and heat production. While promising, some anomalies are still present in the final solution. Lösing et al. (2020) note that when applying the geologically constrained radiogenic heat production data from Burton-Johnson et al. (2017) that their heat flow estimates vary by around 24 mW m^{-2}. Additionally, some suspicious results such as attributing the majority of the West Antarctic rift heat flow to radiogenic heat production may indicate improvements are still required in the separation of crustal and mantle contributions. The results show a strong dependence on the Curie isotherm estimate (being the shallowest of the two geophysical models used), which has been noted by Burton-Johnson et al. (2020) to have questionably low estimated uncertainties, and is discussed briefly here in the following section.

Stål et al. (2021) produced their heat flow model of Antarctic by using a similarity detection approach calibrated from other continents. While this method depends on reference and target observable relationships, some of which showing poor compatibility, their thorough quantification of uncertainty estimates along with a broad range of observables used in the modelling process lead to exceptionally promising results. The model of Stål et al. (2021) also shares a striking spatial resemblance to the model of Shen et al. (2020) which is generated from different methods. Of particular note, the higher heat flow estimates in Eastern Antarctica which show far higher correlation to the independent heat flow estimates discussed in Section 6.4.2, giving further credence that the calibration parameters of Shen et al. (2020) may warrant reconsideration.

The models of Lösing et al. (2020) and Stål et al. (2021) provide the most robust direction to date by combining multidisciplinary estimates of isotherm depths and allowing thermal parameters to vary laterally (although considerable uncertainty still persists). As further geophysical, geochemical, and geological data is collected in Antarctica, the results from similar inversions using integrated frameworks will be refined.

6.4.5 Future work

More vigorous calibrations of thermal parameters may also be possible as knowledge of the Antarctic basement geology increases. A more robust calibration model by making use of once conjoined geological terranes (akin to discussion in Pollett et al., 2019), ages and lithology (as discussed in Gard et al., 2019c), as well as other proxy information may give more meaningful insights to refine distributions in a more robust manner as further data becomes available. As this information is not currently well-defined for the Antarctic continent however, testing the validity of such a pursuit by applying these methods to regions where Curie depth estimates exist alongside well-defined subsurface geology and crustal velocity models would be beneficial.

Consideration of the effects of thermal refraction could also be added in future studies. Heat flow can preferentially flow into or around valleys in the basement-ice interface, a function of large contrasts in thermal conductiv-

ity, and leading to non-trivial deviations in heat flow from the background field (Willcocks and Hasterok, 2019).

While the topic of this manuscript was a discussion around the uncertainties in thermal parameters applied to geophysical proxies for temperature, the variability between Curie depth models must also be addressed. Although mean values are coarsely similar, and show similar long wavelength estimates, local scale estimates suffer from incredible variability in the Antarctic region (Figure 6.2). Significant additional analysis to compare methodologies and ascertain how such large variances can occur when making use of similar data sets is required and will likely be the target of further analysis. This point has been recognised by other authors specifically comparing Antarctic models (Burton-Johnson et al., 2020, e.g.).

6.5 Conclusions

Surface heat flux estimates and uncertainties derived from geophysical proxies are often used as an input parameter for modelling ice sheet dynamics. I have demonstrated that some of the variations in surface heat flow models for the Antarctic continent are not a function of the methodological procedure for estimating the isotherm with depth, but with the extrapolation and vertical models of thermal parameters of heat production and thermal conductivity applied to get to the surface. Quantifying the uncertainty of heat flow estimates derived from these assumptions is particularly important for the Antarctic continent where sub glacial geological information is sparse, and surface heat flow can impart direct influence on models of ice sheet dynamics.

I proposed a generalised layered model, guided by studies of continental average composition and uncertainty bounds for radiogenic heat production estimated from global whole-rock geochemical information. This model was applied to the Curie isotherm estimate of Martos et al. (2017) with updated uncertainty bounds derived via Monte Carlo simulation that mirror the asymmetric distributions of heat flow observed globally. The uncertainty model produced shows around 20% increase over that published by Martos et al. (2017). Uncertainty distributions also closer resemble log-

normal/log-logisitic heat flow distributions observed globally rather than Gaussian assumptions applied by previous studies. Surprisingly, the median model derived from these methods showed to be quite a good fit to the independent heat flow estimates in Antarctica compiled by Guimarães et al. (2020). 47.2% of the Martos et al. (2017) heat flow compilation, 48.39% of the MHB heat flow estimates, and 91.22% of the lake derived heat flow minimums were satisfied, with a mean misfit of the heat flow residuals of 0.71 mW m^{-2} and standard deviation of 27.68 mW m^{-2}. Additional uncertainty sources from variance of rock type, vertical geometry due to complex geological histories and structures observed in other continents are hard to quantify numerically, but are expected to be significant.

CHAPTER

SEVEN

SUMMARY AND CONCLUSION

7.1 Summary

Uncertainties in thermal parameter estimates such as radiogenic heat production result in large uncertainties when modelling the thermal state of the lithosphere. This uncertainty has wide-ranging implications on models of physical parameters such as lithospheric strength, economic benefits via petroleum maturation models and mineral and geothermal exploration, and impacts models relating to climate change such as those involved with ice sheet dynamics and melt rates whereby the sub-glacial heat flow is a critical input variable. In this thesis, I present improved constraints and methods for estimating radiogenic heat production and the thermal state of the continental lithosphere.

Estimating crustal radiogenic heat production requires knowledge of its natural variability. The whole-rock geochemical database compilation of Chaper 3 provides a foundation for assessing the distributions and correlations of the radioactive elements with respect to age, location, lithological types for future studies. This database currently stands at over 1 million unique analyses, with varying amounts of sample data ranging from major element concentrations, trace element concentrations, isotopic ratios and temporal and spatial meta-data. Computed geochemical indices, naming schema and properties such as density and heat production provide

a unique contribution of this database, along with significantly expanded date information particulary for ages older than ~1000 Ma.

The geochemical database stands as the foundation for the analysis of temporal trends in heat production through time in Chapter 4. This chapter demonstrates that radioactive decay describes the first-order decrease in heat production with age, while lithological bias also imparts a significant influence on radiogenic heat production distributions. I propose that super continent-cycle and plate velocities are not observed in the adjusted heat production record as suggested by some previous authors. After corrections, a deficit in heat production of samples older than the Archean–Proterozoic boundary appears to be evident. I suggest this is likely associated with the shift in bulk crust composition postulated by previous authors around this similar time, and in-line with studies of temporal heat production enrichment in sediments of McLennan and Taylor (1980). Alternatively, the heat production record may be biased due to selective preservation to to thermal stability. Regions with high heat production may not have been stable in the early Earth as the crust in high heat producing regions would be hot and weak, making them susceptible to destructive plate forces. Both Chapters 3 and 4 have implications for improving heat production distribution estimates in regions with little to no data, but also in areas where magmatic age and/or dominant lithology may be known. While many correlations have large uncertainties, the benefits lie mostly in constraining the expected distributions of heat production at large scales. For example, a dominantly felsic terrane from the Paleozoic will have a different uncertainty range than a predominantly mafic terrane of Archean age, as derived from this database and temporal trend analysis.

The global Curie depth model, developed in this thesis in Chapter 5, provides a model for the deeper thermal state of the crust which upper crustal heat production samples alone cannot. By making use of an update lithospheric magnetic field model, LCS-1, a laterally variable magnetic susceptibility model, and solving the forward modelling solution with all three vector components of the magnetic field model, I produced an improved global estimate of Curie depth via the equivalent source magnetic dipole method. Regions such as central Africa show the most improvement due to

application of the variable susceptibility model, but continents with poor constraints such as Antarctica require further work.

Finally, I analyse and discuss vertical thermal parameter models applied to geophysical proxies for temperature in the Antarctic continent. I demonstrate that some of the variability in Antarctic heat flow models derived from these methods are as a direct result of stark contrasts in models of thermal parameters of heat production and thermal conductivity applied to extrapolate to the surface. Radiogenic heat production variability is often poorly modelled and uncertainty estimates tend to under-represent the high lateral and vertical changes. By using the models of expected variability derived from the geochemical database of Chapter 3, and guided by studies of average continental crust composition, I generate a Monte Carlo solution for an Antarctic heat flow estimate and its associated uncertainty. I show an increase of around 20% in heat flow uncertainty compared with previous studies. Surprisingly, the median model derived from this 'global average' estimate provides a reasonable fit to the independent heat flow estimates in Antarctica.

7.2 Future directions

The global whole-rock geochemical database permits a plethora of potential studies of global geochemistry and its relationships, and will prove to be a useful tool for hopefully years to come. Refinement of the global geochemical database is a never ending process. Searching for new data as it becomes available is a somewhat laborious process. In the current processing schema updates are infrequent, manual, and primarily driven by our own personal research interests. Transitioning this database to a community driven effort, perhaps through a dynamic website, or assisting with initiatives such as the AuScope Geochemistry Network may be the future of this project. Furthermore, adjustments to the database structure may be warranted as further data entry fields are desired.

The Curie depth model of Chapter 5 has opened up a number of follow up topics and future work. Currently uncertainty estimates relating to the Curie depth are poorly quantified, owing largely to the lack of uncer-

tainty estimates for the input models. This includes uncertainty associated with the remanent magnetic field model for the oceans, the important of remanence for the continents, uncertainty estimates for the magnetic susceptibility model and long-wavelength supplement model for spherical harmonic degrees 1 through 15. These uncertainty estimates are currently very generalised, which filters through to the final Curie depth uncertainty estimates possible.

Further work also needs to be conducted to explain the significant discrepancies between differing methods of Curie depth estimation. Curie models derived via the fractal methods show large variability with each other, as well with the solution derived via the ESMD method in this thesis. Selection of model parameters in both methods seem to significantly influence the final results.

In Chapter 6, I present thermal parameter estimates and considerations for estimates of heat flow from geophysical proxies in Antarctica. As tectonic, geological, and age information continues to expand for subglacial bedrock, more robust calibrations of thermal parameters for the upper crust may become possible. Consideration of the effects of thermal refraction due to subglacial topography may also be warranted and its influence on lensing heat flow.

BIBLIOGRAPHY

Abbott, D., Burgess, L., Longhi, J., and Smith, W. H. F. (1994). An empirical thermal history of the Earth's upper mantle. *Journal of Geophysical Research: Solid Earth*, 99(B7):13835–13850.

Afonso, J. C., Fullea, J., Griffin, W. L., Yang, Y., Jones, A. G., D. Connolly, J. A., and O'Reilly, S. Y. (2013). 3-D multiobservable probabilistic inversion for the compositional and thermal structure of the lithosphere and upper mantle. I: a priori petrological information and geophysical observables. *Journal of Geophysical Research: Solid Earth*, 118(5):2586–2617.

Alessio, K. L., Hand, M., Kelsey, D. E., Williams, M. A., Morrissey, L. J., and Barovich, K. (2018). Conservation of deep crustal heat production. *Geology*, 46(4):335.

An, M., Wiens, D. A., Zhao, Y., Feng, M., Nyblade, A., Kanao, M., Li, Y., Maggi, A., and Lévêque, J.-J. (2015). Temperature, lithosphere-asthenosphere boundary, and heat flux beneath the Antarctic Plate inferred from seismic velocities. *Journal of Geophysical Research: Solid Earth*, 120(12):8720–8742.

Armstrong, R. L., Harmon, R. S., Moorbath, S. E., and Windley, B. F. (1981). Radiogenic Isotopes: The case for crustal recycling on a near-steady-state no-continental-growth Earth [and discussion]. *Philosophical Transactions of the Royal Society of London. Series A, Mathematical and Physical Sciences*, 301(1461):443–472.

Artemieva, I. and Mooney, W. (2001). Thermal thickness and evolution of Precambrian lithosphere: a global study. *J. Geophys. Res.*, 106:16387–16414.

Artemieva, I. M. (2006). Global 1x1 thermal model TC1 for the continental lithosphere: Implications for lithosphere secular evolution. *Tectonophysics*, 416(1):245–277. The Heterogeneous Mantle.

Artemieva, I. M., Thybo, H., Jakobsen, K., Sørensen, N. K., and Nielsen, L. S. (2017). Heat production in granitic rocks: Global analysis based on a new data compilation granite2017. *Earth-Science Reviews*, 172(Supplement C):1–26.

Barette, F., Poppe, S., Smets, B., Benbakkar, M., and Kervyn, M. (2017). Spatial variation of volcanic rock geochemistry in the virunga volcanic province: Statistical analysis of an integrated database. *Journal of African Earth Sciences*, 134:888–903.

Bédard, J. H., Hayes, B., Hryciuk, M., Beard, C., Williamson, N., Dell'Oro, T. A., Rainbird, R. H., Prince, J., Baragar, W. R. A., Nabelek, P. I., Weis, D., Wing, B., Scoates, J., Naslund, H. R., Cousens, B., Williamson, M.-C., Hulbert, L. J., Montjoie, R., Girard, É., Ernst, R., and Lissenberg, C. J. (2016). Geochemical database of Franklin sills, Natkusiak Basalts and Shaler Supergroup rocks, Victoria Island, Northwest Territories, and correlatives from Nunavut and the mainland. Open-file 8009, Geological Survey of Canada.

Behn, M. and Kelemen, P. B. (2003). Relationship between seismic p-wave velocity and the composition of anhydrous igneous and meta-igneous rocks. *Geochem. Geophys. Geosyst.*, 4:1041.

Belousova, E., Kostitsyn, Y., Griffin, W., Begg, G., O'Reilly, S., and Pearson, N. (2010). The growth of the continental crust: Constraints from zircon Hf-isotope data. *Lithos*, 119(3):457–466.

Birch, F. (1954). The present state of geothermal investigations. *Geophysics*, 19:645–659.

Birch, F., Roy, R., and Decker, E. (1968). Heat flow and thermal history in New England and New York. In Zen, E., White, W., Hadley, J., and

Thompson, J., editors, *Studies of Appalachian Geology: Northern and Maritime*, pages 437–451. Interscience, New York.

Blakely, R. J., Brocher, T. M., and Wells, R. E. (2005). Subduction-zone magnetic anomalies and implications for hydrated forearc mantle. *Geology*, 33(6):445–448.

Bouligand, C., Glen, J., and Blakely, R. (2009). Mapping Curie temperature depth in the western United States with a fractal model for crustal magnetization. *J. Geophys. Res.*, 114:B11104.

Brady, R., Ducea, M., Kidder, S., and Saleeby, J. (2006). The distribution of radiogenic heat production as a function of depth in the Sierra Nevada Batholith, California. *Lithos*, 86:229–244.

Brown, M. and Johnson, T. (2018). Secular change in metamorphism and the onset of global plate tectonics. *American Mineralogist*, 103(2):181–196.

Buggle, B., Glaser, B., Hambach, U., Gerasimenko, N., and Marković, S. (2011). An evaluation of geochemical weathering indices in loess–paleosol studies. *Quaternary International*, 240(1):12–21.

Burton-Johnson, A., Dziadek, R., and Martin, C. (2020). Geothermal heat flow in Antarctica: current and future directions. *The Cryosphere Discussions*, 2020:1–45.

Burton-Johnson, A., Halpin, J. A., Whittaker, J. M., Graham, F. S., and Watson, S. J. (2017). A new heat flux model for the Antarctic Peninsula incorporating spatially variable upper crustal radiogenic heat production. *Geophysical Research Letters*, 44(11):5436–5446.

Cammarano, F., Goes, S., Vacher, P., and Giardini, D. (2003). Inferring upper-mantle temperatures from seismic velocities. *Physics of the Earth and Planetary Interiors*, 138(3):197–222.

Campbell, I. (2003). Constraints on continental growth models from Nb/U ratios in the 3.5 Ga Barbarton and other Archaean basalt-komatiite suites. *American Journal of Science*, 303:319–351.

Carbotte, S. M., Marjanović, M., Carton, H., Mutter, J. C., Canales, J. P., Nedimović, M. R., Han, S., and Perfit, M. R. (2013). Fine-scale segmentation of the crustal magma reservoir beneath the East Pacific Rise. *Nature Geoscience*, 6:866–870.

Carson, C. J., McLaren, S., Roberts, J. L., Boger, S. D., and Blankenship, D. D. (2014). Hot rocks in a cold place: high sub-glacial heat flow in East Antarctica. *Journal of the Geological Society*, 171(1):9–12.

Champion, D., Budd, A., Hazell, M., and Sedgmen, A. (2007). Ozchem national whole rock geochemistry dataset. Technical report, Geoscience Australia.

Chapman, D. S. (1986). Thermal gradients in the continental crust. *Geological Society, London, Special Publications*, 24(1):63–70.

Christensen, N. and Mooney, W. (1995). Seismic velocity structure and composition of the continental crust: a global view. *J. Geophys. Res.*, 100:9761–9788.

Clark, D. A. and Emerson, J. B. (1991). Notes on rock magnetization characteristics in applied geophysical studies. *Exploration Geophysics*, 22(3):547–555.

Clauser, C. and Huenges, E. (1995). Thermal conductivity of rocks and minerals. In *Rock Physics & Phase Relations*, pages 105–126. American Geophysical Union (AGU).

Clemens, J., Stevens, G., and Farina, F. (2011). The enigmatic sources of I-type granites: The peritectic connexion. *Lithos*, 126(3-4):174–181.

Clifford, T. (1970). The structural framework of Africa. *African Magmatism and Tectonics*, pages 1–26.

Codd, E. F. (1970). A relational model of data for large shared data banks. *Communications of the ACM*, 13(6):377–387.

Coltice, N., Marty, B., and Yokochi, R. (2009). Xenon isotope constraints on the thermal evolution of the early Earth. *Chemical Geology*, 266(1-2):4–9.

Condie, K. C. (1993). Chemical composition and evolution of the upper continental crust: Contrasting results from surface samples and shales. *Chemical Geology*, 104(1):1–37.

Condie, K. C. and Aster, R. C. (2010). Episodic zircon age spectra of orogenic granitoids: The supercontinent connection and continental growth. *Precambrian Research*, 180(3):227–236.

Condie, K. C. and Aster, R. C. (2013). Refinement of the supercontinent cycle with Hf, Nd and Sr isotopes. *Geoscience Frontiers*, 4(6):667–680. Thematic Section: Antarctica – A window to the far off land.

Condie, K. C., Aster, R. C., and van Hunen, J. (2016). A great thermal divergence in the mantle beginning 2.5 Ga: Geochemical constraints from greenstone basalts and komatiites. *Geoscience Frontiers*, 7(4):543–553.

Cooper, C., Lenardic, A., and Moresi, L. (2004). The thermal structure of stable continental lithosphere within a dynamic mantle. *Earth and Planetary Science Letters*, 222(3):807–817.

Counil, J.-L., Cohen, Y., and Achache, J. (1991). The global continent-ocean magnetization contrast. *Earth and Planetary Science Letters*, 103(1):354–364.

Cox, G. M., Lyons, T. W., Mitchell, R. N., Hasterok, D., and Gard, M. (2018). Linking the rise of atmospheric oxygen to growth in the continental phosphorus inventory. *Earth and Planetary Science Letters*, 489:28–36.

Dalton, C. A., Ekström, G., and Dziewonski, A. M. (2009). Global seismological shear velocity and attenuation: A comparison with experimental observations. *Earth and Planetary Science Letters*, 284(1):65–75.

Daly, R. A. (1925). The Geology of Ascension Island. *Proceedings of the American Academy of Arts and Sciences*, 60(1):3–80.

Davies, J. (2013). Global map of solid Earth surface heat flow. *Geochem. Geophys. Geosys.*, 14:4608–4622.

Davies, J. and Davies, D. (2010). Earth's surface heat flux. *Solid Earth*, 1:5–24.

Dawson, J. (1984). Contrasting types of mantle metasomatism? In Kornprobst, J., editor, *Kimberlites II: the Mantle and Crust-Mantle Relationships*, pages 289–294. Elsevier, Amsterdam.

Debon, F. and Le Fort, P. (1983). A chemical–mineralogical classification of common plutonic rocks and associations. *Transactions of the Royal Society of Edinburgh: Earth Sciences*, 73(3):135–149.

Dhuime, B., Wuestefeld, A., and Hawkesworth, C. J. (2015). Emergence of modern continental crust about 3 billion years ago. *Nature Geoscience*, 8(7):552–555.

Drury, M. J. (1984). Perturbations to temperature gradients by water flow in crystalline rock formations. *Tectonophysics*, 103(1):19–32. Terrestrial Heat Flow Studies and the Structure of the Lithosphere.

Dyment, J. and Arkani-Hamed, J. (1998a). Contribution of lithospheric remanent magnetization to satellite magnetic anomalies over the world's oceans. *Journal of Geophysical Research: Solid Earth*, 103(B7):15423–15441.

Dyment, J. and Arkani-Hamed, J. (1998b). Equivalent source magnetic dipoles revisited. *Geophysical Research Letters*, 25(11):2003–2006.

Eaton, D. W., Darbyshire, F., Evans, R. L., Grütter, H., Jones, A. G., and Yuan, X. (2009). The elusive lithosphere–asthenosphere boundary (LAB) beneath cratons. *Lithos*, 109(1):1–22. Continental Lithospheric Mantle: The Petro-Geophysical Approach.

Engelhardt, H. (2004). Ice temperature and high geothermal flux at Siple Dome, West Antarctica, from borehole measurements. *Journal of Glaciology*, 50(169):251—-256.

Faul, U. H. and Jackson, I. (2005). The seismological signature of temperature and grain size variations in the upper mantle. *Earth and Planetary Science Letters*, 234(1):119–134.

Ferré, E. C., Friedman, S. A., Martín-Hernández, F., Feinberg, J. M., Conder, J. A., and Ionov, D. A. (2013). The magnetism of mantle xenoliths and potential implications for sub-Moho magnetic sources. *Geophysical Research Letters*, 40(1):105–110.

Finlay, C. C., Olsen, N., Kotsiaros, S., Gillet, N., and Tøffner-Clausen, L. (2016). Recent geomagnetic secular variation from Swarm and ground observatories as estimated in the CHAOS-6 geomagnetic field model. *Earth, Planets and Space*, 68(1):112.

Fisher, A. T., Mankoff, K. D., Tulaczyk, S. M., Tyler, S. W., Foley, N., and the WISSARD science team (2015). High geothermal heat flux measured below the West Antarctic Ice Sheet. *Science Advances*, 1(6).

Fountain, D. (1987). The relationship between seismic velocity and heat production—reply. *Earth Planet. Sci. Lett.*, 83:178–180.

Fountain, D. and Salisbury, M. (1981). Exposed cross-sections through the continental crust: implications for crustal structure, petrology, and evolution. *Earth Planet. Sci. Lett.*, 56:263–277.

Fox-Maule, C., Purucker, M. E., and Olsen, N. (2009). Inferring Magnetic Crustal Thickness and Geothermal Heat Flux from Crustal Magnetic Field Models.

Fox-Maule, C., Purucker, M. E., Olsen, N., and Mosegaard, K. (2005). Heat Flux Anomalies in Antarctica Revealed by Satellite Magnetic Data. *Science*, 309(5733):464–467.

French, J., Chacko, T., and Rivard, B. (2004). Global mafic magmatism and continental breakup at 2.2Ga: evidence from the Dharwar craton, India. *Geological Society of America Abstracts with Programs*, 36.

Frost, B. R., Barnes, C. G., Collins, W. J., Arculus, R. J., Ellis, D. J., and Frost, C. D. (2001). A Geochemical Classification for Granitic Rocks. *Journal of Petrology*, 42(11):2033–2048.

Furlong, K. P., Spakman, W., and Wortel, R. (1995). Thermal structure of the continental lithosphere: constraints from seismic tomography. *Tectonophysics*, 244(1):107–117. Heat flow and thermal regimes of continental lithosphere.

Fyfe, W. S. (1974). Heats of Chemical Reactions and Submarine Heat Production. *Geophysical Journal International*, 37(1):213–215.

Gao, S., Luo, T.-C., Zhang, B.-R., Zhang, H.-F., wen Han, Y., Zhao, Z.-D., and Hu, Y.-K. (1998). Chemical composition of the continental crust as revealed by studies in East China. *Geochimica et Cosmochimica Acta*, 62(11):1959–1975.

Gard, M., Hasterok, D., and Halpin, J. (2019a). Global whole-rock geochemical database compilation (data files). DOI: 10.5281/zenodo.2592823.

Gard, M., Hasterok, D., and Halpin, J. A. (2019b). Global whole-rock geochemical database compilation. *Earth System Science Data*, 11(4):1553–1566.

Gard, M., Hasterok, D., Hand, M., and Cox, G. (2019c). Variations in continental heat production from 4 Ga to the present: Evidence from geochemical data. *Lithos*, 342-343:391–406.

Geological Survey of Greenland (2011). Ujarassiorit 1989–2011. Technical report, http://www.ujarassiorit.gl. Downloaded June 2016.

Goes, S., Govers, R., and Vacher, P. (2000). Shallow mantle temperatures under Europe from P and S wave tomography. *Journal of Geophysical Research: Solid Earth*, 105(B5):11153–11169.

Goes, S., Hasterok, D., Schutt, D. L., and Klöcking, M. (2020). Continental lithospheric temperatures: A review. *Physics of the Earth and Planetary Interiors*, 306:106509.

Goodge, J. W. (2018). Crustal heat production and estimate of terrestrial heat flow in central East Antarctica, with implications for thermal input to the East Antarctic ice sheet. *The Cryosphere*, 12(2):491–504.

Goodwin, A. and Smith, I. (1980). Chemical discontinuities in Archean metavolcanic terrains and the development of Archean crust. *Precambrian Research*, 10(3):301–311. Comparative Planetary Evolution: Implications for the Proto-Archean.

Goodwin, A. M. (1996). Chapter 6 - evolution of the continental crust. In Goodwin, A. M., editor, *Principles of Precambrian Geology*, pages 261–280. Academic Press, London.

Gordon, R. (1998). The plate tectonic approximation: Plate nonrigidity, diffuse plate boundaries, and global plate reconstructions. *Annu. Rev. Earth Planet. Sci*, 26:615–642.

Gosnold, W. (1987). Redistribution of U and Th in shallow plutonic environments. *Geophys. Res. Lett.*, 14:291–294.

Goutorbe, B., Lucazeau, F., and Bonneville, A. (2007). Comparison of several BHT correction methods: a case study on an Australian data set. *Geophysical Journal International*, 170(2):913–922.

Guimarães, S. N. P., Vieira, F. P., and Hamza, V. M. (2020). Heat flow variations in the Antarctic Continent. *International Journal of Terrestrial Heat Flow and Applied Geothermics*, 3(1):1–10.

Gupta, M., Sundar, A., and Sharma, S. (1991). Heat flow and heat generation in the Archaean Dharwar cratons and implications for the Southern Indian Shield geotherm and lithospheric thickness. *Tectonophysics*, 194(1):107–122.

Hacker, B. R., Kelemen, P. B., and Behn, M. D. (2011). Differentiation of the continental crust by relamination. *Earth and Planetary Science Letters*, 307(3):501–516.

Hacker, B. R., Kelemen, P. B., and Behn, M. D. (2015). Continental lower crust. *Annual Review of Earth and Planetary Sciences*, 43(1):167–205.

Hand, M. and Sandiford, M. (1999). Intraplate deformation in central Australia, the link between subsidence and fault reactivation. *Tectonophysics*, 305(1):121–140.

Hans Wedepohl, K. (1995). The composition of the continental crust. *Geochimica et Cosmochimica Acta*, 59(7):1217–1232.

Haraguchi, S., Ueki, K., Yoshida, K., Kuwatani, T., Mohamed, M., Horiuchi, S., and Iwamori, H. (2018). Geochemical database of Japanese islands for basement rocks: compilation of domestic article. *Journal of Geological Society of Japan*, 124:1049–1054.

Hasterok, D. (2010). *Thermal State of the Oceanic and Continental Lithosphere*. PhD thesis, University of Utah.

Hasterok, D. and Chapman, D. (2007). Continental thermal isostasy II: Applications to North America. *J. Geophys. Res.*, 112:B06415.

Hasterok, D. and Chapman, D. (2011). Heat production and geotherms for the continental lithosphere. *Earth Planet. Sci. Lett.*, 307:59–70.

Hasterok, D., Chapman, D., and Davis, E. (2011). Oceanic heat flow: Implications for global heat loss. *Earth Planet. Sci. Lett.*, 311:386–395.

Hasterok, D. and Gard, M. (2016). Utilizing thermal isostasy to estimate sub-lithospheric heat flow and anomalous crustal radioactivity. *Earth Planet. Sci. Lett.*, 450:197–207.

Hasterok, D., Gard, M., Bishop, C., and Kelsey, D. (2019a). Chemical identification of metamorphic protoliths using machine learning methods. *Computers & Geosciences*, 132:56–68.

Hasterok, D., Gard, M., Cox, G., and Hand, M. (2019b). A 4 Ga record of granitic heat production: Implications for geodynamic evolution and crustal composition of the early Earth. *Precambrian Research*, 331:105375.

Hasterok, D., Gard, M., and Webb, J. (2018). On the radiogenic heat production of metamorphic, igneous, and sedimentary rocks. *Geoscience Frontiers*, 9(6):1777–1794. Reliability Analysis of Geotechnical Infrastructures.

Hasterok, D. and Webb, J. (2017). On the radiogenic heat production of igneous rocks. *Geoscience Frontiers*, 8(5):919–940.

Haus, M. and Pauk, T. (2010). Data from the PETROCH lithogeochemical database. Miscellaneous release—data 250, Ontario Geol. Surv.

Hawkesworth, C., Cawood, P., Kemp, T., Storey, C., and Dhuime, B. (2009). A matter of preservation. *Science*, 323(5910):49–50.

Hawkesworth, C., Cawood, P. A., and Dhuime, B. (2019). Rates of generation and growth of the continental crust. *Geoscience Frontiers*, 10(1):165–173.

Hawkesworth, C. J., Cawood, P. A., and Dhuime, B. (2016). Tectonics and crustal evolution. *GSA Today*, 26(9):4–11.

He, L., Hu, S., Huang, S., Yang, W., Wang, J., Yuan, Y., and Yang, S. (2008). Heat flow study at the Chinese Continental Scientific Drilling site: borehole temperature, thermal conductivity, and radiogenic heat production. *J. Geophys. Res.*, 113:B02404.

Heaman, L. M. (1997). Global mafic magmatism at 2.45 Ga: Remnants of an ancient large igneous province? *Geology*, 25(4):299–302.

Hemant, K. (2003). *Modeling and interpretation of global lithospheric magnetic anomalies*. PhD thesis, Freien Universität.

Hemant, K. and Maus, S. (2005). Geological modeling of the new CHAMP magnetic anomaly maps using a geographical information system technique. *Journal of Geophysical Research: Solid Earth*, 110(B12).

Herron, M. M. (1988). Geochemical classification of terrigenous sands and shales from core or log data. *SEPM Journal of Sedimentary Research*, 58:820–829.

Herzberg, C., Condie, K., and Korenaga, J. (2010). Thermal history of the earth and its petrological expression. *Earth and Planetary Science Letters*, 292(1):79–88.

Hojat, A., Fox-Maule, C., and Singh, K. H. (2016). Reconnaissance exploration of potential geothermal sites in Kerman province, using Curie depth calculations. *Journal of the Earth and Space Physics*, 41(4):95–104.

Hulot, G., Sabaka, T., Olsen, N., and Fournier, A. (2015). 5.02 - The present and future geomagnetic field. In Schubert, G., editor, *Treatise on Geophysics (Second Edition)*, pages 33–78. Elsevier, Oxford, second edition edition.

Iwamori, H. and Nakamura, H. (2015). Isotopic heterogeneity of oceanic, arc and continental basalts and its implications for mantle dynamics. *Gondwana Research*, 27(3):1131–1152.

Jaupart, C. (1983). Horizontal heat transfer due to radioactivity contrasts: Causes and consequences of the linear heat flow relation. *Geophys. J. R. astr. Soc.*, 75:411–435.

Jaupart, C., Labrosse, S., and Mareschal, J.-C. (2007). Temperatures, heat and energy in the mantle of the Earth. In Shubert, G. and Bercovici, D., editors, *Treatise on Geophysics: Mantle Dynamics*, volume 7, chapter 6, pages 253–303. Elsevier.

Jaupart, C. and Mareschal, J.-C. (2007). Heat flow and thermal structure of the lithosphere. In Shubert, G. and Watts, A., editors, *Treatise on Geophysics: Crust and Lithospheric Dynamics*, volume 6, chapter 5, pages 217–251. Elsevier.

Jaupart, C. and Mareschal, J.-C. (2010). *Heat Generation and Transport in the Earth*. Cambridge University Press.

Jaupart, C. and Mareschal, J.-C. (2014). Constraints on crustal heat production from heat flow data. In *Treatise on Geochemistry*, pages 53–73. Elsevier.

Jaupart, C., Mareschal, J.-C., and Iarotsky, L. (2016). Radiogenic heat production in the continental crust. *Lithos*, 262:398–427.

Jiao, L. and Lei, Y. (2019). Curie point depth inversion and its potential application to geothermal resource exploration. In *International Workshop on Gravity, Electrical & Magnetic Methods and Their Applications*, pages 193–196.

Jiménez-Díaz, A., Ruiz, J., Villaseca, C., Tejero, R., and Capote, R. (2012). The thermal state and strength of the lithosphere in the Spanish Central System and Tajo Basin from crustal heat production and thermal isostasy. *Journal of Geodynamics*, 58:29–37.

Jones, A. G., Afonso, J. C., and Fullea, J. (2017). Geochemical and geophysical constrains on the dynamic topography of the Southern African Plateau. *Geochemistry, Geophysics, Geosystems*, 18(10):3556–3575.

Keller, B. and Schoene, B. (2018). Plate tectonics and continental basaltic geochemistry throughout Earth history. *Earth and Planetary Science Letters*, 481:290–304.

Keller, C. and Schoene, B. (2012). Statistical geochemistry reveals disruption in secular lithospheric evolution about 2.5 Gyr ago. *Nature*, 485:490–493.

Kelsey, D. and Hand, M. (2015). On ultrahigh temperature crustal metamorphism: Phase equilibria, trace element thermometry, bulk composition, heat sources, timescales and tectonic settings. *Geosci. Frontiers*, 6:311–356.

Kent, D. V., Honnorez, B. M., Opdyke, N. D., and Fox, P. J. (1978). Magnetic properties of dredged oceanic gabbros and the source of marine magnetic anomalies. *Geophysical Journal International*, 55(3):513–537.

Ketcham, R. (2006). Distribution of heat-producing elements in the upper and middle crust of southern and west central Arizona: evidence from core complexes. *J. Geophysical Res.*, 101:13611–13632.

Korenaga, J. (2008). Urey ratio and the structure and evolution of Earth's mantle. *Reviews of Geophysics*, 46(2).

Korenaga, J. (2013). Archean Geodynamics and the Thermal Evolution of Earth. In *Archean Geodynamics and Environments*, pages 7–32. American Geophysical Union (AGU).

Kukkonen, I. and Lahtinen, R. (2001). Variation of radiogenic heat production rate in 2.8–1.8 Ga old rocks in the central Fennoscandian Shield. *Phys. Earth Planet. Int.*, 126:279–294.

Kumar, P. and Reddy, G. (2004). Radioelements and heat production of an exposed Archaean crustal cross-section, Dharwar craton, south India. *Earth and Planetary Science Letters*, 224(3):309–324.

la Roche, H. D., Leterrier, J., Grandclaude, P., and Marchal, M. (1980). A classification of volcanic and plutonic rocks using R1R2-diagram and major-element analyses – Its relationships with current nomenclature. *Chemical Geology*, 29(1):183–210.

Labrosse, S. and Jaupart, C. (2007). Thermal evolution of the Earth: Secular changes and fluctuations of plate characteristics. *Earth Planet. Sci. Lett.*, 260:465–481.

Lachenbruch, A. (1970). Crustal temperature and heat production: implications for the linear heat flow relation. *J. Geophys. Res.*, 75:3291–3300.

Langel, R. A. and Hinze, W. J. (1998). *The Magnetic Field of the Earth's Lithosphere: The Satellite Perspective*. Cambridge University Press.

Laske, G., Masters, G., Ma, Z., and Pasyanos, M. E. (2012). CRUST1.0: An Updated Global Model of Earth's Crust. In *EGU General Assembly Conference Abstracts*, EGU General Assembly Conference Abstracts, page 3743.

Le Bas, M. and Streckeisen, A. (1991). The IUGS systematics of igneous rocks. *J. Geol. Soc., London*, 148:825–833.

Le Pichon, X. and Heirtzler, J. R. (1968). Magnetic anomalies in the Indian Ocean and sea-floor spreading. *Journal of Geophysical Research (1896-1977)*, 73(6):2101–2117.

Lee, C.-T. A. and Bachmann, O. (2014). How important is the role of crystal fractionation in making intermediate magmas? Insights from Zr and P systematics. *Earth and Planetary Science Letters*, 393:266–274.

Lee, Y. and Deming, D. (1998). Evaluation of thermal conductivity temperature corrections applied in terrestrial heat flow studies. *Journal of Geophysical Research: Solid Earth*, 103(B2):2447–2454.

Lei, Y., Jiao, L., and Chen, H. (2018). Possible correlation between the vertical component of lithospheric magnetic field and continental seismicity. *Earth, Planets and Space*, 70(1):179.

Lesur, V., Hamoudi, M., Choi, Y., Dyment, J., and Thébault, E. (2016). Building the second version of the World Digital Magnetic Anomaly Map (WDMAM). *Earth, Planets and Space*, 68(1):27.

Lett, R. and Ronning, C. (2005). BC rock geochemical database - British Columbia Geological Survey Geofile 2005-14. Technical report, British Columbia Ministry of Energy and Mines.

Li, C.-F., Lu, Y., and Wang, J. (2017). A global reference model of Curie-point depths based on EMAG2. *Scientific Reports*, 7(1):45129.

Liu, H.-P., Anderson, D. L., and Kanamori, H. (1976). Velocity dispersion due to anelasticity; implications for seismology and mantle composition. *Geophysical Journal International*, 47(1):41–58.

Lowes, F. J. and Olsen, N. (2004). A more realistic estimate of the variances and systematic errors in spherical harmonic geomagnetic field models. *Geophysical Journal International*, 157(3):1027–1044.

Lucazeau, F. (2019). Analysis and mapping of an updated terrestrial heat flow data set. *Geochemistry, Geophysics, Geosystems*, 20(8):4001–4024.

Lucazeau, F., Poort, J., Goutorbe, B., and Raillard, S. (2011). Global heat flow trends resolved from multiple geological and geophysical proxies. *Geophysical Journal International*, 187(3):1405–1419.

Lösing, M., Ebbing, J., and Szwillus, W. (2020). Geothermal heat flux in Antarctica: Assessing models and observations by Bayesian inversion. *Frontiers in Earth Science*, 8:105.

Macdonald, K. C. and Holcombe, T. (1978). Inversion of magnetic anomalies and sea-floor spreading in the Cayman Trough. *Earth and Planetary Science Letters*, 40(3):407 – 414.

Mamani, M., Worner, G., and Sempere, T. (2010). Geochemical variations in igneous rocks of the Central Andean orocline (13 S to 18 S): Tracing crustal thickening and magma generation through time and space. *Geological Society of America Bulletin*, 122:162–182.

Mareschal, J. and Jaupart, C. (2004). Variations of surface heat flow and lithospheric heat production beneath the North American Craton. *Earth Planet. Sci. Lett.*, 223:65–77.

Mareschal, J.-C. and Jaupart, C. (2013). Radiogenic heat production, thermal regime and evolution of continental crust. *Tectonophysics*, 609:524–534.

Mareschal, J.-C. and West, G. (1980). A model for Archean tectonism. Part 2. Numerical models of vertical tectonism in greenstone belts. *Canadian Journal of Earth Sciences*, 17:60–71.

Martos, Y. M., Catalán, M., Jordan, T. A., Golynsky, A., Golynsky, D., Eagles, G., and Vaughan, D. G. (2017). Heat Flux Distribution of Antarctica Unveiled. *Geophysical Research Letters*, 44(22):11,417–11,426.

Mason, B. (1952). *Principles of Geochemistry*. J Wiley & Sons.

Mather, B., Moresi, L., and Rayner, P. (2019). Adjoint inversion of the thermal structure of Southeastern Australia. *Geophysical Journal International*, 219(3):1648–1659.

Maus, S., Barckhausen, U., Berkenbosch, H., Bournas, N., Brozena, J., Childers, V., Dostaler, F., Fairhead, J. D., Finn, C., von Frese, R. R. B., Gaina, C., Golynsky, S., Kucks, R., Lühr, H., Milligan, P., Mogren, S., Müller, R. D., Olesen, O., Pilkington, M., Saltus, R., Schreckenberger, B., Thébault, E., and Caratori Tontini, F. (2009). EMAG2: A 2–arc min resolution Earth Magnetic Anomaly Grid compiled from satellite, airborne, and marine magnetic measurements. *Geochemistry, Geophysics, Geosystems*, 10(8).

Maus, S. and Haak, V. (2002). Is the long wavelength crustal magnetic field dominated by induced or by remanent magnetisation? *J. Ind. Geophys. Union*, 6:1–5.

Maus, S., Rother, M., Holme, R., Lühr, H., Olsen, N., and Haak, V. (2002). First scalar magnetic anomaly map from CHAMP satellite data indicates weak lithospheric field. *Geophysical Research Letters*, 29(14):45–1–47–4.

Mayhew, M. A. (1982). Application of satellite magnetic anomaly data to Curie isotherm mapping. *Journal of Geophysical Research: Solid Earth*, 87(B6):4846–4854.

McCay, A. T., Harley, T. L., Younger, P. L., Sanderson, D. C. W., and Cresswell, A. J. (2014). Gamma-ray Spectrometry in Geothermal Exploration: State of the Art Techniques. *Energies*, 7:4757–4780.

McDonough, W. F. (2021). K, Th, U, and radiogenic heat production. In Alderton, D. and Elias, S. A., editors, *Encyclopedia of Geology (Second Edition)*, pages 198–205. Academic Press, Oxford, second edition edition.

McKenzie, D. (1967). Some remarks on heat flow and gravity anomalies. *J. Geophys. Res.*, 72:6261–6273.

McKenzie, D., Jackson, J., and Priestley, K. (2005). Thermal structure of oceanic and continental lithosphere. *Earth Planet. Sci. Lett.*, 233:337–349.

McKenzie, D. and Priestley, K. (2016). Speculations on the formation of cratons and cratonic basins. *Earth and Planetary Science Letters*, 435:94–104.

McLaren, S., Sandiford, M., Hand, M., Neumann, N., Wyborn, L., and Bastrakova, I. (2003). The hot southern continent: heat flow and heat production in Australian Proterozoic terranes. In *Evolution and Dynamics of the Australian Plate*, volume 372 of *Special Pub.*, pages 151–161. Geological Society of Australia.

McLennan, S. and Taylor, S. (1996). Heat flow and the chemical composition of continental crust. *Journal of Geology*, 104(4):369.

McLennan, S. M., Nance, W., and Taylor, S. (1980). Rare earth element-thorium correlations in sedimentary rocks, and the composition of the continental crust. *Geochimica et Cosmochimica Acta*, 44(11):1833–1839.

McLennan, S. M. and Taylor, S. R. (1980). Th and U in sedimentary rocks: crustal evolution and sedimentary recycling. *Nature*, 285(5767):621–624.

Middlemost, E. A. (1994). Naming materials in the magma/igneous rock system. *Earth Sci. Rev.*, 37:215–224.

Middleton, M. F. (2016). Radiogenic Heat Generation in Western Australia — Implications for Geothermal Energy. In Ismail, B. I., editor, *Advances in Geothermal Energy*, chapter 3. IntechOpen, Rijeka.

Morgan, P. (1985). Crustal radiogenic heat production and the selective survival of ancient continental crust. *J. Geophys. Res.*, 90:C561–C570.

Mörner, N.-A. and Etiope, G. (2002). Carbon degassing from the lithosphere. *Global and Planetary Change*, 33(1):185–203. The global carbon cycle and its changes over glacial-interglacial cycles.

Nataf, H.-C. and Ricard, Y. (1996). 3SMAC: An a priori tomographic model of the upper mantle based on geophysical modeling. *Physics of the Earth and Planetary Interiors*, 95(1):101–122.

National Geophysical Data Center (2006). 2-minute Gridded Global Relief Data (ETOPO2) v2. Accessed 07.07.2020.

Nesbitt, H. W. and Young, G. M. (1989). Formation and diagenesis of weathering profiles. *The Journal of Geology*, 97(2):129–147.

Neumann, N., Sandiford, M., and Foden, J. (2000). Regional geochemistry and continental heat flow: implications for the origin of the South Australian heat flow anomaly. *Earth Planet. Sci. Lett.*, 183:107–120.

Newfoundland and Labrador Geological Survey (2010). Newfoundland and Labrador GeoScience Atlas OnLine. Technical report.

Nisbet, E., Cheadle, M., Arndt, N., and Bickle, M. (1993). Constraining the potential temperature of the Archaean mantle: A review of the evidence from komatiites. *Lithos*, 30(3–4):291–307.

Okubo, Y. and Matsunaga, T. (1994). Curie point depth in northeast Japan and its correlation with regional thermal structure and seismicity. *Journal of Geophysical Research: Solid Earth*, 99(B11):22363–22371.

Olsen, N., Ravat, D., Finlay, C. C., and Kother, L. K. (2017). LCS-1: A high-resolution global model of the lithospheric magnetic field derived from CHAMP and Swarm satellite observations. *Geophysical Journal International*, 211(3):1461–1477.

Palumbo, F., Main, I. G., and Zito, G. (1999). The thermal evolution of sedimentary basins and its effect on the maturation of hydrocarbons. *Geophysical Journal International*, 139(1):248–260.

Pappa, F., Ebbing, J., and Ferraccioli, F. (2019). Moho depths of Antarctica: Comparison of seismic, gravity, and isostatic results. *Geochemistry, Geophysics, Geosystems*, 20(3):1629–1645.

Parker, A. (1970). An index of weathering for silicate rocks. *Geological Magazine*, 107(6):501–504.

Pattyn, F. (2010). Antarctic subglacial conditions inferred from a hybrid ice sheet/ice stream model. *Earth and Planetary Science Letters*, 295(3):451–461.

Perry, H. K. C., Jaupart, C., Mareschal, J.-C., and Bienfait, G. (2006). Crustal heat production in the Superior Province, Canadian Shield, and

in North America inferred from heat flow data. *Journal of Geophysical Research: Solid Earth*, 111(B4).

Pinet, C. and Jaupart, C. (1987). The vertical distribution of radiogenic heat production in the Precambrian crust of Norway and Sweden: Geothermal implications. *Geophysical Research Letters*, 14(3):260–263.

Pollack, H. and Chapman, D. (1977a). Mantle heat flow. *Earth Planet. Sci. Lett.*, 34:174–184.

Pollack, H. and Chapman, D. (1977b). On the regional variation of heat flow, geotherms, and lithospheric thickness. *Tectonophysics*, 38:279–296.

Pollack, H., Hurter, S., and Johnson, J. (1993). Heat flow from the Earth's interior: analysis of the global data set. *Rev. Geophys.*, 31:267–280.

Pollard, D., DeConto, R. M., and Nyblade, A. A. (2005). Sensitivity of cenozoic Antarctic ice sheet variations to geothermal heat flux. *Global and Planetary Change*, 49(1):63–74.

Pollett, A., Hasterok, D., Raimondo, T., Halpin, J. A., Hand, M., Bendall, B., and McLaren, S. (2019). Heat flow in Southern Australia and connections with East Antarctica. *Geochemistry, Geophysics, Geosystems*, 20(11):5352–5370.

Pujol, M., Marty, B., Burgess, R., Turner, G., and Philippot, P. (2013). Argon isotopic composition of Archaean atmosphere probes early Earth geodynamics. *Nature*, 498(7452):87–90.

Purucker, M. and Ishihara, T. (2005). Magnetic images of the Sumatra region crust. *Eos, Transactions American Geophysical Union*, 86(10):101–102.

Purucker, M., Langlais, B., Olsen, N., Hulot, G., and Mandea, M. (2002). The southern edge of cratonic North America: Evidence from new satellite magnetometer observations. *Geophysical Research Letters*, 29(15):56–1–56–4.

Purucker, M., Sabaka, T., Le, G., Slavin, J. A., Strangeway, R. J., and Busby, C. (2007). Magnetic field gradients from the ST-5 constellation:

Improving magnetic and thermal models of the lithosphere. *Geophysical Research Letters*, 34(24).

Purucker, M. and Whaler, K. (2007). 5.06–Crustal magnetism. In Schubert, G., editor, *Treatise on Geophysics*, pages 195–235. Elsevier, Amsterdam.

Purucker, M. E. (2013). Antarctica basal heat flux. url: http://websrv.cs.umt.edu/isis/index.php/Antarctica_Basal_Heat_Flux, date accessed: 02/08/2020.

Purucker, M. E. and Dyment, J. (2000). Satellite magnetic anomalies related to seafloor spreading in the South Atlantic Ocean. *Geophysical Research Letters*, 27(17):2765–2768.

Rajaram, M., Anand, S., Hemant, K., and Purucker, M. (2009). Curie isotherm map of Indian subcontinent from satellite and aeromagnetic data. *Earth and Planetary Science Letters*, 281(3):147–158.

Ramana, M., Ramprasad, T., and Desa, M. (2001). Seafloor spreading magnetic anomalies in the Enderby Basin, East Antarctica. *Earth and Planetary Science Letters*, 191(3):241–255.

Rasilainen, K., Lahtinen, R., and Bornhorst, T. (2007). The Rock Geochemical Database of Finland Manual. (online). Report of Investigation 164, Geol. Surv. Finland.

Regan, R. D. and Marsh, B. D. (1982). The Bangui Magnetic Anomaly: Its geological origin. *Journal of Geophysical Research: Solid Earth*, 87(B2):1107–1120.

Robin, G. d. Q. (1955). Ice movement and temperature distribution in glaciers and ice sheets. *Journal of Glaciology*, 2(18):523—-532.

Roy, R., Blackwell, D., and Birch, F. (1968). Heat generation of plutonic rocks and continental heat flow provinces. *Earth Planet. Sci. Lett.*, 5:1–12.

Roy, S., Ray, L., Bhattacharya, A., and Srinivasan, R. (2008). Heat flow and crustal thermal structure in the Late Archaean Closepet Granite batholith, south India. *International Journal of Earth Sciences*, 97(2):245–256.

Rudnick, R. (1992). Xenoliths–samples of the lower continental crust. In Fountain, D., Arculus, R., and Kay, R., editors, *Continental Lower Crust*, number 23 in Geodynamics, chapter 7, pages 269–316. Elsevier, New York.

Rudnick, R. and Fountain, D. (1995). Nature and composition of the continental crust: a lower crustal perspective. *Rev. Geophys.*, 33:267–309.

Rudnick, R. and Gao, S. (2003). Composition of the continental crust. In Rudnick, R., editor, *Treatise on Geochemistry: The Crust*, volume 3, chapter 1, pages 1–64. Elsevier.

Rybach, L. (1988). Determination of heat production rate. In Hänel, R., Rybach, L., and Stegena, I., editors, *Terrestrial Handbook of Heat-Flow Density Determination*, chapter 4.2, pages 125–142. Kluwer Academic Publishers, Dordrecht.

Rybach, L. and Buntebarth, G. (1984). The variation of heat generation, density and seismic velocity with rock type in the continental lithosphere. *Tectonophysics*, 103:335–344.

Sahr, K., White, D., and Kimerling, A. J. (2003). Geodesic discrete global grid systems. *Cartography and Geographic Information Science*, 30(2):121–134.

Sandiford, M. and McLaren, S. (2002). Tectonic feedback and the ordering of heat producing elements within the continental lithosphere. *Earth Planet. Sci. Lett.*, 204:133–150.

Sandiford, M. and McLaren, S. (2006). Thermo-mechanical controls on heat production distributions and the long-term evolution of the continents. In Brown, M. and Rushmer, T., editors, *Evolution and Differentiation of the Continental Crust*, pages 67–91. Cambridge University Press, London.

Sandiford, M., McLaren, S., and Neumann, N. (2002). Long-term thermal consequences of the redistribution of heat-producing elements associated with large-scale granitic complexes. *J. Metamorphic Geol.*, 20:87–98.

Sawka, W. N. and Chappell, B. W. (1988). Fractionation of uranium, thorium and rare earth elements in a vertically zoned granodiorite: Implications for heat production distributions in the Sierra Nevada batholith, California, U.S.A. *Geochimica et Cosmochimica Acta*, 52(5):1131–1143.

Scholl, D. W. and von Huene, R. (2007). Crustal recycling at modern subduction zones applied to the past—Issues of growth and preservation of continental basement crust, mantle geochemistry, and supercontinent reconstruction. In *4-D Framework of Continental Crust*. Geological Society of America.

Schroeder, D. M., Blankenship, D. D., Young, D. A., and Quartini, E. (2014). Evidence for elevated and spatially variable geothermal flux beneath the West Antarctic Ice Sheet. *Proceedings of the National Academy of Sciences*, 111(25):9070–9072.

Schubert, G. (1997). Mantle convection. In *Encyclopedia of Planetary Science*, pages 416–421. Springer Netherlands, Dordrecht.

Sclater, J., Jaupart, C., and Galson, D. (1980). The heat flow through the oceanic and continental crust and the heat loss of the Earth. *Rev. Geophys. Space Phys.*, 18:269–311.

Sekiguchi, K. (1984). A method for determining terrestrial heat flow in oil basinal areas. *Tectonophysics*, 103(1):67–79. Terrestrial Heat Flow Studies and the Structure of the Lithosphere.

Shapiro, N. M. and Ritzwoller, M. H. (2004). Inferring surface heat flux distributions guided by a global seismic model: particular application to Antarctica. *Earth and Planetary Science Letters*, 223(1):213–224.

Shen, W., Wiens, D. A., Lloyd, A. J., and Nyblade, A. A. (2020). A Geothermal Heat Flux Map of Antarctica Empirically Constrained by Seismic Structure. *Geophysical Research Letters*, 47(14):e2020GL086955.

Simons, F. J. and Dahlen, F. A. (2006). Spherical Slepian functions and the polar gap in geodesy. *Geophysical Journal International*, 166(3):1039–1061.

Slagstad, T. (2008). Radiogenic heat production of Archean to Permian geological provinces in Norway. *Norwegian Journal of Geology*, 88:149–166.

Sobolev, S. V., Zeyen, H., Stoll, G., Werling, F., Altherr, R., and Fuchs, K. (1996). Upper mantle temperatures from teleseismic tomography of French Massif Central including effects of composition, mineral reactions, anharmonicity, anelasticity and partial melt. *Earth and Planetary Science Letters*, 139(1):147–163.

Sonder, L. J. and England, P. (1986). Vertical averages of rheology of the continental lithosphere: relation to thin sheet parameters. *Earth and Planetary Science Letters*, 77(1):81–90.

Strong, D., Turnbull, R., Haubrock, S., and Mortimer, N. (2016). Petlab: New Zealand's national rock catalogue and geoanalytical database. *New Zealand J. Geol. Geophys.*, 53:475–481.

Stål, T., Reading, A. M., Halpin, J. A., and Whittaker, J. M. (2021). Antarctic Geothermal Heat Flow Model: Aq1. *Geochemistry, Geophysics, Geosystems*, 22(2):e2020GC009428.

Sun, X., Zhan, Y., Zhao, L., Chen, X., Sun, J., Li, C., Cui, T., and Han, J. (2019). Electrical structure of the Kunlun–Qinling fault system, northeastern Tibetan Plateau, inferred from 3-D inversion of magnetotelluric data. *Journal of Asian Earth Sciences*, 181:103910.

Szwillus, W., Afonso, J. C., Ebbing, J., and Mooney, W. D. (2019). Global crustal thickness and velocity structure from geostatistical analysis of seismic data. *Journal of Geophysical Research: Solid Earth*, 124(2):1626–1652.

Takei, Y. (2017). Effects of partial melting on seismic velocity and attenuation: A new insight from experiments. *Annual Review of Earth and Planetary Sciences*, 45(1):447–470.

Tang, M., Chen, K., and Rudnick, R. L. (2016). Archean upper crust transition from mafic to felsic marks the onset of plate tectonics. *Science*, 351(6271):372–375.

Taylor, P. T. and Frawley, J. J. (1987). Magsat anomaly data over the Kursk region, U.S.S.R. *Physics of the Earth and Planetary Interiors*, 45(3):255–265.

Taylor, S. and McLennan, S. (1985). *The Continental Crust: Its Composition and Evolution*. Blackwell, Oxford.

Taylor, S. R. and McLennan, S. M. (1995). The geochemical evolution of the continental crust. *Reviews of Geophysics*, 33(2):241–265.

Thébault, E. (2010). The Magnetic Field of the Earth's Lithosphere. *Space Science Reviews*, 155:95–127.

Thébault, E., Hemant, K., Hulot, G., and Olsen, N. (2009). On the geographical distribution of induced time-varying crustal magnetic fields. *Geophysical Research Letters*, 36(1).

Thébault, E. and Vervelidou, F. (2015). A statistical spatial power spectrum of the Earth's lithospheric magnetic field. *Geophysical Journal International*, 201(2):605–620.

Turcotte, D. and Schubert, G. (2002). *Geodynamics*. Cambridge University Press, Cambridge, U.K., 2nd edition.

Turekian, K. (1969). The oceans, streams and atmosphere. In *Handbook of geochemistry*, volume 1, pages 297–323. Springer-Verlag Berlin, Heidelberg, New York.

Unsworth, M., Wenbo, W., Jones, A. G., Li, S., Bedrosian, P., Booker, J., Sheng, J., Ming, D., and Handong, T. (2004). Crustal and upper mantle structure of northern Tibet imaged with magnetotelluric data. *Journal of Geophysical Research: Solid Earth*, 109(B2).

Urey, H. C. (1955). The cosmic abundances of potassium, uranium, and thorium and the heat balances of the Earth, the Moon, and Mars. *Proceedings of the National Academy of Sciences of the United States of America*, 41(3):127–144.

Van Liefferinge, B. and Pattyn, F. (2013). Using ice-flow models to evaluate potential sites of million year-old ice in Antarctica. *Climate of the Past*, 9(5):2335–2345.

Van Liefferinge, B., Pattyn, F., Cavitte, M. G. P., Karlsson, N. B., Young, D. A., Sutter, J., and Eisen, O. (2018). Promising oldest ice sites in East Antarctica based on thermodynamical modelling. *The Cryosphere*, 12(8):2773–2787.

Veizer, J. (1983). Geologic evolution of the Archean-Early Proterozoic Earth. In *Earth's earliest biosphere: Its origin and evolution*, pages 240–259.

Vieira, F. P. and Hamza, V. M. (2019). Assessment of Geothermal Resources of South America - A New Look. *International Journal of Terrestrial Heat Flow and Applied Geothermics*, 2(1):46–57.

Vilà, M., Fernández, M., and Jiménez-Munt, I. (2010). Radiogenic heat production variability of some common lithological groups and its significance to lithospheric thermal modeling. *Tectonophysics*, 490(3):152–164.

Vitorello, I. and Pollack, H. (1980). On the variation of continental heat flow with age and the thermal evolution of the continents. *J. Geophys. Res.*, 85:983–995.

Vosteen, H.-D. and Schellschmidt, R. (2003). Influence of temperature on thermal conductivity, thermal capacity and thermal diffusivity for different types of rock. *Physics and Chemistry of the Earth, Parts A/B/C*, 28(9):499–509. Heat Flow and the Structure of the Lithosphere.

Walker, J. D., Bowers, T. D., Black, R. A., Glazner, A. F., Lang Farmer, G., and Carlson, R. W. (2006). A geochemical database for western North American volcanic and intrusive rocks (NAVDAT). In *Geoinformatics: Data to Knowledge*. Geological Society of America.

Wasilewski, P. J. and Mayhew, M. A. (1992). The Moho as a magnetic boundary revisited. *Geophysical Research Letters*, 19(22):2259–2262.

Wasserburg, G. J., MacDonald, G. J. F., Hoyle, F., and Fowler, W. A. (1964). Relative contributions of uranium, thorium, and potassium to heat production in the earth. *Science*, 143(3605):465–467.

Whittington, A. G., Hofmeister, A. M., and Nabelek, P. I. (2009). Temperature-dependent thermal diffusivity of the Earth's crust and implications for magmatism. *Nature*, 458(7236):319–321.

Willcocks, S. and Hasterok, D. (2019). Thermal refraction: Impactions for subglacial heat flux. *ASEG Extended Abstracts*, 2019(1):1–4.

Williams, M., Dumond, G., Mahan, K., Regan, S., and Holland, M. (2014). Garnet-forming reactions in felsic orthogneiss: Implications for densification and strengthening of the lower continental crust. *Earth and Planetary Science Letters*, 405:207–219.

Wollenberg, H. and Smith, A. (1987). Radiogenic heat production of crustal rocks: an assessment based on geochemical data. *Geophys. Res. Lett.*, 14(3):295–298.

Workman, R. and Hart, S. (2005). Major and trace element composition of the depleted MORB mantle (DMM). *Earth Planet. Sci. Lett*, 231:53–72.

Worsley, T. R., Nance, D., and Moody, J. B. (1984). Global tectonics and eustasy for the past 2 billion years. *Marine Geology*, 58(3):373–400.

Xing, Z. and Beghein, C. (2015). A Bayesian approach to assess the importance of crustal corrections in global anisotropic surface wave tomography. *Geophysical Journal International*, 203(3):1832–1846.

Xu, X., O'Reilly, S., Zhou, X., and Griffin, W. (1996). A xenolith-derived geotherm and the crust-mantle boundary at Qilin, southeastern China. *Lithos*, 38(1):41–62.

Y. O'Reilly, S. and Griffin, W. (1985). A xenolith-derived geotherm for southeastern Australia and its geophysical implications. *Tectonophysics*, 111(1):41–63.

Zhu, P. P. (2016). Frictional strength and heat flow of southern San Andreas Fault. *Journal of Seismology*, 20(1):291–304.

Čermák, V. and Bodri, L. (1995). Three-dimensional deep temperature modelling along the European geotraverse. *Tectonophysics*, 244(1):1–11. Heat flow and thermal regimes of continental lithosphere.